ORTA DOĞU TEKNİK ÜNİVERSİTESİ
FEN BİLİMLERİ ENSTİTÜSÜ MÜDÜRLÜĞÜ

TEZ ŞABLONU ONAY FORMU
THESIS TEMPLATE CONFIRMATION FORM

1. Şablonda verilen yerleşim ve boşluklar değiştirilmemelidir.
2. **Jüri tarihi** Başlık Sayfası, İmza Sayfası, Abstract ve Öz'de ilgili yerlere yazılmalıdır.
3. İmza sayfasında jüri üyelerinin unvanlarıdoğru olarak yazılmalıdır. Tüm imzalar **mavi pilot kalemle** atılmalıdır.
4. **Disiplinlerarası** programlarda görevlendirilen öğretim üyeleri için jüri üyeleri kısmında tam zamanlı olarak çalıştıkları anabilim dalı başkanlığının ismi yazılmalıdır. Örneğin: bir öğretim üyesi Biyoteknoloji programında görev yapıyor ve biyoloji bölümünde tam zamanlı çalışıyorsa, İmza sayfasına biyoloji bölümü yazılmalıdır. İstisnai olarak, disiplinler arası program başkanı ve tez danışmanı için disiplinlerarası program adı yazılmalıdır.
5. Tezin **son sayfasının sayfa** numarası Abstract ve Öz'de ilgili yerlere yazılmalıdır.
6. Bütün chapterlar, referanslar, ekler ve CV sağ sayfada başlamalıdır. Bunun için **kesmeler** kullanılmıştır. **Kesmelerin kayması** fazladan boş sayfaların oluşmasına sebep olabilir. Bu gibi durumlarda paragraf (¶) işaretine tıklayarak kesmeleri görünür hale getirin ve yerlerini **kontrol edin**.
7. Figürler ve tablolar kenar boşluklarına taşmamalıdır.
8. Şablonda yorum olarak eklenen uyarılar dikkatle okunmalı ve uygulanmalıdır.
9. Tez yazdırılmadan önce PDF olarak kaydedilmelidir. Şablonda yorum olarak eklenen uyarılar PDF dokümanında yer almamalıdır.
10. **Bu form aracılığıyla oluşturulan PDF dosyası arkalı-önlü baskı alınarak tek bir spiralli cilt haline getirilmelidir.**
11. Spiralli hale getirilen tez taslağınızdaki ilgili alanları imzalandıktan sonra, Tez Juri Atama Formu ile birlikte bölüm sekreterliğine teslim edilmelidir.
12. Tez taslaklarının kontrol işlemleri tamamlandığında, bu durum öğrencilere METU uzantılı öğrenci e-posta adresleri aracılığıyla duyurulacaktır.
13. Tez yazım süreci ile ilgili herhangi bir sıkıntı yaşarsanız, **Sıkça Sorulan Sorular (SSS)** sayfamızı ziyaret ederek yaşadığınız sıkıntıyla ilgili bir çözüm bulabilirsiniz.

1. Do not change the spacing and placement in the template.
2. Write **defense date** to the related places given on Title page, Approval page, Abstract and Öz.
3. Write the titles of the examining committee members correctly on Approval Page. **Blue ink** must be used for all signatures.
4. For faculty members working in **interdisciplinary programs**, the name of the department that they work full-time should be written on the Approval page. For example, if a faculty member staffs in the biotechnology program and works full-time in the biology department, the department of biology should be written on the approval page. Exceptionally, for the interdisciplinary program chair and your thesis supervisor, the interdisciplinary program name should be written.
5. Write **the page number of the last page** in the related places given on Abstract and Öz pages.
6. All chapters, references, appendices and CV must be started on theright page. **Section Breaks** were used for this. **Change in the placement** of section breaks can result in extra blank pages. In such cases, make the section breaks visible by clicking paragraph (¶) mark and **check their position.**
7. All figures and tables must be given inside the page. Nothing must appear in the margins.
8. All the warnings given on the comments section through the thesis template must be read and applied.
9. Save your thesis as pdf and Disableall the comments before taking the printout.
10. **Print two-sided the PDF file that you have created through this form and make a single spiral bound.**
11. Once you have signed the relevant fields in your thesis draft that you spiraled, submit it to the department secretary together with your Thesis Jury Assignment Form.
12. This will be announced to the students via their METU students e-mail addresses when the control of the thesis drafts has been completed.
13. If you have any problems with the thesis writing process, you may visit our **Frequently Asked Questions (FAQ)** page and find a solution to your problem.

☒ **Yukarıda bulunan tüm maddeleri okudum, anladım ve kabul ediyorum. / I have read, understand and accept all of the items above.**

Name : Nazlı Seray
Surname : BOSTANCI
E-Mail : seray.bostanci@metu.edu.tr
Date :
Signature : _____

DEVELOPMENT OF 3D PRINTED PECTIN AND GELATIN BASED BIOACTIVE SKIN GRAFTS

A THESIS SUBMITTED TO
THE GRADUATE SCHOOL OF NATURAL AND APPLIED SCIENCES
OF
MIDDLE EAST TECHNICAL UNIVERSITY

BY

NAZLI SERAY BOSTANCI

IN PARTIAL FULFILLMENT OF THE REQUIREMENTS
FOR
THE DEGREE OF MASTER OF SCIENCE
IN
BIOTECHNOLOGY

AUGUST 2021

Approval of the thesis:

DEVELOPMENT OF 3D PRINTED PECTIN AND GELATIN BASED BIOACTIVE SKIN GRAFTS

submitted by **NAZLI SERAY BOSTANCI** in partial fulfillment of the requirements for the degree of **Master of Science in Biotechnology, Middle East Technical University** by,

Prof. Dr. Halil Kalıpçılar
Dean, Graduate School of **Natural and Applied Sciences** _____

Prof. Dr. Candan Gürakan Gültekin
Head of the Department, **Biotechnology** _____

Prof. Dr. Ayşen Tezcaner
Supervisor, **Dept. of Biotechnology, METU** _____

Prof. Dr. Nesrin Hasırcı
Co-Supervisor, **Chemistry, METU** _____

Examining Committee Members:

Prof. Dr. Dilek Keskin
Dept. of Engineering Sciences, METU _____

Prof. Dr. Ayşen Tezcaner
Dept. of Biotechnology, METU _____

Assoc. Prof. Dr. Aylin Şendemir
Dept. of Bioengineering, Ege University _____

Assoc. Prof. Dr. İrem Erel Göktepe
Dept. of Chemistry, METU _____

Assoc. Prof. Dr. Halime Kenar
Dept. of Medical Engineering, Acıbadem University _____

Date: 10.08.2021

I hereby declare that all information in this document has been obtained and presented in accordance with academic rules and ethical conduct. I also declare that, as required by these rules and conduct, I have fully cited and referenced all material and results that are not original to this work.

Name Last name: Nazlı Seray Bostancı

Signature :

ABSTRACT

DEVELOPMENT OF 3D PRINTED PECTIN AND GELATIN BASED BIOACTIVE SKIN GRAFTS

Bostancı, Nazlı Seray
Master of Science, Biotechnology
Supervisor: Prof. Dr. Ayşen Tezcaner
Co-Supervisor: Prof. Dr. Nesrin Hasırcı

August 2021, 119 pages

The aim of this study was to develop an easily applicable and bioactive skin graft composed of methacrylated pectin (PeMA) and methacrylated gelatin (GelMA), containing curcumin and/or Vitamin-C as antimicrobial and healing accelerating agents, respectively. Grafts were prepared in slab, 3D printed and 3D bioprinted forms and different properties were evaluated. Preparation parameters were optimized using slabs having different compositions (PeMA:GelMA as P:G 1:1, 1:2 and 1:3, v/v). P1:G1 solution did not have proper viscosity and eliminated from printing studies. Based on the characterization studies, P1:G3 was chosen as the optimum composition. Curcumin (loaded as 100 or 150 µg/mL) release from the gels was higher at pH 7.4 than pH 5.0. The gels having higher curcumin demonstrated higher antibacterial effect on *S.aureus* but lower cell proliferation. For Vitamin-C (0.75 or 0.25 mM), spectroscopic detection was not succesful due to the interference of photo-crosslinker (Irgacure 2959). Therefore, the effect of Vitamin-C on collagen synthesis of fibroblasts was evaluated, where higher Vitamin-C containing gels generated higher collagen synthesis and enhanced cell proliferation. According to

Live/Dead analyses, cell viability was above 80% for the samples having both bioactive agents upto 14 days. Bioprinted P1:G3 hydrogels containing L929 cells, curcumin and Vitamin-C resulted in high shape stability, viability and proliferation of the cells. The results indicated that curcumin and Vitamin-C containing P1:G3 hydrogels (either slab, printed or bioprinted) have high potential as skin graft and can be applied for the treatment of chronic wounds. *In vivo* studies are needed before any clinical application.

Keywords: Photocrosslinked Hydrogels, 3D Printing, Pectin, Gelatin, Skin Graft

ÖZ

3 BOYUTLU (3D) BASILMIŞ PEKTİN VE JELATİN ESASLI BİYOAKTİF CİLT GREFTLERİNİN GELİŞTİRİLMESİ

Bostancı, Nazlı Seray
Yüksek Lisans, Biyoteknoloji
Tez Yöneticisi: Prof. Dr. Ayşen Tezcaner
Ortak Tez Yöneticisi: Prof. Dr. Nesrin Hasırcı

Ağustos 2021, 119 sayfa

Bu çalışmanın amacı, antimikrobiyal ve iyileşmeyi hızlandırıcı ajanlar olarak sırasıyla kurkumin ve/veya Vitamin-C içeren metakrilatlı pektin (PeMA) ve metakrilatlı jelatinden (GelMA) oluşan, kolay uygulanabilir ve biyoaktif bir deri grefti geliştirmektir. Greftler disk, 3B basım ve 3B biyobasım formlarında hazırlanmış ve farklı özellikleri değerlendirilmiştir. Hazırlanma paramaetreleri farklı kompozisyonlardaki (PeMA:GelMA hacimsel oranları P:G 1:1, 1:2 ve 1:3) disk jellerde optimize edilmiştir. P1:G1 solüsyonu uygun viskoziteye sahip olmadığı için 3B basım çalışmalarından çıkıarılmıştır. Karakterizasyon çalışmalarının sonucunda en uygun kompozisyon olarak P1:G3 seçilmiştir. Jellerden zerdeçal (100 or 150 µg/mL olarak yüklenmiş) salınımı pH 7.4'te pH 5.0'e göre daha yüksek bulunmuştur. Daha yüksek zerdeçal içeren jeller, *S.aureus* üzerinde daha yüksek antibakteriyal etki sağlamış, ancak daha düşük hücre proliferasyonu göstermiştir. Vitamin-C (0.25 mM veya 0.75 mM) için, foto çapraz bağlayıcı (Irgacure 2959) ile etkileşimi sebebiyle spektroskopik olarak tespiti başarılı olamamıştır. Bu nedenle, Vitamin-C'nin fibroblastların kolajen sentezi üzerine etkisi değerlendirilmiş, ve daha yüksek Vitamin-C içeren jellerin daha yüksek kolajen sentezi ürettiği ve hücre

proliferasyonunu arttırdığı gözlemlenmiştir. Canlı/Ölü analizlerine göre 14 güne kadar her iki biyoaktif maddeye sahip örneklerde hücre canlılığı %80'in üzerinde bulunmuştur. L929 hücreleri, zerdeçal ve Vitamin-C içeren 3B biyobasım P1:G3 hidrojellerinin yüksek şekilsel stabilite ve hücreler üzerinde canlılık ve çoğalmasıyla sonuçlanmıştır. Sonuçlar, zerdeçal ve Vitamin-C içeren P1:G3 hidrojellerinin (disk, 3B basım veya 3B biyobasım) deri grefti olarak yüksek potansiyele sahip olduğunu ve kronik yaraların tedavisi için uygulanabileceğini göstermiştir. Herhangi bir klinik uygulamadan önce *in vivo* çalışmalara ihtiyaç vardır.

Anahtar Kelimeler: Foto-çapraz Bağlı Hidrojeller, 3B Basım, Pektin, Jelatin, Deri Grefti

To my beloved family, the Bostancı's

ACKNOWLEDGMENTS

I am grateful to my advisor Prof. Dr. Ayşen TEZCANER for her tolerance, support and encouragements throughout my study. I would also like to express my gratitude to my co-advisor Prof. Dr. Nesrin HASIRCI for sharing her valuable experiences and knowledge with me. I am so happy and lucky for having Dr. Senem BÜYÜKSUNGUR as a mentor, as a neighbor and also, as a friend.

I would like to thank my thesis committee members, Prof. Dr. Dilek KESKİN, Assoc. Prof. Dr. Aylin ŞENDEMİR, Assoc. Prof. Dr. İrem EREL GÖKTEPE and Assoc. Prof. Dr. Halime KENAR for their valuable contributions.

I would like to thank Prof. Dr. Vasıf HASIRCI for allowing me to conduct my experiments in BIOMATEN. I would like to thank Dr. Arda BÜYÜKSUNGUR, Engin PAZARÇEVİREN, Mustafa NAKİPOĞLU, Buşra YEDEKÇİ and Emine Ayşe TURHAN for all the help they have given, Mahsa MONİRİ and Selenay ÖZSOY for the good times.

I cherish all the the moments I have spent with my best friends Büşra ALTUĞ, Feyza N. KABATAŞ, İpek İDAYE, Gunes S. SERİN, Dilşat ÇELİK and Naz YURDAER.

Lastly, I offer my deep and sincere thanks to my wondeful family whom I love dearly. I would like to thank my mother, Semra BOSTANCI, for always being there for me. And my father, Sezai BOSTANCI for all the valuable lessons he has taught me for my whole life and my brother, Sezer BOSTANCI for always cheering me up and motivating me. I appreciate everything my family has ever done for me and I will do my best to honor them in every single thing I do in life.

I gratefully acknowledgeMiddle East Technical University Scientific Research Unit Project Number for the scholarship (GAP-10645).

TABLE OF CONTENTS

LIST OF TABLES

TABLES

LIST OF FIGURES

FIGURES

LIST OF ABBREVIATIONS

ABBREVIATIONS

3D	Three dimensional
ADSC	Adipose derived stem cells
AFSC	Human mesenchymal amniotic fluid stem cells
BSA	Bovine serum albumin
CA	Contact angle
CB	Carbonate buffer
$CaCl_2$	Calcium chloride
ChMA	Methacrylated chitosan
cm	centimeter
CO_2	Carbon dioxide
Cur	Curcumin
d_2O	Deuterium oxide
DE	Degree of esterification
dH_2O	Distilled water
DM	Degree of Methacrylation
DMEM	Dulbecco's Modified Eagle Medium
DMSO	Dimethyl sulfoxide
E.coli	Escherichia coli
ECM	Extracellular matrix
EGF	Epidermal growth factor
FBS	Fetal bovine serum
FDA	Food and Drug Administration
FGF	Fibroblast growth factor

FTSG	Full-thickness skin grafts
GalA	α-(1,4) linked D-galacturonic acid
GelMA	Methacrylated gelatin
H_2O_2	Hydrogen peroxide
h	hour
HA	Hyaluronic acid
HASCs	Human adipose
HCl	Hydrogen chloride
HM	High methoxy
HMECs	Human microvascular endothelial cells
HRP	Horseradish peroxide
HUVEC	Primary human umbilical vein endothelial cells
IL-1	Interleukin 1
kPa	Kilopascal
LAA	L-Ascorbic acid
LB	Luria broth
LM	Low methoxy
M	Molarity
MA	Methacrylic anhydride
MB	Methylene blue
MF	Mafenide acetate
MIC	Minimum inhibitory concentration
mM	milimolar
mm	milimeter
mTGase	Microbial transglutaminases
$Na_2S_2O_2$	Sodium thiosulfate

NaI	Sodium iodide
NaOH	Sodium hydroxide
NHDF	Normal human dermal fibroblasts
NIH-3T3	Mouse embryonic fibroblasts
O/W	Oil in water
P1:G1	Pectin:GelMA (1:1, v/v)
P1:G2	Pectin:GelMA (1:2, v/v)
P1:G3	Pectin:GelMA (1:3, v/v)
P	Passage
P.aeruginosa	Pseudomonas aeruginosa
PBS	Phosphate buffer saline
PCL	Poly(ε-caploractone)
PDGF	Platelet-derived growth factor
PDMS	Poly dimethylsiloxane
PEG	Poly(ethylene glycol)
PeMA	Methacrylated pectin
Pen-Strep	Pencillin-streptomycin
PFA	Paraformaldehyde
PHDF	Primary human dermal fibroblasts
PHEK	Primary human epidermal keratinocytes
PI	Photoinitiator
PLA	Poly(Lactic Acid)
PLGA	Poly(lactic-co-glycolic acid)
PVA	Poly(vinylalcohol)
PVP	Poly(vinylpyrrolidone)
RGD	Arginine-glycine-aspartate peptide sequence

RT	Room temperature
s	seconds
S.aureus	Staphylococcus aureus
SA/V	Surface are to volume ratio
SEM	Scanning electon microscopy
SGF	Simulated gastric fluid
SIF	Simulated intestinal fluid
SLA	Stereolithography
STSG	Split-thickness skin grafts
TBSA	Total body surface areas
TGF-α	Transforming growth factor- α
TGF-β	Transforming growth factor- β
UV	Ultraviolet
v/v	volume to volume ratio
VEGF	Vascular endothelial growth factor
w/v	weight to volume ratio
wd	dried weight
wi	initial weight
ws	swollen weight
WVTR	water vapor transmission rate
µL	microliter
µM	micromolar

CHAPTER 1

INTRODUCTION

1.1 Skin Structure and Organization

Skin is the largest organ in the human body effectuating 15% of the total body weight of an average adult (Vig et al. 2017). The fundamental role of human skin is to act as a barrier to protect the internal organs from external factors such as pathogens and mechanical destruction (W.-C. Yan et al. 2018; Pereira et al. 2017). Skin is also in charge of regulating the body temperature and moisture, eliminating biological waste and producing Vitamin-D (Huyan et al. 2020; Przekora 2020). Human skin is composed of three regions, named from the outer to inner layers; epidermis, dermis and subcutaneous tissue (hypodermis). The thickness and the composition of the skin alter from location thus, each layer has separate biostructure, components and functions (Figure 1.1) (Suhail et al. 2019).

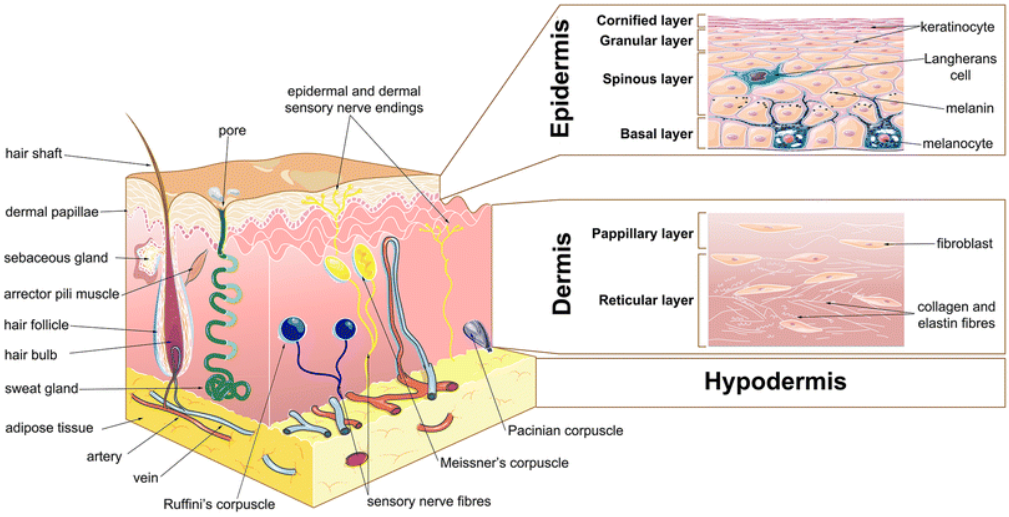

Figure 1.1 Schematic illustration of human skin (Pereira et al. 2017).

Epidermis is the exterior layer of the skin and its thickness varies from 0.05 mm to 1.55 mm. It consists of keratinocytes, melanocytes, Langerhans cells and Merkel cells (Suhail et al. 2019). Each component is responsible for different functions for instance, melanocytes produce melanin which protects the skin from UV, while Langerhans cells commence the first immune response to pathogens and Merkel cells provide the sensory function to skin tissue (Tavakoli and Klar 2020; Castañeda-Reyes et al. 2020; Sridhar, Venugopal, and Ramakrishna 2015). Nevertheless, the majority of epidermis layer is composed of keratinocytes which produce keratin (Castañeda-Reyes et al. 2020).

Epidermis has five sublayers named from the deepest to the superficial as; stratum basale, stratum spinosum, stratum granulosum, stratum lucidum and stratum corneum. Among these five layers, stratum corneum plays crucial role in water diffusion and its balance within skin (Wickett and Visscher 2006). Epidermis has an avascular structure thus the necessary oxygen and nutrients are provided to epidermis from the primary papillary region in dermis (Keirouz et al. 2020). Nonetheless, epidermis has self-renewable property that depends mainly on keratinization. As keratinocytes differentiate, cells move from stratum basale to upper hydrophobic stratum corneum layer.

The middle layer *dermis* has variable thickness from 0.3 to 3.0 mm depending on the area (Castañeda-Reyes et al. 2020). Unlike epidermis, dermis contains enormous amount of ECM (involving collagen, polysaccharides, elastin etc.). Thus, dermis is responsible for the strength and the elasticity of the skin. Along with the ECM insoluble components, dermis contains of fibroblasts, endothelial cells, vascular cells, nerve cells and as well as hair follicles, sensory receptors, sweat glands, and sebaceous glands (Naves et al. 2016). Fibroblasts are the primary cells of the dermis which produce structural components as collagen and elastin that support the mechanical stability and flexibility (Tavakoli and Klar 2020; Nourian Dehkordi et al. 2019). In addition, the blood vessels present in this layer, promote nutrient and

oxygen passage (Augustine 2018). Therefore, dermis plays an important role in wound healing.

Hypodermis is the deepest of the three layers of the skin. It is comprised of loose connective tissue and majorly from adipose tissue. The adipose tissue and adequately vascularized structure of subcutaneous tissue have a significant role in thermoregulation, nutritional storage and insulation (Naves et al. 2016). This layer is rich in blood and lymph vessels and also includes sweat glands and nerves. Primary cells of hypodermis are adipocytes however, fibroblasts and mast cells, macrophages and pre-adipocytes are also abundant (Ambekar and Kandasubramanian 2019).

1.2 Skin Defects and Regeneration

1.2.1 Classification of Skin Wounds

A skin wound is defined as the disruption in the function and the structure of the skin due to variety of reasons as diseases and thermal or physical damages (Ghomi et al. 2019). Commonly, wounds are categorized depending on the depth and the healing time as *acute* and *chronic wounds*.

Acute wounds mostly occur due to exogenous based deformations such as burns, cuts and surgical scars etc. (Okur et al. 2020). Although, the healing time can alter from the depth and the type of the wound, acute wounds show progressive healing in three months (Ghomi et al. 2019). Acute wounds follow the healing order and the wound heals without the need of treatments. However, in serious cases, certain external supports as debridements can be applied (Okur et al. 2020; Ambekar and Kandasubramanian 2019). In comparison to chronic wounds, acute wounds do not have bacterial colonization problem nor show cellular abnormalities in and around the wound bed.

Chronic wounds, occur due to the internal conditions that deform cellular unity (Okur et al. 2020). The main distinctive property of chronic wounds is that, they do not show full and natural recovery. The natural healing order is interrupted thus, instead of full recovery, partial healing is observed and the wound can stay active unpredictably, through minimum 3 months to years. The main reason of the delayed healing is bacterial contamination as *E.coli, S.aureus* and *B.subtilis* which leads to longer inflammation stage (Dart, Bhave, and Kingshott 2019). It is also reported that the presence of chronic wound changes the pH of human skin, increasing it from 4.0 - 6.0 to 7.15 - 8.00 which causes water loss and infections (Abrigo, McArthur, and Kingshott 2014; Ono et al. 2015). Non-healing and/or repeating wounds as in diabetic leg and foot ulcers, pressure ulcers, second and higher degree burns can be given as examples for this type of wounds. Furthermore, the treatment methods of chronic wounds are currently not fully effective. Moreover, the treatments cause an economical burden on both to the patient and health care system, as well as causing physical and mental challenges to the patient. It was reported that only in the United States, almost 80.000 people are hospitalized over a year due to serious burn injuries and average treatment/person costs US$36.000 – 117.000 (Naves et al. 2016).

1.2.2 Phases of Wound Healing

When the skin is damaged the natural functions are disrupted therefore, the immune response commences a cascade of actions urgently, to heal the damaged or traumatized skin. The healing process of the body is complex and it involves variety of components and pathways as immune cells (leukocytes, microphages), body cells (fibroblasts, keratinocytes), growth factors (TGF-β, PDGF, VEGF, FGF) and cytokines (Suhaeri et al. 2018). Throughout an optimal healing, the skin shows four overlapping stages as (i) hemostasis, (ii) inflammation, (iii) proliferation (re-epithelization) and (iv) remodeling (Figure 1.2). Although, these stages are generally synchronized, in the case of chronic wounds they might be prolonged, interrupted and even do not occur (Rieger, Birch, and Schiffman 2013).

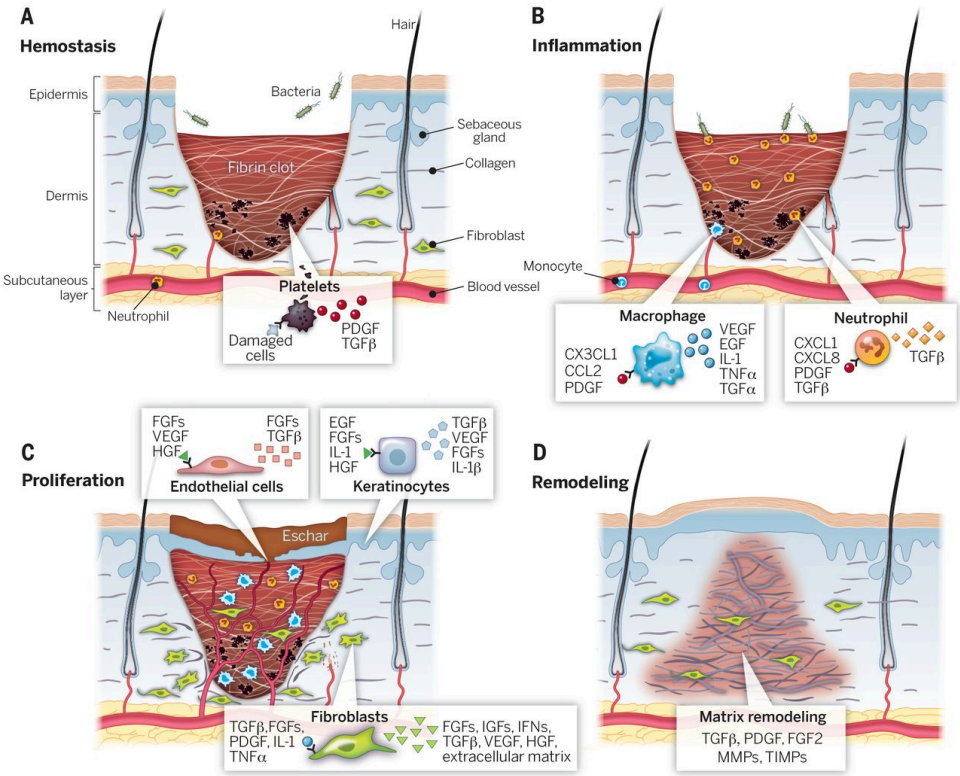

Figure 1.2 Schematic representation of the phases and components in charge of the wound healing cascade (Sun, Siprashvili, and Khavari 2014).

The first stage, *hemostasis* takes place right after the tissue is injured. The main role of this stage is to prevent blood loss. Thus, thrombocytes are coagulated and blood vessels narrow down. In addition, accumulated platelets form fibrin matrix which covers the wound, prevents bacterial infection and migration of immune cells (Brown, Ashley, and Koh 2018). After the blood clot is formed and hemostasis is obtained, the second stage called *inflammation* begins. In this phase, vasodilation allows the passage of neutrophils, growth factors, nutrients and cells to the wounded area (Okur et al. 2020). Neutrophils and macrophages are in charge of removing foreign organisms. During this phase, indications as swelling heat, pain and oedema occur (Serra et al. 2017).

In *proliferation*, endothelial cells form new or restore damaged blood vessels that allow oxygen and nutrient passage to the wound bed. Angiogenesis also stimulates granulation by promoting fibroblast migration for re-building the basement membrane (Ambekar and Kandasubramanian 2019; Okur et al. 2020). Lymphocytes and growth factors as PDGF and EGF are also involved for the closure of the wound and during the re-epithelization skin starts to contract (Brown, Ashley, and Koh 2018). This stage usually takes for 4-21 days (Figure 1.3) and ends when granulation tissue is formed (Čoma et al. 2021), (Gizaw et al. 2018).

The final phase is also known as *maturation* and it takes minimum three weeks and can last for months and even years (Przekora 2020). In this stage, skin tries to balance the synthesis, deposition and degradation of compounds. Thus, the ratio of collagen type I increases and as a result of this change, skin reaches the highest limit of its tensile strength and promoting wound closure (Gizaw et al. 2018).

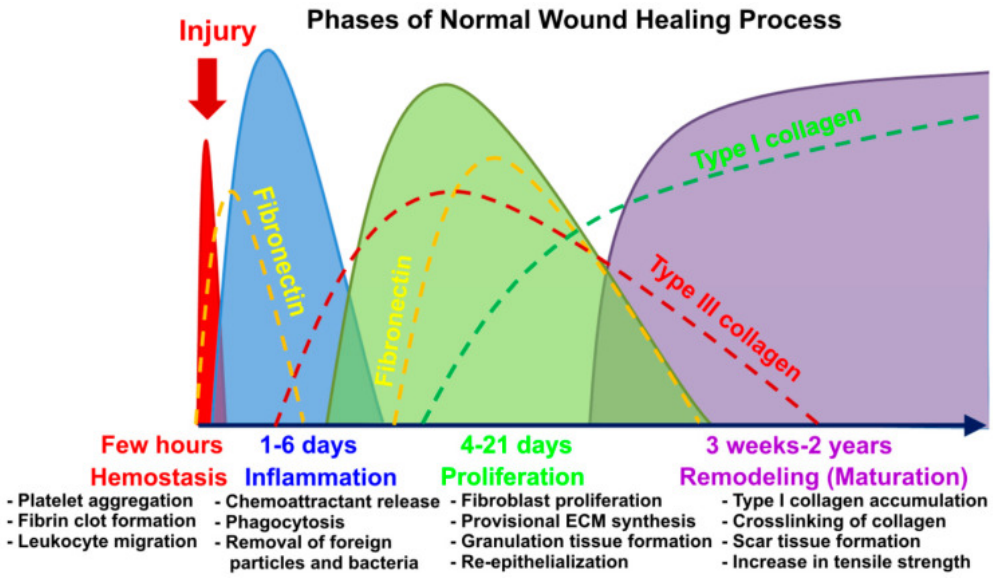

Figure 1.3 The timeline for overlapped wound healing stages during an acute wound (Przekora 2020).

1.3 Skin Grafts in Wound Healing

The treatment of chronic skin wounds remains challenging. Nowadays, debridements and antibacterial therapies are offered to the patient. However, they are not fully effective and each method has its own risks. For instance, it was reported that silver containing wound dressings were found inadequate for providing re-epithelization and also, causing a color change on the wound (II Stone et al. 2018). Prior to the complications of the healing procedure of deep wounds as second and higher degree burns, skin grafting has been used as an optimal medication. The success of skin grafting higher when the graft is applied onto the wounded skin immediately. Briefly, skin grafting is a surgical procedure allowing the use of removed skin tissue as a patch, to cover the wound bed of wounds that are wider and deeper than 4 cm (Vig et al. 2017).

American Burn Association categorizes skin grafts as *skin replacements (transplantation)* and *skin substitutes* based on the origin of the tissues. Skin replacements include harvesting of the healthy skin tissue from various origins as the patient him/herself, a donor from same species or another species (II Stone et al. 2018). Meanwhile, skin substitutes are tissue engineered artificial grafts made of biomaterials and cells (Przekora 2020). Depending on the source of the harvested tissues; skin replacements are divided into three groups as autografts, allografts and xenografts.

1.3.1 Autografts (Autologous Skin Grafts)

Autografts are obtained from the uninfected tissues of the patient him/herself. Autografts are considered as the primary and permanent treatment method for traumatic wounds because of its low mortality rate and better outcomes in wound closure (Naves et al. 2016). These grafts are harvested from the patient via a surgery while the patient is usually under anesthesia. Depending on the depth of the harvested tissue, autografts are divided into two categories as full-thickness skin grafts (FTSG)

or split-thickness skin grafts (STSG). STSG includes the harvesting of epidermis and a slight section of papillary dermis (II Stone et al. 2018). On the other hand, FTSG requires the removal of thicker skin piece than STSG, starting from epidermis, covering dermis to fat layer. Due to removal of wider dermis layer, FTSGs are less preferred since they have higher recovery time and risk of failure (Browning and Cindass 2020).

Autografts are superior than the other grafts on providing vascularization and having lower risk of immune rejection. However, limited availability of donor tissue and blood loss during tissue harvesting plays a crucial role in the search for alternative methods. Especially, for patients that are burnt more than the half of their total body surface area (TBSA), autografting is a risky procedure (Yiwei Wang et al. 2018).

1.3.2 Allografts

Skin allografts are recognized as a promising method for patients who cannot provide sufficient volume of healthy skin to cover their wound surface (Rezaei et al. 2017). These grafts are obtained either from the donors of same species or their cadavers (Yamamoto et al. 2018). Allografts have the advantage of supporting the expression of growth factors and cytokines in the wound bed (Vig et al. 2017). Moreover, allografts are easier to find in larger volumes that allow their usage on full thickness wounds. However, the major drawback of these groups is the risk of contamination from foreign pathogens and the preservation conditions of allografts limit their preferences (Sheikh et al. 2017). Thus, allografts do not present a permanent solution.

1.3.3 Xenografts

Xenografts are harvested from non-human species. As in allografts, xenografts are also used in brief time to reestablish human skin tissue (Vig et al. 2017). Over the years, many animal based grafts as chicken, dog, rat etc. have been used as a grafting

on humans. Nowadays, porcine skin is extensively used due to the histological resemblance of porcine skin to human (Yamamoto et al. 2018). The main downsides of xenografts are ethical and personal or religious issues (Naves et al. 2016).

1.3.4 Artificial Skin Grafts (Skin Substitutes)

The complications of conventional skin replacements as immune rejection, scar formation, slow healing and limited harvesting tissue lead to the utilization of tissue engineered artificial skin grafts to minimize patient discomfort (Kannaiyan et al. 2019). Tissue engineering consists of three principles as cells, scaffolds and growth factors to revitalize, preserve and to improve the tissue activity (De Isla et al. 2010). Thus, the primary goal of skin tissue engineering is to fabricate a skin substitute which can accelerate cellular activity and healing while allowing the formation of new skin meshes (Zhao et al. 2017). Although, there are currently a variety of acellular and cellular commercialized skin substitutes (Table 1.1) none of them effectively simulates the biological structure and/or functions of natural skin (Metcalfe and Ferguson 2007). These grafts are unsuccessful on suitable engraftment especially on full thickness burn wounds. For instance, an advertised graft named Biobrane® is inadequate on protecting the wound bed from infections (Przekora 2020). Table 1.1. gives the details on commercially available skin grafts, their cellular composition and insufficient properties. Because of these mentioned limitations, the research for an ideal tissue engineered skin graft is still in progress.

Table 1.1 Commercialized skin grafts and their features

Cellular Composition	Substitute Type	Name of the Product	Targeted Layer (Epidermis/Dermis)	Material	Drawbacks	Reference
Cellular	Autologous	Epicel®	Epidermal	-	Although, Epicel® fulfills FDA guidelines on safety and quality, the efficiency of Epicel® has not been confirmed.	Capo et al. 2014
	Allogenic	Dermagraft	Dermal	Polyglycolic acid	Although the graft has no rejection problems, it has inadequate mimicry to ECM that leads to infection.	Vig et al. 2017
	Xenogenic	Oasis®	Epidermal	Glycosaminoglycans, fibronectin, proteoglycans, and growth factors, Collagen type I, III and V	Average healing duration is 12 weeks and the product require change every 7 days. In addition, 3 of 5 studies reported this product cause wound serious infections.	Snyder et al. 2012
	Autologous	Bioseed-S®	Epidermal	Fibrin sealent	Has limited shelf life	Zeng et al. 2011
	Allogenic	Apligraft®	Dermo-epidermal	Bovine collagen type I	Only bilayered product that is accepted by FDA. However, not effective on deep chronic wounds.	Capo et al. 2014
Acellular	Hyalomatrix®		Dermo-epidermal	Silicone, hyaluronic acid	Silicone membrane slows down colonization at wound bed.	Myers et al. 2007
	Suprathel®		Epidermal	DL-lactide, trimethylcarbonate, and alpha-caprolactone	Graft was found effective on pain however it was found inadequate on wound contamination and adhesion.	Rashaan et al. 2017)
	Integra		Dermal	Silicone, bovine collagen, chondroitin-6-sulfate	No specific complication was reported, however the wound should be cleared from pathogens before using this graft.	Capo et al. 2014
	Alloderm®		Dermal	Cadaveric	Overpriced method also causes the spreading of the diseases.	Vig et al. 2017
	Biobrane®		Dermo-epidermal	Porcine collagen, silicone, polypeptides	Insufficient on protecting the wound bed from infections	Przekore et al. 2020

1.3.4.1 Aspired Characteristics of Skin Substitutes

Skin substitutes are fabricated to reduce the need for autografts. Depending on the architecture of the skin substitute, it can be a temporary application or a permanent graft which will not require the replacement with an autograft (Varkey, Ding, and Tredget 2015). Therefore, in both cases, the skin substitute must present a biocompatible environment for weeks to support the release of growth factors, vascularization and migration and proliferation of cells. Moreover, as in other skin replacements and wound dressings, artificial skin grafts must have the following properties; (i) should be biocompatible and do not show toxic effects, (ii) should regulate water loss and gaseous diffusion, (iii) should maintain the barrier behavior and overcome infection problems, (iii) should be easy to apply and store; (iv) should have a reasonable price, (v) should be mechanically and functionally compliant to skin (Naves et al. 2016; Varkey, Ding, and Tredget 2015).

1.4 Hydrogel Scaffolds in Tissue Engineering

Hydrogels are a class of three-dimensional polymeric networks which can be used as scaffold matrices for many tissue types. They attract attention especially in skin tissue engineering, due to having carboxyl, amino and hydroxyl groups in their backbone that provide high hydrophilic property (El-Sherbiny and Yacoub 2013). High water retention and semi-permeability of hydrogels supports mass and gaseous transportation while, having soft and porous structure allow flexibility that provide better mimicking of natural tissue environment (S. Wang, Lee, and Yeong 2015). In addition, having adjustable properties as pore sizes, allow control on the release of drug containing systems that aid in skin healing (Alven, Nqoro, and Aderibigbe 2020). The biological, mechanical and chemical properties of the hydrogel skin substitute are dependent on the production parameters including the chosen material(s), covalent bonding of the polymer network and the manufacturing method.

1.4.1 Preparation of of Hydrogels

Although, hydrogels are considered as promising matrices for tissue engineering and drug delivery applications, the characteristics of hydrogels differ from manufacturing techniques. In order to provide an effective treatment, scaffolds must have sufficient interconnected pore structure that would support cellular migration and growth also diffusion of gas and waste materials (O'Brien 2011). Depending on the needs, there are many methods for obtaining a hydrogel from traditional techniques as to more modern techniques as 3D printing (Mantha et al. 2019).

One of the techniques is *lyophilization* (*freeze drying*) which involves fast cooling of the polymer solution and removal of the frozen water in the material to sublimate. The advantage of lyophilization is allowing the formation of highly porous hydrogels however, it is not possible to control pore size or the shape (El-Sherbiny and Yacoub 2013). The geometries of lyophilized scaffolds are dependent on the molds used for the polymer solutions. Thus, even though freeze drying is used in many tissues, only planar shaped scaffolds are obtained with this method (Brougham et al. 2017). *Electrospinning* is another method which is based on an electric field created between the polymer and a grounded collector. A simple electrospinning setup consists of a (*i*) a syringe(s) that contains the polymer solution(s), (*ii*) a pump that ejects the polymer solution under defined rate, (*iii*) high voltage power supply that generates an electrical charge between the syringe and the collector that forms the fiber (*iv*) metal collector that compiles the exerted polymer (Esentürk, Erdal, and Güngör 2016). Electrospun fibers attract attention in tissue engineering applications prior to their adjustable properties as fiber diameters, mechanical strength and surface topography (Jin et al. 2012). Moreoever, electrospun fibers have high surface to volume ratio which promote their cellular proliferation (Rnjak-Kovacina and Weiss 2011). Among all these methods, 3D printing is considered as a novel technology and is popular in tissue engineering scaffolds.

1.4.1.1 3D Bioprinting (Additive Manufacturing)

3D Bioprinting is a state-of-the-art manufacturing technique involving a computer aided layer by layer design (De Mori et al. 2018). 3D bioprinting is considered as a superior method than the other fabrication techniques by providing control over the properties of the scaffolds as pore size, pore pattern, toughness and topography that would mimic the natural ECM of the targeted tissue (D. Singh, Singh, and Han 2016; Maver et al. 2018). In addition, 3D bioprinting allows cell encapsulation as in a bioink form, or cell seeding on 3D printed scaffolds which restraints cell distribution (Derakhshanfar et al. 2018). 3D printers are divided into three categories based on the ejection principles of polymers as inkjet printing, extrusion printing and laser assisted printing (Figure 1.4).

Inkjet 3D bioprinting requires either thermal, piezoelectric or electromagnetic apparatus to retain small ink droplets through the nozzles (Augustine 2018). Attention should be paid on the viscosity of the polymeric ink should be less-viscous thus far, needs to be mechanically stable enough right after printing (S. Wang, Lee, and Yeong 2015). Inkjet printing is preferable prior to its rapid fabrication time and affordability. However, bioink applications involve lower cell densities and cannot provide homogenous distribution of cells within scaffolds (Augustine 2018).

Extrusion based 3D bioprinters, eject the polymeric ink either by piston, screw or air pressure mechanisms (Rider et al. 2018). The advantage of this device is that it allows high cell densities and distribution in bioprinting. However, the ink should not be too viscous that could clog the nozzle or not too liquid to prevent the shape fidelity (Derakhshanfar et al. 2018).

Laser assisted bioprinting does not involve nozzles thus clogging is not a problem. The mechanism is different, briefly energy is transferred to the ribbon then, in the laser absorbing layer a bubble is formed to which generate pressure for creating droplets (Tamay et al. 2019). This method offers high resolution processing of solid

or liquid polymers (Ghilan et al. 2020). The drawbacks are high expense of the method and being the slowest fabrication among the three (Augustine 2018).

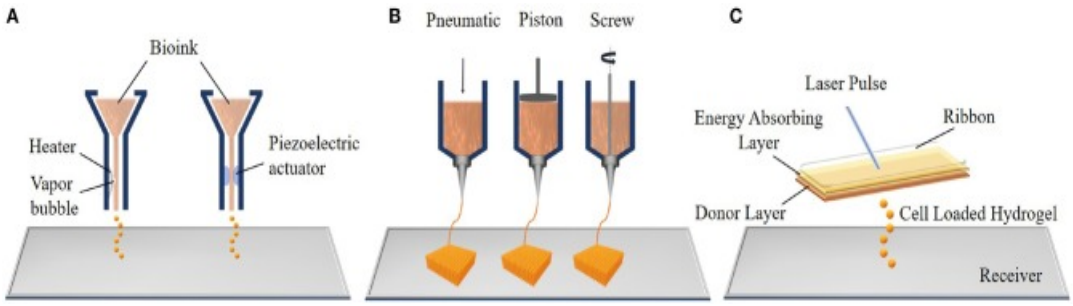

Figure 1.4 A comparative illustration of the 3D printing setups, inkjet printing (A), extrusion printing (B) and laser assited printing (C) (Tamay et al. 2019).

3D bioprinted scaffolds are adapted into all tissue types and some of them include bioactive agents for recovering the damaged site. For instance, Long et al. developed an extrusion based 3D printed wound dressing from two biopolymers: chitosan and pectin. In order to support the wound healing activity, the polymer ink included the drug lidocaine hydrochloride. Their results suggested that the solutions showed good printability as well as printed the scaffold had proper self-adhesiveness, mechanical strength, water uptake and drug release that would be used as a dressing (Long et al. 2019). Another study for 3D printed wound dressing was reported by Ilhan et al. The hydrogel was prepared from sodium alginate and polyethylene glycol to cover epidermis and to target diabetic wound ulcers the authors used an extraction of *Satureja cuneifolia* as a drug. The antibacterial property of *S.cuneifolia* was assessed on *E.coli* and *S.aureus*. Their results showed that *S.cuneifolia* was as effective as amphicillin on inhibiting bacterial proliferation however, their viability studies on L929 cells showed decrease in cell viability after 7 days of incubation (Ilhan et al. 2020). In bone tissue engineering, Curti et al. combined Wollastonite ($CaO-SiO_2$) with fish gelatin in different compositions in order to fabricate a promising bioink that can mimic the composition of bone and support osseointegration and

osseoinduction. Among four compositions, the bioink that consisted of 77% (w/v) Wollastonite and 23% (w/v) was found better in 3D printing preserving the shape fidelity. The Young's Modulus was found 2.05 ± 0.34 MPa and Ca/P ratio around 2.2. The viability of the 3D printed scaffolds were determined by seeding AFSCs. Cell density remained high during the 72 h study (Curti et al. 2020). A more general study was performed by Basara et al. in order to improve the pattern fidelity of 3D printed constructs. Briefly, the authors compared 3D printed GelMA with two different photocrosslinking time with dual crosslinked GelMA hydrogels via treatment with mTGase for the same UV exposure time. In result, it was observed that treatment with the enzyme mTGase reduced the water uptake ratio of the scaffolds, however it improved stiffness and preservation of pattern configuration. Human breast cancer cell line HCC1806 was encapsulated in the bioinks and it was observed that treatment with or without mTGase did not change the cytocompatibility of GelMA prints (Basara, Yue, and Zorlutuna 2019). With this study, it was observed that the properties of the hydrogels can be adjusted with the appropriate crosslinking mechanism.

1.4.1.2 Photocrosslinking of Hydrogels

Photocrosslinking creates irreversible reactions and transforms pre-polymer solutions into 3D network structures when exposed to light. The free radical initiated chain polymerization occurs with the presence of a photo-initiator (Choi et al. 2019). Irgacure 2959 is the most popular photo-initiator type in tissue engineering applications. It is a water soluble compound that separates into two radicals as bezoyl and alkyl that starts the polymerization (Tomal and Ortyl 2020).

The advantages of photocrosslinking are that the reaction takes place under biological conditions and is cost-effective (Chou and Nicoll 2009). In addition, the properties of the hydrogels can be adjusted by changing the concentrations and the type of photo-initiator, the power of the light source and the exposure time, the biopolymer type and concentration (GhavamiNejad et al. 2020). For instance, the

impact of polymer concentration and UV exposure time on 3D printability and other properties of GelMA hydrogels was studied. It was reported that GelMA solutions from 7 to 15 % (w/v) were found printable and the increase in GelMA benefitted on the mechanical properties. However, solutions below 5% (w/v) could not be printed. At the same time, increase in UV exposure time from 10 to 60 s also increased the elastic modulus from 2.6 ± 0.6 kPa to 60.3 ± 9.5 kPa. However, 3D printed GelMA hydrogels prepared with 10 s UV exposure were found inadequate on having shape fidelity. Meanwhile, one day viability studies showed that among all groups, cell viability on GelMA hydrogels which were exposed to 60 s of UV was the poorest (Bertassoni et al. 2014). Thus, having a wide range of adjusting options lead photo-crosslinking a highly preferred method in hydrogel preparation especially in 3D bioprinting. Table 1.2 presents tissue engineering studies involving via photo-crosslinking.

Table 1.2 Tissue engineering studies based on photo-crosslinked scaffolds.

Biomaterial(s)	Fabrication Method	Exposure time	Cell Type	Target Tissue	Findings	Reference
Methacrylated chitosan (ChMA) + GelMA	Hydrogel	10 min	NHDF	Not specified	Higher ChMA ratio, showed more porous structure and better cell viability.	Saraiva et al. 2015
Methacrylated κ-carrageenan + GelMA	Extrusion based 3D Printing	10 min	Human ASCs	Adipose Tissue	3D printed hydrogels promoted adipogenic differentiation.	Tytgat et al. 2019
Methacrylated Gellan Gum + GelMA	Two step photocrosslinked Hydrogel	120 s	NIH 3T3 fibroblasts	Cartilage Tissue	Double network hydrogels made by immersion of photocrosslinked gellan gum gels into Gelma solution; showed better mechanical strength that suits the cartilage applications	Shin et al. 2012
Bovine serum albumin glycidylmethacrylate	Hydrogel	45 s	NIH 3T3 fibroblasts	Not specified	Glycidyl methacrylate concentration improved the compressive moduluswhile decreasing water retention which makes them suitable for wound dressings and bone implants.	Lantigua et al. 2020
GelMA + Methacrylated hyaluronic acid	Hydrogel	40 s	Adipose Derived Stem Cells	Skin Tissue	NIH 3T3 cells showed similar proliferation rate in pure PulMA and GelMA while higher elongation in pure GelMA hydrogels.	Eke et al. 2017
Methacrylated Alginate	Microfluidic Fabricated Hydrogel	0-15-30-45-60 s	HUVEC	Not specified	Increasing UV exposure time increased the gel density however lowered the swelling ratio. Cell viability decreased with increasing UV exposure and AlgMA concentration.	Gao et al. 2019

1.5 Biomaterials and Bioactive Agents Used in Skin Tissue Engineering

1.5.1 Biomaterials

The decision of biomaterial(s) plays a crucial role in the properties of the scaffold. The biodegradation profile, biocompatibility, mechanical stability and viscosity (for ink based applications as electrospinning and 3D printing) are all dependent on the type of the material (Kaur et al. 2019). In artificial skin graft studies, natural and synthetic polymers are being used.

1.5.1.1 Natural Polymers (Biopolymers)

Natural polymers can be a polysaccharide (as chitosan, alginate, pectin, gellan gum etc.) or a protein (as collagen, gelatin, hyaluronic acid etc.) origin. Biopolymers show superior properties like biological affinity, recovering physiologic performance of damaged ECM (Kaur et al. 2019; Przekora 2020). Therefore, they are more preferred. However, they show limited mechanical strength and stiffness that may require the involvement of synthetic polymers and/or cross-linkers (W.-C. Yan et al. 2018).

1.5.1.1.1 Collagen

Collagen is known for its exquisite biocompatible and non-immunogenic properties. It is found in the dermis layer of the skin providing the mechanical strength (Esentürk, Erdal, and Güngör 2016). Collagen also comprises the primary element of ECM thus, it is highly used in studies and commercialized skin grafts and displays a vital role in tissue regeneration (Kaur et al. 2019). As an example, Ying et al. fabricated a hydrogel from collagen and HA to use onto skin wounds. The gelation of the two compounds was achieved through covalent interaction with H_2O_2 and an enzyme horse radish peroxidase (HRP). To compare the effectiveness of Col-HA

gels, pure Col crosslinked with HRP only were used as the control hydrogels. All of the hydrogels showed similar anti-bacterial property by preventing the *E.coli* and *S.aureus* proliferation around 47% and 55%, respectively only in 3 h of incubation. COS-7 fibroblasts and HMECs cells were encapsulated separately in Col-HA hydrogels. Although, both types of cells showed increase in number at the determined time points, VEGF expression of HMECs was lower at day 7 than the earlier time points. In vivo healing assay on mice showed that Col-HA hydrogels showed faster healing by reducing wound area by $96.44 \pm 0.47\%$ in 14 days. Other control groups, the pure gels, were also found effective on wound closure yet slightly lower than Col-HA (Ying et al. 2019).

1.5.1.1.2 Gelatin

Gelatin is obtained through hydrolysis and denaturation of the protein collagen (Tavakoli and Klar 2020). It can be extracted from many tissues (skin, bone and connective tissue) of many animals (fish, porcine, bovine etc.) (Mogoşanu and Grumezescu 2014). As a derivative of collagen, gelatin possesses the RGD sequence which provides cytocompatibility that promotes its usage in tissue engineering applications. In skin tissue engineering, Mishra et al. produced a hydrogel membrane by crosslinking different amounts of gelatin with pectin via glutaraldehyde. In result, all configurations showed higher viability than 88%. In addition, increase in gelatin amount increased the water vapor transmission rate (WVTR) which favors the membrane as a promising wound dressing (Mishra, Majeed, and Banthia 2011).

The major drawback of gelatin based hydrogels are their instability at physiological temperatures. To overcome this issue, gelatin is blended with other polymers or modified chemically (Tytgat et al. 2019). Therefore, gelatin is highly used in photopolymerization. There are numerous studies regarding on GelMA for cartilage, skin, bone etc. tissues (GhavamiNejad et al. 2020). For instance, Zhao et al. performed a comparative study on the wound healing abilities of electrospun GelMA hydrogels by using pure porcine gelatin and PLGA electrospun fibers as controls.

First, the optimizations were made on GelMA hydrogels photocrosslinked for different times (2 min, 6 min and 10 min). It was found out that, GelMA exposed to UV for 2 min showed faster degradation (5% in 3 days) while other scaffolds were stable for 28 days. Meanwhile GelMA-2 and GelMA-10 had the two lowest Young's Moduli of 290 kPa and 350 kPa, respectively. Thus, for viability studies GelMA-10 was chosen for comparison with gelatin and PLGA. Both gelatin and GelMA electrospun hydrogels showed high proliferation of BJ-6s cells while PLGA had the lowest. However, the main difference between gelatin and GelMA was observed in in vivo healing study conducted on mice. GelMA fibers had more collagen deposition than pure gelatin fibers and showed visible reduction wound in 14 days. Within this study, GelMA hydrogels were shown as effective scaffolds for wound healing studies (Zhao et al. 2017). Another study was reported by Eke et al. which involved a blend of photocrosslinked GelMA and HAMA in 15:1 ratio. The hydrogels had adequate compressive modulus (6 kPa) and preserved half of its mass after 21 days of incubation in PBS. Vascularization capacity of ADSCs encapsulated in the hydrogel was assessed for 21 days. For positive control VEGF was included along with cells. Starting from day 14, cells started to elongate and contact with the other cells (Eke et al. 2017).

1.5.1.1.3 Pectin

Pectin is an anionic polysaccharide consist of the repeating units of α-(1,4) linked D-galacturonic acid (GalA) and other sugars as L-rhamnose, D-arabinose, D-galactose (Gawkowska, Cybulska, and Zdunek 2018). It is extracted from variety of plants and depending on the extraction conditions and methods, the yield and the characteristics of pectin differs. Pectins are divided into two groups based on their degree of esterification (DE) as low methoxy (LM) and high methoxy (HM). DE determines the conditions for pectin to gel. For instance, LM pectin needs multivalent ions as Ca^{+2} and Mn^{+2} for gelation while HM pectin gels in acidic media with the inclusion of sugars (Noreen et al. 2017). Although, the requirements are different, pectins are

known for their excellent gelation especially in food industries. Furthermore, having a pH sensitive ability, adapted pectin's usage in drug delivery and tissue engineering applications (Lara-Espinoza et al. 2018).

Andriotis et al. produced a 3D printed skin patch from HM apple pectin blended with Manuka honey. The ink also included cyclodextrin and prepolis for providing anti-bacterial property to the patches. Another 3D printed skin substitute study was reported by Pereira et al. LM citrus pectin was modified with RGD sequences than methacrylated for the first time. The authors assessed the printability of pectin by using three different concentrations as 1.0% 1.5% 2.5% (w/v). The 3D printed scaffolds were dual crosslinked with UV light at different times and different molarity of $CaCl_2$. The results showed that increasing both polymer concentration and UV exposing time have improved the mechanical properties and gel fraction. However, hNDF proliferation and migration was higher on bioinks with 1.5% (w/v) polymer than 2.5% (w/v) showing that stiffness of the gel has an inverse correlation on the spreading of cells. Moreover, the printability of the bioinks were also assessed with $CaCl_2$ concentration as 0-1-3-5 mM. It was reported that at 0 and 1 mM the bioinks were too fluid to flow through the nozzle thus, bioprinting could not be completed. The problem was overcomed by increasing the concentration to 3 mM however, this amount was found toxic on cells. Therefore, in the study 1.8 mM of $CaCl_2$ was used as an ionic crosslinker (Pereira et al. 2018).

1.5.1.2 Synthetic Polymers

Synthetic polymers are known for their remarkable mechanical strength and spinnability. However, some of them do not show biodegradable or biocompatible properties (Alven, Nqoro, and Aderibigbe 2020). Sterilization of synthetic polymers also limits their utilization in tissue engineering applications (Mantha et al. 2019). Thus, they are generally combined with the biopolymers.

1.5.1.2.1 PEG

PEG is an inert, hydrophilic and biodegradable synthetic polymer (Choi et al. 2019). It has exquisite thermal defiance and water retention that allowed its usage as hydrogels in biomedical applications (Ahmed et al. 2018). Ahmed et al. developed a hydrogel film wound dressing from PEG and PVA via freeze thaw method. The polymers were crosslinked by autoclaving then, the drug asiaticoside was included. The results suggested that the drug release from hydrogels obeyed zero-order kinetics by releasing almost 90% of asiaticoside in 12 h. The gels were also seeded with HDF and HaCaT and even though the viability study was performed for 24 h, cells showed high viability as 97.83% and 98.74%, respectively (Ahmed et al. 2018).

1.5.1.2.2 PCL

PCL is a FDA approved synthetic polymer used frequently on tissue engineering applications (Kannaiyan et al. 2019). Although, it has good mechanical strength, it was reported that does not provide a sufficient environment for keratinocyte proliferation (Franco, Nguyen, and Lee 2011). Wei et al. developed scaffolds based on PCL, bovine skin gelatin and collagen for skin tissue engineering. PCL was included at two different concentrations into lyophilized Col-Gel. SEM analysis of the scaffolds showed that increasing PCL content has reduced the pore sizes and smoothened surface. The viabilities of the scaffolds were tested by seeding PHEK, PHDF cells and ASCs and all three cell types were found well attached and proliferated (Wei et al. 2019).

1.5.2 Bioactive Agents

Skin substitutes obtained from aforementioned biomaterials can be limited in supporting wound healing. Therefore, bioactive compounds are included (Alven, Nqoro, and Aderibigbe 2020).

1.5.2.1 Vitamin-C (L-Ascorbic Acid)

Vitamin-C also known as L-Ascorbic acid, is a water soluble compound that human body cannot produce. The consumption of Vitamin-C is highly important for human health since Vitamin-C is responsible for eliminating toxic free radicals and supporting collagen biosynthesis. Vitamin-C is also an anti-oxidant that can inhibit skin damage. It also possesses anti-agent properties that allow its utilization into cosmetic, pharmaceutical industries and wound healing applications (Q. Wang et al. 2018; Karakurt et al. 2020). However, Vitamin-C is a delicate compound that gets easily oxidized in acidic conditions and high temperature which limits its usage (Hu et al. 2020).

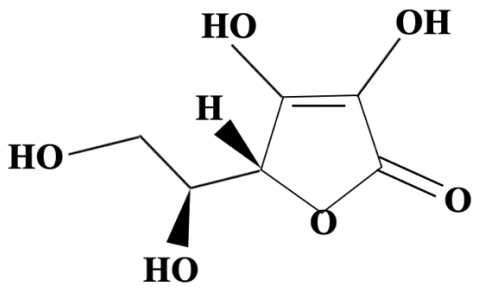

Figure 1.5 Chemical structure of Vitamin-C ($C_6H_8O_6$).

In wound healing applications, Mansuroğlu et al. developed a lyophilized hydrogel of chitosan and dextran sulphate sodium, later immersed in Vitamin-C and quercetin mixture solution. 0.02 mg/mL of Vitamin-C solution was used and in situ release showed that almost 60% of the Vitamin-C was released in PBS (pH 7.4) in 6 h. In addition, the impact of the drugs was analyzed by seeding L929 cells onto the hydrogels. Compared with the control, sole Vitamin-C loaded gels had 114.40% and blend of Vitamin-C and quercetin loaded gels had 94.16% viability at the end of day 7 (Mansuroğlu et al. 2020).

Recently, Karakurt et al. used SLA printer for preparing Vitamin-C (1%, w/v) loaded PEGDMA hydrogels. They have chosen riboflavin as photoinitiator (PI) and investigated the release kinetics of Vitamin-C from the hydrogels with different pore patterns (honeycomb, 4 circles, coaxial annulus, large and small tablets). In the study, the gels were first immersed in simulated gastric fluid (SGF) for 2 h then, in simulated intestinal fluid (SIF) for 4 h. Among the five designs, honeycomb pore pattern has the highest SA/V ratio, followed by coaxial annulus. In result, designs with higher SA/V ratio showed faster Vitamin-C release than the rest, showing that geometry of the scaffold affects the release kinetics. Although the study was not targeting a specific wound dressing, the authors reported that their scaffolds can be promising matrices in drug delivery applications (Karakurt et al. 2020). Hu et al. developed a hydrogel composed of chitosan and salecan via polyelectrolyte complex. Vitamin-C was loaded into the gel by the immersion method. To study a pH dependent release, the hydrogel was first placed in SGF (pH 1.2) media for 2 h then switched to SIF (pH 6.8) for 8 h. In vitro release study showed that in SGF approximately 10% of Vitamin-C was released while 92% of Vitamin-C was released in SIF in the following 8 h. The viability of L929 and 3T3-L1 fibroblasts on Vitamin-C loaded hydrogels was assessed for two days. It was reported that for both cell types, the viability was above 95% (Hu et al. 2020).

1.5.2.2 Curcumin

Curcumin is a yellow polyphenolic compound extracted from the plant Curcuma longa also known as turmeric (Figure 1.6) (Minzanova et al. 2018). Curcumin is a frequently used compound in wound healing applications due to its anti-inflammatory and antimicrobial properties. However, it has poor aqueous solubility and bioavailability which limits its usage (J.-K. Yan et al. 2017).

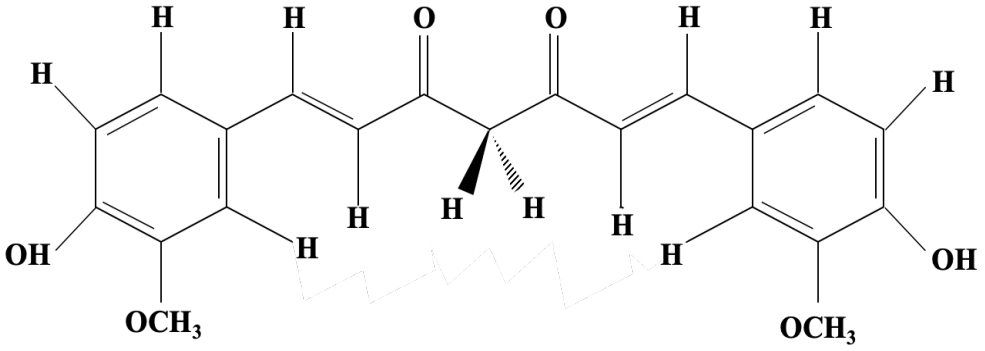

Figure 1.6 Chemical structure of curcumin ($C_{21}H_{20}O_6$).

Khamrai et al. developed a film composed of gelatin and cellulose derived from *Glucanoacetobacter xylinus*. Wound healing activity of the patches was studied by immersing the films composed of different amounts of cellulose into 5 mg/mL of curcumin solution. The antibacterial property of curcumin was assessed via disk method on *E.coli* and *S.aureus* strains. It was shown that curcumin was effective on inhibiting the growth of both strains. Moreover, higher cellulose amount improved the drug uptake into the film and showed sustained release in PBS media (pH 7.4). While, hydrogel film with lower cellulose amount, showed burst release in 40 h and had limited NIH 3T3 proliferation on the film (Khamrai et al. 2019). Another curcumin based wound dressing study was reported by Sharma et al. They have conjugated curcumin with hyaluronic acid (HA) to assess its influence on wound healing. It is reported that conjugating curcumin to HA at doses which might be toxic in free form supported cell proliferation immensely. Meanwhile, in vivo wound closure assay performed in diabetic mice revealed faster healing in HA-Cur group compared to than sole HA (Sharma et al. 2018). The results on curcumin preventing keratinocyte migration was in correlation with the other studies. For instance, Tummalapalli et al. also reported the negative influence of curcumin on fibroblasts in terms of apoptosis, yet improved the anti-bacterial properties of their wound dressing based on pectin and gelatin (Tummalapalli et al. 2016a). Fereydouni et al. (2021) produced corn zein electrospun fibers containing different concentrations of

oil in water (O/W) nanoemulsions of curcumin. The authors reported that, the increase in the curcumin concentration increased the ultimate tensile strength from 0.73 ± 0.06 to 3.21 ± 0.21 MPa. It was also stated that nanofibers showed good cell viability for both L929 and HDF cells (Fereydouni et al. 2021).

Table 1.3 Bioactive compounds used in artificial skin graft and wound dressing studies

Biomaterial(s)	Bioactive Compound(s)	Scaffold Fabrication Method	Cell Type	Findings	References
Chitosan, pectin	lidocaine hydrochloride (LDC)	lidocaine hydrochloride (LDC)	N/A	3D printed hydrogel was sufficient for water absorption c elasticity. Increase in LDC concentration lowered the pore size, however increased the porosity.	(Long et al. 2019)
κ-carrageenan, locust bean gum	cranberry extract	Hydrogel film	NIH 3T3	Anthocyanin in cranberry powders, provided visible color change in different pH values, also efficient on inhibiting anti-bacterial growth.	Zepon et al. 2019)
Chitosan, agarose	Vitamin-C	Hydrogel film	human skin fibroblasts, human epidermal keratinocytes and	Skin substitute supported the adhesion and proliferation of all cells however, the burst release of Vitamin-C did not result in a specific different cell response.	(Vivcharenko et al 2020)
Oxidized pullulan, oxidized cellulose, PVA	L-arginine	Lyophilized Hydrogel	Primary fibroblast cells from rabbit dermis	Chemical interaction between oxidized pullulan and L-arginine provided prolonged release.	(Barn et al. 2019)
PVA	Ciprofloxacin	Freeze thaw-membrane hydrogel	Freeze thaw-membrane hydrogel	Ciprofloxacin inhibited bacterial infection on mice. In addition, at day 21, drug included groups showed higher collagen synthesis.	(Suhaeri et al. 2018)
GelMA	Silver + PDGF	3D Printed Hydrogel	HaCaT cells (human keratinocyte cell line)	PDGF first showed burst release but remained active for 14 days, silver remained active over 14 days. Silver completely prevented proliferation of gram negative bacteria (*E.coli* and *P. aeruginosa*)	(Wang et al. 2019)
PVA, PVP, pectin and MF	Ag^+ nanoparticles	Electrospinning	HSF-PI 18 fibroblast like cells	AgNPs slightly decreased fibroblast viability however, prevented *E.coli* and *S.aureus* infection. *In vivo* study on rats showed that wound area reduced more in AgNPs containing groups.	(Tummalapalli et al. 106b)

1.6 The Aim of The Study

The treatment of chronic wound such as ulcers and burns remains a delicate issue. It creates a major burden on the patient economically, physically and mentally while causing financial burden on health care. Despite there are many commercialized wound dressings or skin grafts, all products and methods have their own limitations thus, the search for an optimal artificial graft is still proceeded.

The aim of the study was to fabricate a 3D bioprinted photo-crosslinkable methacrylated pectin and methacrylated gelatin hydrogel skin graft which can be utilized in the treatment of chronic wounds. Gelatin, was chosen prior to its optimal mechanical strength and high cytocomptability. On the other hand, the polysaccharide pectin was preferred due to its excellent water retention and stability under acidic environments. The novelty of this study comes from incorporation of the two bioactive agents, namely Vitamin-C and curcumin to accelerate tissue regeneration. Vitamin-C is chosen for enhancing the synthesis of collagens, while curcumin is chosen for its antioxidant properties. It is expected that PeMA would provide a pH sensitive release of the drugs and GelMA would promote L929 migration and proliferation while the Vitamin-C would support collagen synthesis of L929 cells and curcumin would prevent bacterial infections.

As schematically illustrated at Figure 1.7, this thesis is divided into three parts. In the first section, synthesis of pectin and gelatin with suitable DMs would be performed and photocrosslinkable slab gels from different PeMA:GelMA (P:G, 1:1, 1:2, 1:3, v/v) compositions would be obtained and characterization studies are conducted.

In the second section, the same blend compositions were 3D printed with honeycomb pore patterns. The characterizations of photocrosslinked 3D printed hydrogels were performed and an optimal composition of PeMA:GelMA was chosen. Vitamin-C and curcumin was loaded in the inks at determined concentrations and drug release was studied at two different pHs to mimic the physiology of skin wounds.

The final section consists of 3D bioprinting of the determined polymer composition along with the determined drug dosages. The viability of L929 cells and the release of drugs from the scaffold was analyzed. Along with this study, a promising dermo-epidermal artificial skin graft was aimed to be obtained for the treatment chronic wounds.

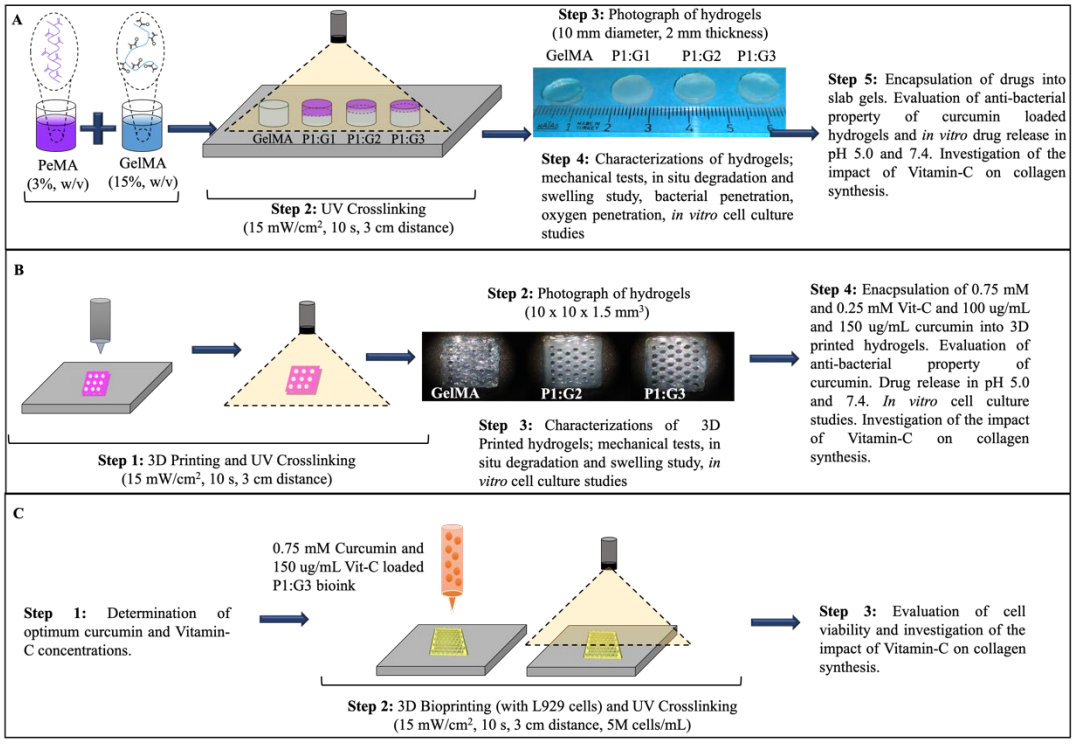

Figure 1.7 An illustration of the experimental steps of this thesis study. Part 1 involves polymer synthesis, slab gel production, drug loading and characterization (A). Part 2 involves the production of 3D printed hydrogels and the characterizations, drug encapsulation and analyses. Part 3 involves the fabrication of 3D bioprinted hydrogels and their characterizations.

CHAPTER 2

MATERIALS AND METHODS

2.1 Materials

Porcine skin gelatin type A (100 bloom), methacrylic anhydride (MA), 2-hydroxy-1-(4-(hydrox-yethoxy)phenyl)-2-methyl-1-propanone (Irgacure 2959) and Curcumin from Curcumin longa (Turmeric) powder were provided from Sigma-Aldrich (Germany). High methoxy pectin was provided from Benosen (Turkey). Trypsin/EDTA, Live-Dead cell viability/cytotoxicity kit, Alexa Fluor™ 488 phalloidin, dimethyl sulfoxide (DMSO) were purchased from Thermo Fisher Scientific (USA). Triton-X 100 was purchased from PanReac Applichem (Germany). Fetal bovine serum (FBS) was obtained from Biowest (France). Alamar Blue cell proliferation assay solution was purchased from Invitrogen Inc. (USA). Dulbecco's Modified Eagle Medium (DMEM) High glucose (glucose concentration: 4.5 g/L) and L-glutamine (200 mM in 0.85% NaCl solution) were obtained from Lonza (Switzerland). Penicillin/streptomycin (100 U/mL-100 µg/mL), Direct Red 80 and L-Ascorbic Acid were the product of Fluka (Switzerland). Recombinant Anti-Collagen I antibody (ab138492) was obtained from ABCAM.

2.2 Methods

2.2.1 Synthesis of Methacrylated Gelatin (GelMA)

Synthesis of methacrylated gelatin was performed according to the protocol reported by Lee et al. (Lee et al. 2015). Briefly, 20% (w/v) gelatin (type A, 100b) was dissolved in carbonate buffer (0.25 M, pH 9.0) at 50ºC, then methacrylic anhydride was added into the gelatin solution as 2% (v/v) and mixed for 3h at 50ºC. The

reaction was ended when pH was adjusted to 7.4. The solution was filtered, dialyzed against distilled water (dH_2O) (SnakeSkin, ThermoFisher) at 40ºC for 1 day and stored at -80ºC until lyophilized.

2.2.2 Synthesis of Methacrylated Pectin (PeMA)

Methacrylated pectin was synthesized according to the protocol reported by Pereira et al. with some modifications (Pereira et al. 2018). Briefly, 1.5% (w/v) pectin was fully dissolved in PBS (0.1 M, pH 7.4) at room temperature (RT), then 15 fold excess of MA was added into the solution dropwise at 0.5 mL/min while pH was being adjusted to 8.0 by adding 5.0 M NaOH. After 24 h, the reaction was stopped by precipitating the mixture in cold acetone at +4ºC. The solution was filtered and methacrylated pectin was dried in the incubator at 37ºC overnight. Later, dried pectin was dissolved in dH_2O and dialyzed (12kDa dialysis bag, Sigma Aldrich) for a week, stored at at -80ºC overnight then lyophilized.

2.2.3 Proton Nuclear Magnetic Resonance Spectroscopy (^{1}H NMR) Analysis

^{1}H-NMR analyses were conducted to determine the degree of methacrylation (DMs) of GelMA and PeMA. Freeze dried GelMA and PeMA were dissolved separately in 500 µL d_2O (deuterium oxide) at a final concentration of 3% (w/v). GelMA was dissolved by incubating at 60ºC while PeMA dissolved at RT. After homogenously dissolved, the solutions were pipetted into NMR tubes and analyzed at RT. DM of each material was calculated via MestreNova NMR analysis program (version 6.0.2, Mestrelabs Research, SL, Spain) with the following equation:

$$\text{DM (\%)} = \left(\frac{Number\ of\ methacrylate\ groups}{Number\ of\ amine\ groups\ of\ unreacted\ polymer}\right) \text{x100 (Shin et al. 2012)} \quad (1)$$

2.2.4 Attenuated Total Reflectance Fourier Transform Infrared (ATR-FT-IR) Analysis

The chemical modifications of pectin and gelatin powders, lyophilized PeMA and GelMA were confirmed by ATR FT-IR (Frontier, Perkin Elmer, USA) analysis.

2.2.5 Preparation of PeMA/GelMA Blend Solutions

Hydrogel precursor solutions were prepared by dissolving 15% (w/v) GelMA and 3% (w/v) PeMA separately in PBS (0.1 M, pH 7.4) containing 0.5% (w/v) Irgacure 2959 as the photoinitiator. After the polymers were dissolved separately, different volume to volume ratios of PeMA and GelMA (1:1, 1:2, and 1:3, v/v) were prepared which were designated by P1:G1, P1:G2, and P1:G3, respectively. The obtained hydrogel solutions were used in the fabrication of slab gels and 3D printed scaffolds.

2.2.6 Rheological Analysis

The rheological behavior of the polymer solutions (GelMA, P1:G1, P1:G2, P1:G3) was investigated to determine the viscosity for 3D printability. Analyses were performed at METU Department of Food Engineering using a TA rheometer (AR 2000ex, Rheometer). Temperature sweep tests were carried out between 10 - 40°C with constant frequency at 1 Hz and strain rate 1%. The storage modulus (G') and loss modulus (G'') were obtained from temperature sweep tests (Yin et al. 2018). The viscosities of the solutions were assessed by frequency sweep test, after equilibrating the solutions for 15 min at 20°C and analyzing at shear rate from 0.1 to 100 s^{-1}.

2.2.7 Preparation of Slab Gels

Slab gels were prepared by pouring the hydrogel solutions into round poly (dimethylsiloxane) (PDMS) molds with 1 cm diameter and 1.5 mm height and then photo-crosslinked with application of UV light (OmniCure S2000 UV lamp, Lumen Dynamics, Canada) (365 nm, 15 W/cm^2, 3 cm distance) for 10 seconds. For mechanical (compression) tests, PDMS molds with 1 cm diameter and 4 mm height were used to obtain thicker gels.

2.2.8 Optimization of UV Exposure Time

In order to determine the optimal UV exposure time, 3D bioprinted GelMA samples (the preparation process is given in detail in Section 2.2.13.2.) were exposed to UV light for 5, 10, 15 and 20 seconds, separately. The cell viability in GelMA bioinks was studied via Live/Dead staining as described in Section 2.2.13.5.1. The optimal exposure time was chosen from the viability analysis and the gelation ability of the inks.

2.2.9 Preparation of 3D Printed Scaffolds

3D printed hydrogels were obtained with EnvisionTec 3D Bioplotter (Germany). In the same manner with slab gels, pure GelMA and PEMA:GelMA composite solutions were prepared by dissolving lyophilized materials in PBS (0.1 M, pH 7.4) containing 0.5% (w/v) Irgacure 2959. Later, the solutions were poured into the syringe and placed onto the cartridge of the 3D printer. The hydrogels were printed in a defined square shape with the dimensions 10 x 10 x 1.5 mm^3 in 10 layers via 25G gauge (250 µm) along with honeycomb pore patterns (Figure 2.1). The parameters for printing of each hydrogel types are given in Table 2.1. The illustration of the 3D printed hydrogels is presented in Figure 2.2. For mechanical (compression) testing, 30 layers were printed with a volume of 10 x 10 x 4.5 mm^3. After the printing

was completed, hydrogels were photo-crosslinked under OmniCure S2000 UV lamp (Lumen Dynamics, Canada) (365 nm, 15 W/cm^2, 3 cm distance) for 10 seconds.

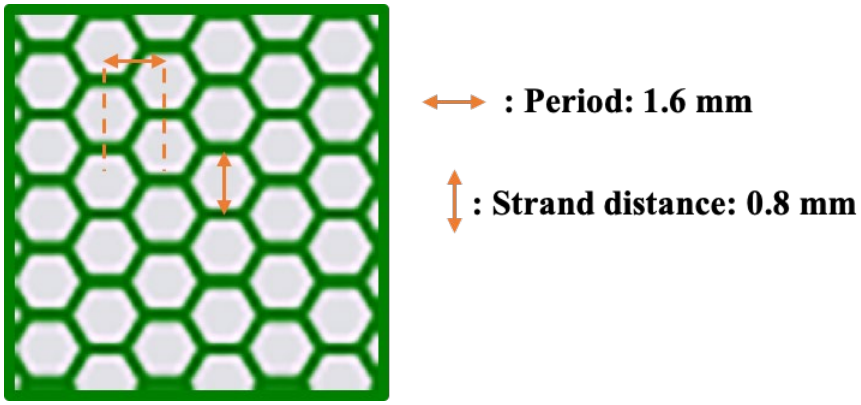

Figure 2.1 Illustration of extrusion based 3D printed honey comb pore patterned hydrogels. Distance between strands were set as 0.8 mm, period was set as 1.6 mm and 250 µm gauge was used for 3D printing.

Table 2.1 3D printing parameters of the hydrogels.

Sample	**RT (°C)**	**Pre/Post flow (mm/s)**	**Pressure (bar)**	**Flow rate (mm/s)**
GelMA	21	Pre: 0.05	1.6	8
P1:G2	21	Pre: 0.05	1.5	8
P1:G3	21	Pre: 0.05	2.0	8

2.2.10 Physical and Chemical Characterization of Slab Gels and 3D Printed Hydrogel Scaffolds

2.2.10.1 Scanning Electron Microscopy (SEM) Analyses

The morphology of the pure and composite slab gels and 3D printed hydrogels were investigated with Scanning Electron Microscopy (SEC, NanoEye, South Korea) at Middle East Technical University – Center of Excellence in Biomaterials and Tissue Engineering (METU BIOMATEN). Prior to SEM, the hydrogels were washed with distilled water and lyophilized. The scaffolds obtained were coated with gold before analysis. Average pore sizes of the hydrogels were determined from the micrographs using NIH ImageJ software.

2.2.10.2 Mechanical Analyses

Mechanical properties of 3D printed hydrogels with dimensions 10 x 10 x 4.5 mm^3, were analyzed with a Mechanical Tester (Shimadzu AGS-X Universal Test Machine, Japan) at METU BIOMATEN while the mechanical properties of slab gels were investigated with a Mechanical Tester (CellScale Univert, Canada) at METU-TAF Modeling and Simulation Research&Development Center (Modsimmer). The compressive speed was set at 1 mm/min. Before mechanical testing, all hydrogels were immersed in PBS (0.1 M, pH 7.4) for 24 h. The compressive modulus of the hydrogels was calculated from the slope of linear region in the 0-10% strain of the stress-strain curve (Tytgat et al. 2019).

2.2.10.3 *In Situ* Degradation Profile

The stability of photo-crosslinked hydrogel formulations was determined by the difference of weight before and after incubating in PBS. The gels were incubated in PBS (0.1 M, pH 7.4) for 21 days at 37°C and under 5% CO_2 atmosphere. At

predetermined time points (1, 3, 7, 14, 21 days), the scaffolds were taken out, washed with distilled water three times, frozen at -80°C overnight, then lyophilized and weighed. The weight remained of hydrogels was calculated by using the following equation:

Weight remained (%) = $(1 - \frac{wi-wt}{wi})$x100 (Saraiva et al. 2015) (2)

w_i and w_t correspond to the initial weight at day zero and the weight at predetermined time points, respectively.

2.2.10.4 Equilibrium Water Content of Hydrogels

The water retention capacity of hydrogels was assessed. For this purpose, the hydrogels were immersed in 2 mL of dH_2O and incubated at 37°C, under 5% CO_2 atmosphere. At predetermined time points, the hydrogels were taken out, extra water dropping from the surface was wiped out with a filter paper with extreme care, and the samples were weighed. The process was repeated until an equilibrium was reached. The water uptake profile was calculated by the equation given below:

Water uptake ratio (%) = $\left(\frac{ws-wd}{wd}\right) x100$ (Long et al. 2019) (3)

w_s corresponds to the weight of the swollen hydrogel while, w_d is the initial dry weight.

2.2.10.5 Oxygen Permeability of Slab Gels

Oxygen permeability was assessed via Winkler method, based on the protocol reported by McCormick (McCormick 1972). Briefly, the cap of a bottle containing dH_2O, was covered with freeze dried hydrogel (1.5 cm diameter, 3 mm height) to prevent the passage of air. The setup was placed onto the stirrer and media were left mixing for 24 h at room temperature. After one day, 100 µL manganese (ii) sulfate monohydrate solution (0.22 M) was added into water to fix oxygen present in water.

Later, 50 µL basic iodide solution of NaOH (0.06 M) was added and brown colored precipitate of manganese hydroxide was formed. This process was followed by the addition of 20 µL 97% sulfuric acid which dissolves the precipitates. Then sodium thiosulfate (00375 M, $Na_2S_2O_3$) was added dropwise to to titrate the yellow colored solution until a clear color was obtained. The added volume of $Na_2S_2O_3$ was recorded for the evaluation of the amount of oxygen. Finally, the endpoint was determined by adding starch into the water.

The stoichiometric equations of the reaction are given below:

$Mn^{+2} + 2OH^- \rightarrow Mn(OH)_2$

$2Mn(OH)_2 + 1/2O_2 + H_2O \rightarrow 2MnO(OH)_2$

$2Mn(OH)_3 + 2I^- + 6H^+ \rightarrow 2Mn^{+2} + I_2 + 6H_2O$

$I^{2+} + I^- \leftrightarrow I^{-3}$

$I^{3-} + 2S_2O_3^{-2} \rightarrow 3I^- + S_4O_6^{-2}$

The amount of oxygen was calculated according to the added volume of sodium thiosulfate. From the reaction, the mole of dissolved Na_2S_2O is found 4 times higher than the oxygen. The unit of the present oxygen will be given as mg per liter (McCormick 1972).

Oxygen permeability tests were performed on slab gels of GelMA, P1:G1, P1:G2 and P1:G3. Negative control was the bottle with closed lid and positive control was set as an open bottle. For each group, test was performed in triplicates.

2.2.10.6 Water Contact Angle Measurements of Slab Gels

Water contact angle study was performed to assess the wettability of the surfaces of pure and composite hydrogels. Contact angle measurements were obtained via a goniometer (Attension, Biolin Scientific, Sweden) by adding a 7 µL of water onto each hydrogel. The angle created on the surface of the hydrogel was measured. The tests were performed in triplicates.

2.2.11 Preparation of Drug Loaded Hydrogels and *In Vitro* Release Studies

2.2.11.1 Curcumin Loading and *In Vitro* Release

Two dosages were chosen from the dose dependent cytotoxicity study for curcumin which are given in detail in Section 2.2.13.1.

The determined concentration of curcumin (100 and 150 µg/mL of polymer solution) was added into Irgacure 2959 (0.5% w/v) containing PBS (0.1 M, pH 7.4) media in a beaker and mixed until to obtain a homogenous solution. Lyophilized polymer was added into the mixture, placed onto the tube heater (Stuart Scientific) at 60°C and heated until polymer was dissolved completely. The ink was either poured into the mold to prepare slabs, or into the syringe of the 3D printer and printed with the parameters given in Table 2.1, and photo-crosslinked by UV application.

Curcumin release from the 3D Printed hydrogels was studied in PBS (0.1 M) with two different pH (5.0 and 7.4). The, hydrogels were placed in well plates containing 2 mL of ethanol:PBS (1:9, v/v) (0.1 M, pH 7.4) and incubated in dark at 37°C in a shaking incubator with a shaking rate of 50 rpm (New Brunswick Scientific, Innova 4000, USA). Ethanol was added in order to provide a medium which enhances the release of curcumin since it's a highly hydrophobic agent. At predetermined time points (30 min, 1.5h, 3h, 1days, 8 days, 14 days), 2 mL of release medium was removed and replaced with fresh medium. The removed solution was frozen at -80°C and lyophilized. The curcumin in the eppendorfs was dissolved in ethanol and PBS (0.1 M, pH 7.4), (1:1, v/v), absorbance of the solution was measured at 425 nm with UV spectrophotometer (Bruker DPX 400 spectrometer). The amount of curcumin released from the hydrogels was determined using the calibration curve constructed with different concentrations of curcumin in ethanol:PBS (1:1, v/v), (0-10 µM) (Appendix A). The study was performed in triplicates.

2.2.11.2 Vitamin-C Loading and *In Vitro* Release

Optimal concentration of Vitamin-C (0.75 mM) was chosen from the dose dependent cytotoxicity study and loaded into the hydrogels. The method followed is given in detail in Section 2.2.13.2. Vitamin-C in powder form was added into Irgacure 2959 containing (PBS 0.1 M, pH 7.4) solution and vortexed at RT in dark. Lyophilized polymer was added into this solution at RT and dissolved completely. Then the solution was poured into syringe, loaded into the cartridge of the 3D printer. Scaffolds were obtained by using the parameters mentioned in Table 2.1. Vitamin-C release from the 3D printed hydrogels was assessed in PBS (0.1 M) at two different pH (5.0 and 7.4). However, it was observed that the photoinitator, Irgacure 2959, interacts with Vitamin-C immediately, and causes reduction in the absorbance values (Appendix B). Thus, the amount of released Vitamin-C could not be detected in PBS media. It was reported by Dilgin et al that the amount of Vitamin-C can be detected via a reduction reaction with methylene blue (MB). Briefly, MB reduced to leucomethylene blue in the presence of Vitamin-C. Moreover, increase in Vitamin-C concentration was reported to decrease both absorbance and fluorescence peaks of methylene blue (Dılgın and Nışlı 2003). To determine the amount of Vitamin-C released a calibration curve of Vitamin-C (5-100 μM) in 0.025 M MB in the presence of Igracure was prepared (Appendix C). Although a decrease in absorbance with increasing Vitamin C concentration, due to large deviations this calibration curve could not be used. Therefore, in this study the in vitro release of Vitamin-C could not be performed and only the impact of Vitamin-C on cells was assessed via collagen staining at different time points.

2.2.12 Anti-bacterial Studies

2.2.12.1 Bacterial Penetration

The penetration test was performed by the protocol reported by Ehterami et al (Ehterami et al. 2018). Briefly, 10 mL of nutrient broth was added into the sterile vials and each vial was covered with freeze dried hydrogels (15 mm diameter and 4 mm height). For negative control, vials were capped with their lids and for positive control open vials were used. The test was performed in triplicates. The blurriness of the broths was assessed by measuring absorbance at 600 nm using a microplate reader (µQuant, Biotek, USA).

2.2.12.2 Determination of Anti-Bacterial Activity

The impact of curcumin loaded 3D printed hydrogels are investigated on gram positive and gram negative bacterial with a zone of inhibition test. Overnight cultured colonies of *E.coli* ATCC 25922 and *S.aureus* ATCC 29213 in Luria Broth (LB broth) were adjusted to 0.5 McFarland turbidity standards (Ilhan et al. 2020). 100 µg/mL and 150 µg/mL curcumin containing slab gels, 3D printed hydrogels and unloaded hydrogels as controls were produced, and all hydrogels were sterilized under UV light (254 nm) for 15 min for each side. Later, hydrogels were placed on agar plates and incubated for 24 h at 37°C. Zones of inhibition around the hydrogels were measured and analyzed via NIH ImageJ software.

2.2.13 *In Vitro* Cell Culture Studies

2.2.13.1 Dose Dependent Cytotoxicity Study of Curcumin and Vitamin-C

In order to determine the optimal dosage of curcumin to be included in the slab and 3D printed hydrogels, the dose dependent cytotoxicity study was conducted using

different concentrations (from 0 to 14.7 µg/mL) of curcumin. L929 mice fibroblasts (P.26) were cultured in T-75 flasks in growth media which consists of DMEM high glucose, 1% (v/v) Pen-Strep and 10% (v/v) FBS. The growth media were changed in every 2 days and the fibroblast cells were incubated in a carbon dioxide incubator (MCO-5AC, Panasonic Corp., Japan) at 37°C with 5% CO_2. When cell confluency reached 80%, the cells were detached from the flasks by incubating in trypsin/EDTA (1X, 0.25% trypsin) for 5 minutes. Later, cell suspension was centrifuged for 5 min at 3000 rpm. The pellet was re-suspended with media, cell suspension of 200 µL containing 10.000 cells was seeded in each well of 96 well plates and left for 4 h for cells to adhere on the wells. Curcumin solutions were prepared in DMSO:DMEM High (1:10, v/v) mixture to obtain the final concentrations of curcumin as 1.84, 3.7, 5.5, 7.4 and 14.7 µg/mL. Curcumin solutions were added to each well without changing the final volume of the wells. The study was performed in five replicates for each concentration. After 24 and 48 h of incubation, cell viability in the curcumin containing wells and control group wells was assessed with Alamar Blue assay, at emission wavelength of 575 nm and excitation wavelength of 600 nm. Cell numbers were determined with previously obtained Alamar blue calibration curve given in Appendix D.

Dose Dependent Cytotoxicity was also performed for Vitamin-C. Since Vitamin-C is water soluble, it was dissolved only in DMEM and diluted to different concentrations as 0.1, 0.25, 0.50, 0.75, 1, and 5 mM. After 24 and 48 hours of incubation, the cell number in the presence of Vitamin-C included media and control groups (without Vitamin-C) was determined via the calibration curve constructed with different cell number ($2x10^3$, $5x10^3$, $7.5x10^4$, $1x10^4$, $1.5x10^4$, $2x10^4$ and $4x10^4$ per well).

2.2.13.2 Cell Seeding on Slab Gels and 3D Printed Hydrogels

For cell culture studies, the hydrogel precursor solutions were prepared as mentioned in Sections 2.2.7 and 2.2.9 however, instead of PBS (0.1 M, pH 7.4), DMEM was

used as the solvent. L929 fibroblasts were cultured in growth media which consists of DMEM high glucose, 1% (v/v) Pen-Strep and 10% (v/v) FBS. The growth media were changed every 2 days and the fibroblast cells were incubated in a humidified CO_2 incubator (37°C, 5% CO_2) until 80% confluency was reached. The hydrogels were placed on non-adhesive 12 well plates and seeded at a seeding density of $8x10^4$ cells/hydrogel for Alamar Blue assay and $3x10^4$ cells/hydrogel for Live/Dead analysis. The cells were allowed to attach on the surfaces for 4 hours in the carbon dioxide incubator. After 4 hours, 2 mL of media was added to each well and cells were incubated in a carbon dioxide incubator at 37°C.

2.2.13.3 Preparation of L929 Loaded 3D Bioprinted Hydrogels

For 3D cell encapsulation, confluent L929 cells in T-75 flasks were trypsinized and centrifuged. The pellet was re-suspended in media then suspension with cell density of $3x10^6$ cells were centrifuged. Polymer solution in DMEM was poured into cell pellet and suspended. The suspension was transferred to sterile syringes and 3D bioprinted at parameters given below in Table 2.2.

Table 2.2 3D bioprinting parameters of the hydrogels.

Sample	RT (°C)	Pre/Post flow (mm/s)	Pressure (bar)	Flow rate (mm/s)
GelMA	21	Pre: 0.05	2.2	8
P1:G2	21	Pre: 0.05	2.0	8
P1:G3	21	Pre: 0.05	2.5	8

2.2.13.4 Determination of L929 Proliferation on Hydrogels

3D bioprinted hydrogels and cell seeded slabs, also 3D printed hydrogels and their controls used to determine the proliferation of L929 cells. Cell proliferation was

determined with Alamar Blue assay. At predetermined time points (on days 1, 3 and 7) all samples were washed with DMEM Colorless. Alamar Blue solution (89% DMEM high modified colorless, 10% Alamar Blue and 1% Pen/Strep) was added to each well and incubated for 1 h for cell seeded samples and 4 h for bioprinted samples in a humidified CO_2 incubator (37°C, 5% CO_2). 200 µL of each well were pipetted into 96 black-bottom well plates and analyzed at microplate reader at the wavelength of 575 nm. In order to determine the cell number using Alamar Blue assay, a calibration curve was prepared by seeding different amounts of cells as $2x10^3$, $5x10^3$, $7.5x10^4$, $1x10^4$, $1.5x10^4$, $2x10^4$ and $4x10^4$ cells per well (n=5). Fluoresence alamar blue assay was performed. Measurements were conducted at an emission wavelength of 575 nm and an excitation wavelength of 600 nm and the calibration curve was constructed from the readings (R^2=0.99) (Appendix D).

2.2.13.5 Microscopy Studies

2.2.13.5.1 Live/Dead Cell Viability/Cytotoxicity Assay

Viability of L929 cells was examined with Live/Dead staining. The dye was prepared from 2 µM Calcein AM and 0.5 µM Ethidium-homodimer in PBS (0.1 M, pH 7.4). At predetermined time points cell seeded slab gels (on days 1, 4 and 7), cell seeded 3D printed hydrogels and 3D bioprinted hydrogels (on days 1, 4, 7 and 14), were washed with PBS, immersed in staining solution in dark for 20 minutes then washed with PBS. Then, the hydrogels were investigated on confocal laser scanning microscope (CLSM) (Zeiss LSM 800, Germany). Live and dead cells were counted in these images (n=3) via NIH ImageJ software using the equation given below:

$$\% \text{ Live Cells} = \left(\frac{Number\ of\ live\ cells\ (green)}{Number\ of\ total\ cells\ (green+red)}\right)x100$$

2.2.13.5.2 DAPI/Phalloidin Staining

At final days of incubation (7 for slab and 14 for 3D printed gels), cells on the slab gels and 3D printed hydrogels which were initially seeded with $8x10^4$ cells, were fixed with the following procedure. First, samples were washed with PBS (0.1 M, pH 7.4) then incubated with 4% paraformaldehyde (PFA) solution for 15 min. After discarding the PFA solution, samples were washed twice with PBS (0.1 M, pH 7.4). For DAPI/Phalloidin staining, the hydrogels were firstly incubated in Triton X-100 (0.1%, v/v in 10 mM Tris-HCl buffer) for 5 min at RT followed by an incubation in BSA (1%, w/v in PBS) at 37°C for 30 minutes. Then, Alexafluor 488-Phalloidin was added into the wells and incubated at 37°C for 1 h. The excess dye was removed and samples were washed with PBS (0.1 M, pH 7.4). The samples were analyzed with confocal laser scanning microscope (CLSM) (Zeiss LSM 800, Germany).

2.2.13.5.3 Immunocytochemistry (ICC) Staining

In order to investigate the collagen deposited by L929 cells, collagen type I staining was performed on the hydrogels. Fixed hydrogels were incubated in 1% Triton X for 5 min (and 15 min for bioprinted samples) and washed with PBS twice. Then, samples were incubated with anti-blocking solution for 1 h in 37°C. After washing with PBS, the primary antibody, Collagen type I antibody solution was poured into each well and left overnight at +4°C. The following day, collagen type I antibody was removed and secondary antibody was added and incubated for 1 h in 37°C. Secondary antibody was removed then, AlexaFluor 488 Phalloidin staining was added and incubated for another hour at 37°C, after samples were washed with PBS, DAPI staining was added and incubated for 15 min at RT. Vitamin-C containing hydrogels after immunostaining were analyzed with confocal microscopy excited at 405, 488 and 561 nm for DAPI, Phalloidin and collagen I polyclonal antibody (AlexaFluor 555), respectively and the areas stained with pink indicate collagen

expression. Area of collagen positive staining to the total number of cells were calculated (Liu et al. 2018).

2.2.13.5.4 Sirius Red Staining

Sirius red staining was also performed to determine the impact of Vitamin-C loaded hydrogels on collagen synthesis of the fibroblasts. Briefly, the dye was prepared by dissolving Direct Red 80 (1.5% w/v) in picric acid solution. Then, the dye was added to the fixed cellsand incubated at RT for 1 h. The excess dye was removed and samples were washed with 0.1 M HCl three times until no dye was released (Onat et al. 2019). Vitamin-C loaded and unloaded 3D printed hydrogels seeded with $3x10^4$ cells were fixed with PFA by the previously mentioned method at days 1 and 7 (day 14 for 3D printed hydrogels). Hydrogel samples without Vitamin-C which were seeded with $3x10^4$ cells were used as the control. Stained hydrogels were analyzed under confocal microscopy excited at 488 and 561 nm and images from 3 different regions were taken. The bright red areas indicate collagens. The images were analyzed with NIH ImageJ software, and area of collagen expressed by the total number of cells were calculated.

2.2.14 Statistical Analyses

Unless specified otherwise, all tests were performed in triplicates. Statistical analyses were obtained via GraphPad Prism 8 (GraphPad, San Diego, USA). p values ≤ 0.05 were considered significant.

CHAPTER 3

RESULTS AND DISCUSSIONS

3.1 Degree of Methacrylation of PeMA and GelMA

Pectin and gelatin were methacrylated in order to have crosslinked hydrogel structures and the mechanisms of methacrylation and photocrosslinking are presented in Appendix E. Proton Nuclear Magnetic Resonance Spectroscopy (^{1}H NMR) analysis was applied to confirm the success of the methacrylation process as well as to calculate the degree of methacrylation (DM) of the polymers. The DM plays a crucial role in the properties of hydrogels such as the mechanical stability, water retention capacity and biocompatibility (Bencherif et al. 2008). ^{1}H-NMR spectra of PeMA and GelMA are presented in Figure 3.1. New peaks around ∂=1.8 ppm, 5.64 ppm and 6.05 ppm in Fig.3.1A come from methacrylate moieties and are in correlation with literature for other methacrylated polysaccharides (Shin, Olsen, and Khademhosseini 2012). For GelMA, peak at ∂=7.24 ppm is a characteristic peak coming from gelatin, and new peaks at 5.56 and 5.32 belong to hydrogens of methacrylic groups.

DM values were calculated as 32% for PeMA and 83% for GelMA. DM is dependent on the volume of methacrylic anhydride used in the reaction (Yihu Wang et al. 2018), and DM results in this study, are in parallel with literature. For instance, DMs of other methacrylated polysaccharides were reported as 24.5% for gellan gum (Shin, Olsen, and Khademhosseini 2012), 33% for chitosan (Saraiva et al. 2015), 37% for k-carrageenan (Mihaila et al. 2013), and 16.5% for pullulan (Bae et al. 2011). GelMA which is the most commonly used methacrylated polymer in tissue engineering applications and its reported DM values cover a wide range varying from 29 to 95% (Pepelanova et al. 2018). Meanwhile, Pereira et al. reported a comparative study of PeMA having a wide range of DMs from 21.7 - 56.6% (Pereira et al. 2018).

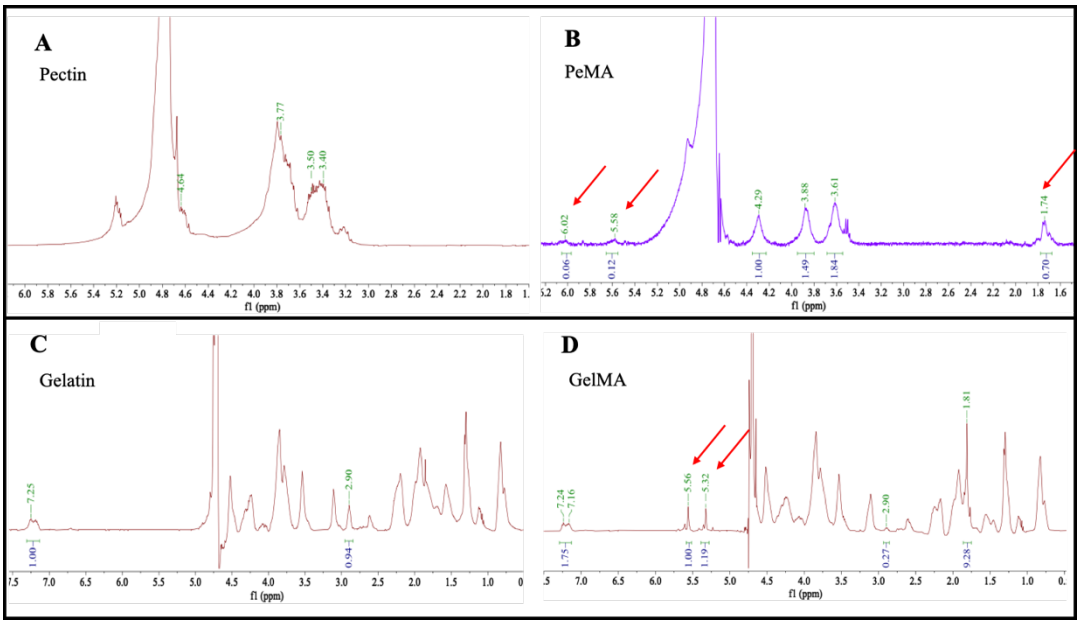

Figure 3.1 ^{1}H NMR spectra of pectin (A); PeMA (B); gelatin (C) and GelMA (D). Red arrows indicate new peaks coming from methacrylation.

3.2 Chemical Structures Obtained via Attenuated Total Reflectance Fourier Transform Infrared (ATR-FTIR) Analysis

ATR-FTIR was performed to analyze the absorption characteristics of PeMA and GelMA. The areas pointed in grey in Fig.3.2A indicate a region of 1724 cm^{-1} and 1629 cm^{-1} which correspond to pectin's C=O ester bond and increases with methacrylation. Coutinho et al. reported that this peak increases with the increased DM ratio on their methacrylated gellan gum (Coutinho et al. 2010). In addition, the shoulder peak around 1620 cm^{-1} shows C=C bond of pectin, again increased with methacrylation. The peaks at around 3200 - 3350 cm^{-1} indicate stretching of O-H bonds present in both pectin and PeMA (Chan et al. 2016).

Fig.3.2B presents ATR-FTIR spectum of gelatin and GelMA. Absorption at 2926 cm^{-1} stems from C-H stretching. Peak at 3243 cm^{-1} indicates N-H stretching, at 1620

cm^{-1} indicates C=C stretching, and at 1515 cm^{-1} indicates N-H bending of amide groups present in gelatin structure (Saraiva et al. 2015).

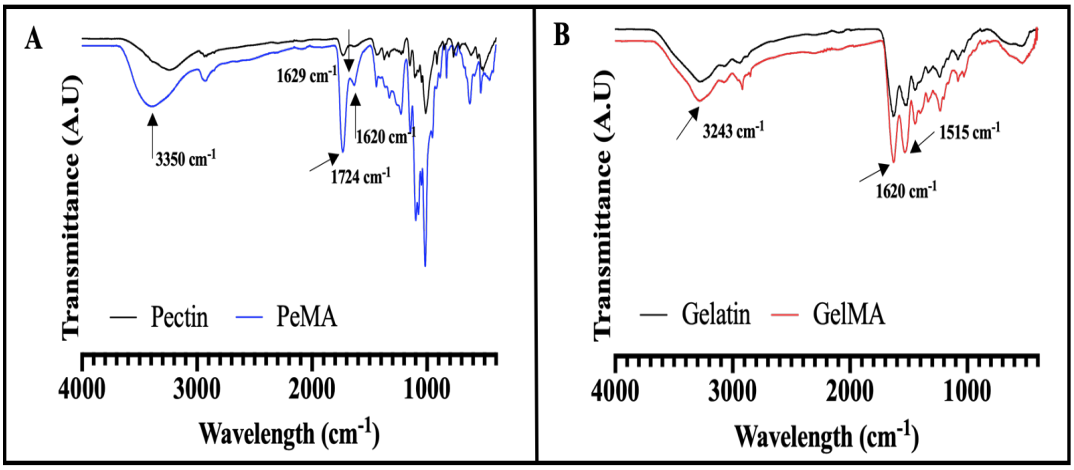

Figure 3.2 ATR-FT-IR spectra of pectin and methacrylated pectin (A), gelatin and methacrylated gelatin(B).

3.3 Effects of UV on Photocrosslinking of Hydrogels

Application of UV on the solutions containing methacrylated polymers and a photoinitiator cause crosslinking of the polymers. Extreme high UV dose may lead to hard structures while very low dose may not cause any solidification. On the other hand, UV effects the cells and high doses cause death of the cells. In this study, in order to determine the optimal UV exposure time, 0.5% (w/v) Irgacure 2959 was dissolved in DMEM media later 15% (w/v) GelMA was added. Meanwhile L929 cells (p.25) was trypsinized, counted, centrifuged and $100x10^4$ cells were added into the prepared GelMA solutions. UV was applied on these solutions for four different durations and GelMA was photocrosslinked. The viability of the cells encapsulated in GelMA hydrogels were analyzed via Live/Dead assay (Fig.3.3A) and the viability percentages were calculated via ImageJ software (Fig.3.3B).

From the images, cell viability percentages were found as 91 ± 3 %, 89 ± 3%, 80 ± 5% and 76 ± 3% for 5 s, 10 s, 15 s and 20 s UV application, respectively. Thus, it is observed that UV exposure was an important parameter for cell viability. L929 showed highest viability after 5 s UV exposure however, this time was not sufficient for the gelation of PeMA blended solutions. Therefore, 10 s UV application was chosen as optimum duration suitable for both; providing proper gelation for the polymers and high viability for the cells.

On the other hand, 15% (w/v) GelMA and 3% (w/v) PeMA solutions were prepared in PBS (0.1 M, pH 7.4) containing 0.5% (w/v) Irgacure 2959. The solutions were mixed in different volume ratios as 1:1, 1:2, 1:3 (v/v) in order to prepare P1:G1, P1:G2 and P1:G3 hydrogels, respectively. These viscous solutions were vibrated in ultrasonic bath (CPX1800H-E, Branson Ultrasonic Corp, USA) to remove the air bubbles. Later the homogenous solutions were poured into PDMS molds and photocrosslinked with application of UV for 10 s. The obtained GelMA gels were transparent, but the color of the PeMA containing ones changed towards to opaque whitish color depending on the amount of PeMA as seen in Fig.3.3C.

The inks for 3D printed hydrogels were prepared in the same manner as the slab gels in PBS solution containing 0.5% (w/v) Irgacure 2959. The printing parameters are given in Table 2.1. After the solutions were poured into syringes and placed onto cartridges, each ink was kept on hold for 30 min to reach the equilibrium temperature. 3D printing parameters were optimized and then GelMA, P1:G2 and P1:G3 inks were printed. It was observed that presence of PeMA improved the quality of printed samples by allowing shape fidelity. Honeycomb pore patterns were clearly visible in P1:G2 and P1:G3 compared to pure GelMA scaffolds (Fig.3.3D). Similar result was reported by Jia et al. where 3% (w/v) alginate promoted the printability of 7% (w/v) GelMA (Jia et al. 2016). The shape fidelity of PeMA containing groups may arise from the interactions of opposite charges formed between negatively charged pectin and positively charged gelatin. Although, P1:G2 and P1:G3 inks were successfully printed, it was not possible to obtain a 3D printed hydrogel from P1:G1 solution. The ink did not have proper viscosity ant it was highly

fluid that either clogged the nozzle which inhibited 3D printing, or exerted in high volumes so that it could not retain its printed honeycomb patterns. Therefore, even though characterizations were made for P1:G1 slab gels, in 3D printing P1:G1 bioink was not considered for further evaluation.

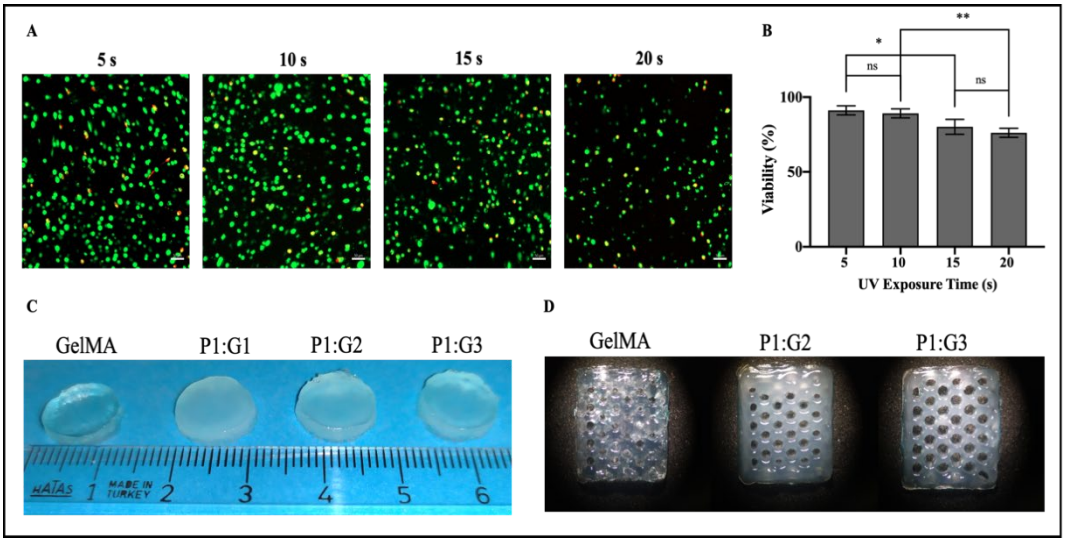

Figure 3.3 Optimization of UV exposure time for slab and 3D printed hydrogels. Live/Dead images of bioprinted GelMA hydrogels subjected to different UV times, from R to L, 5-10-15-20 s. Live cells are imaged green and stained with Calcein AM while dead cells are imaged red and stained with ethidium homodimer-1 (A). Viability percentages of L929 present in bioprinted GelMAs after different UV exposure (B). Photocrosslinked GelMA-P1:G1-P1:G2-P1:G3 slab gels (C). Photocrosslinked 3D printed GelMA-P1:G2-P1:G3 hydrogels (D). Statistical analysis was carried out using one-way ANOVA. *$p<0.1$, **$p < 0.01$ and ns: not-significant (n=3).

3.4 Rheological Properties of GelMA and PeMA Inks

PeMA and GelMA solutions were prepared by dissolving the components in different compositions in PBS without adding Irgacure 2959. The rheological properties of these inks were determined with rheology analyses. Fig.3.4 A-D display the divergence of shear storage (G') and loss moduli (G'') of polymer solutions with respect to temperature. At temperatures where loss modulus exceeding storage modulus (G''>G') the solutions show liquid behavior (Yin et al. 2018). Moreover, Fig.3.4E shows the viscosity of the solutions as a function of shear rate. It was observed that, addition of PeMA into GelMA reduced the viscosity of the blend solutions, especially in P1:G1. Nevertheless, P1:G2 and P1:G3 also GelMA, showed reduction in viscosity as the shear rate was increasing. This phenomenon is defined as shear-thinning behavior and is crucial for inks in 3D printing. Shear thinning behavior of inks prevent the possibility of clogging of solution through nozzle (Jia et al. 2016). The rheology analyses proved that P1:G1 solution is too fluid for 3D printing. Thus, P1:G1 composition was eliminated for further 3D printing studies.

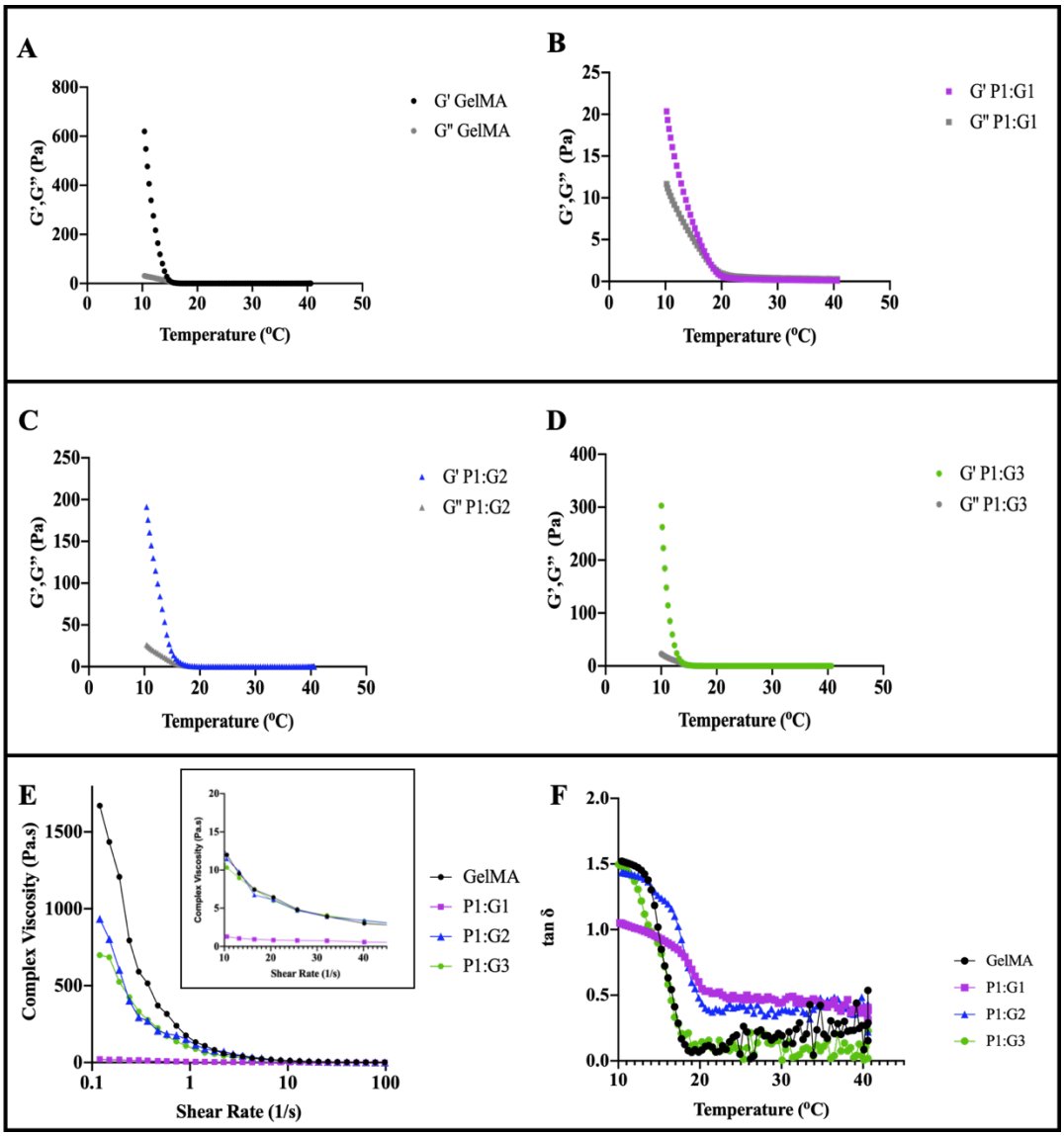

Figure 3.4 Rheology analyses of blend groups. Storage modulus (G') and loss modulus (G'') of GelMA (A), P1:G1 (B), P1:G2 (C) and P1:G3 (D). Complex viscosity of blend solutions as a fucntion of shear rate (E), tan∂ (∂=G''/G'), the value determines the elasticity of solutions (F).

The variation of viscoelastic loss tangent versus temperature is presented in Fig.3.4F. This graph is based on a protocol developed by Winter and Chambon. ∂ value consist of the ratio of G'' to G', and decrease in the gaps in tan∂ show that the material is

forming a gel and becoming elastic (Nordby et al. 2003). It can be seen that for GelMA and P1:G3 solutions, gelation starts around 19°C while it is between 20 to 22°C for P1:G1 and P1:G2.

3.5 Physical and Chemical Properties of Slab Gels and 3D Printed Hydrogel Scaffolds

3.5.1 Scanning Electron Microscopy (SEM) Results

It is important for tissue engineered scaffolds to have porous networks in order to promote oxygen and nutrient passage to cells and to eliminate wastes from tissues (Lin et al. 2018). Therefore, the microstructure of lyophilized hydrogel scaffolds was analyzed via SEM and the average pore sizes were measured from SEM images (Fig.3.5) via ImageJ software. It was found that the average pore sizes were 43.58 ± 5.6 µm, 31.43 ± 15 µm, 26.78 ± 4.8 µm and 26.30 ± 7.4 µm for P1:G1, P1:G2, P1:G3 and GelMA slab gels, respectively. It is observed that the pore sizes are increased as the ratio of PeMA increases. This is in correlation with other results in this study as water contact angle measurements, water uptake ratio and compression studies. P1:G1 slab gel has the highest pore sizes which was also the most hydrophilic gel among other blends. In parallel with the slab gels, Wang et al. reported that their pure GelMA hydrogels had the average pore size of 35 µm and addition of different ratios of dextran glycidyl methacrylate reduced the pore sizes to almost 20 µm. The slight difference between GelMA from the reported study and this study might be due to the difference in the protocol for GelMA synthesis. In that study, GelMA was derived from porcine gelatin as in this study however, 10% (w/v) gelatin was used in the preparation and GelMA content was 5% (w/v) in the study of H. Wang et al. (2014). Higher gelatin and GelMA content inthe slab gelsresulted in an increase in the fiber density thus, reduced the pore sizes. In addition, Pettinelli et al. compared the addition of the polysaccharides pectin and k-carrageenan sepereately in chitosan hydrogels. Similarly, they observed that the addition of polysaccharides increased

the pore sizes and wall thickness of the hydrogels compared to pure chitosan gels (Pettinelli et al. 2019). For 3D printed hydrogels, similar trend was observed. The average pore sizes measured were 31.4 ± 8.3 µm, 25.18 ± 9.6 µm and 22.2 ± 6.0 µm for P1:G2, P1:G3 and GelMA hydrogels, respectively. The difference between 3D printed and slab gels might have stemmed from higher fiber interaction occuring during 3D printing which also improved the *in situ* degradation times (Figure 3.7).

It was previously reported that pore size of 20 - 125 µm is required for the regeneration of adult mammalian skin in order to promote the transmission of sufficient nutrients and other low molecular weight substances (Pettinelli et al. 2019). As a result, the average pore size of both slab gels and 3D printed hydrogels was suitable for mammalian skin tissue regeneration.

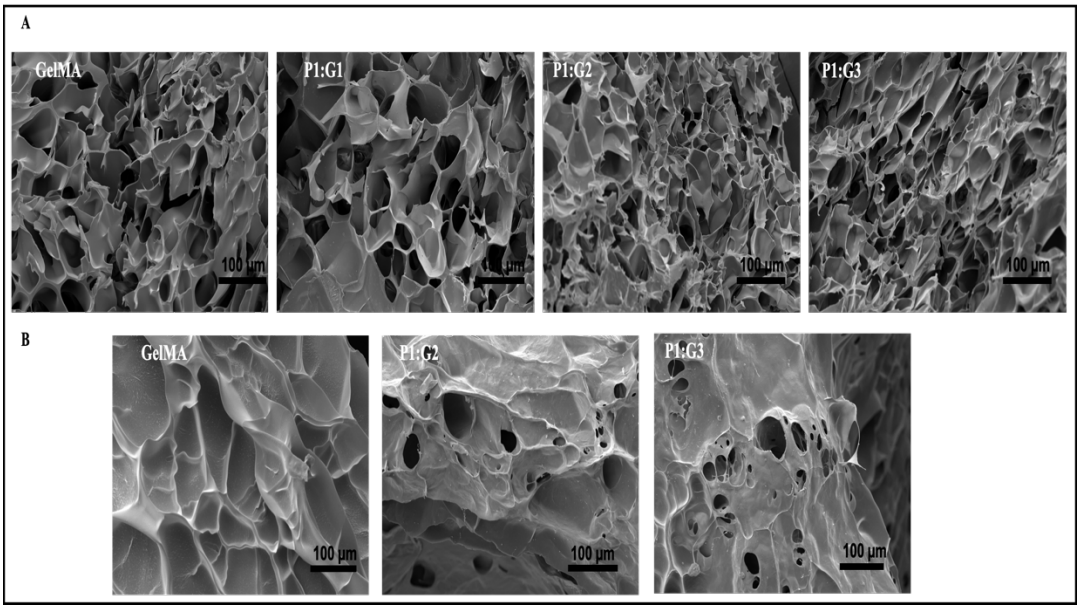

Figure 3.5 SEM images of slab gels (GelMA, P1:G1, P1:G2, P1:G3) A, and 3D printed hydrogels (GelMA, P1:G2, P1:G3) B.

3.5.2 Mechanical Properties of Hydrogels

Mechanical properties of both slab and 3D printed hydrogels were quantified via compression test. For slab gels, compressive moduli were found as 15 ± 3 kPa, 25 ± 5 kPa, 22 ± 3 kPa and 23 ± 6 kPa for P1:G1, P1:G2, P1:G3 and GelMA, respectively (Fig.3.6A). As it can be seen from the results, compressive moduli decrease as PeMA content increases. The mechanical analyses of the gels were performed after immersing them into PBS (0.1 M, pH 7.4) for 24 h. Thus, the difference in moduli among groups, especially between P1:G1 and GelMA, can be explained with the swelling properties and the pore sizes of the hydrogels. P1:G1 had the highest PeMA content and water uptake ratio (97 ± 1%), and these samples demonstrated the lowest modulus. Meanwhile, GelMA had the lowest water uptake ratio (92 ± 1%) and showed the highest compressive modulus as expected. However, it should be noted that there is no significant difference between P1:G2, P1:G3 and GelMA slab gels.

Compression tests were also performed for 3D printed hydrogels. As presented in Fig.3.6B. the compressive moduli were found for 1.7 ± 0.4 kPa, 2 ± 0.2 kPa and 2.1 ± 0.1 kPa for GelMA, P1:G2 and P1:G3 hydrogels, respectively. As in slab gel conjugates, there is no significant difference between groups. However, when compared with slab gel equivalents, 3D printed hydrogels demonstrated lower compressive modulus values. This could arise from the change in the area of the of the hydrogels. 3D printed hydrogels have multiple honeycomb pattern pores with sizes 0.8 mm and the area that the force was applied is reduced due to the pores.

On the other hand, the compressive moduli in this study were in correlation with the data of Tytgat et al. They performed compression tests on 3D printed GelMA and GelMA/methacrylated carrageenan hydrogels prepared in three different pore sizes. It was reported that higher pore sized hydrogels had lower moduli. Also, they reported that the pure GelMA hydrogel had the moduli varying from 1.2 to 2.2 kPa and the blend gels demonstrated 2.2 - 2.5 kPa (Tytgat et al. 2019).

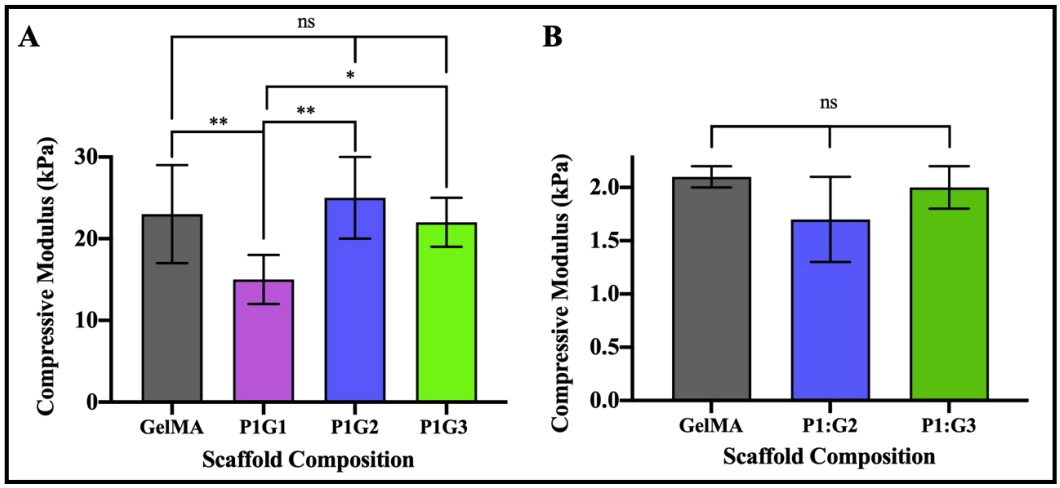

Figure 3.6 Compressive moduli of slab (A) and 3D printed (B) hydrogels. Statistical analysis was carried out using one-way ANOVA. $^{**}p < 0.01$ and ns: not-significant (n=5).

3.5.3 *In situ* Degradation Profile

Degradation profile of the hydrogels plays an important role in the regeneration of natural ECM especially for drug and/or cell encapsulated systems (Rice et al. 2006). It must be considered that the rate of degradation must meet the time required for new tissue formation. In addition, the biodegradation products must not be toxic for the cells. Therefore, degradation rate is an important criterion for scaffolds (Saraiva et al. 2015). Degradation studies were performed both on slab gels and 3D printed hydrogels by incubating the samples in PBS (0.1 M, pH 7.4) at 37ºC for 21 days. The results are presented in Fig.7.

P1:G1 slab gels dissolved fast and degradation completed in 21 days (Fig.3.7A). By the end of day 21, GelMA, P1:G2 and P1:G3 remained 22 ± 2%, 25 ± 3% and 37 ± 3% of their initial amounts, respectively. Among the three groups, P1:G2 was the only group which lost its shape. Parallel to the findings of this study, Zhao et al. used hydrogels prepared from solutions having different GelMA concentrations and investigated their degradation profiles. In their study, 15% GelMA lost 35 ± 4% of

its mass after 7 days of incubation. On the other hand, at the end of the three weeks of incubation period, 3D printed P1:G2, P1:G3 and GelMA, remained 29 ± 2, 60 ± 7% and 43 ± 5% of their initial amounts, respectively. When compared to slab gel conjugates, each 3D printed group showed better stability as well preserving their honeycomb shape. This might occur as a benefit of 3D printing, on providing non-discrete and organized fiber formation during exertion through the nozzle (Lim et al. 2021).

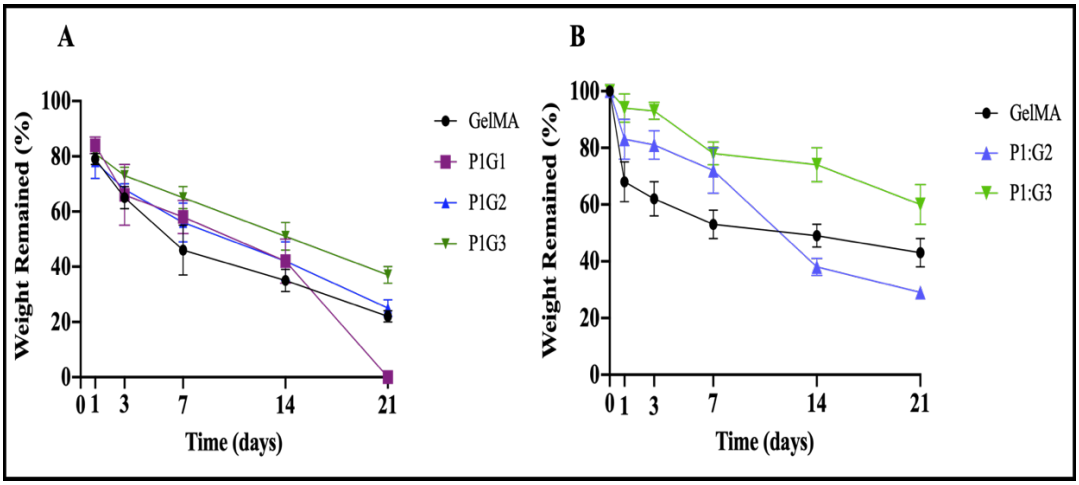

Figure 3.7 *In situ* degradation study performed on slab (A) and 3D printed (B) hydrogels for 21 days in PBS media (0.1 M, pH 7.4) at 37°C (n=3).

3.5.4 Equilibrium Water Contents of Hydrogels

A skin substitute must have sufficient water retention capacity in order to absorb the wound exudate and therefore to provide a proper healing (Abrigo, McArthur, and Kingshott 2014). Water retention property was determined on slab gels and 3D printed hydrogels by weighing at different time points. It was obtained that both hydrogel types have shown fast initial swelling and reached equilibria in about 3 h. As presented in Fig.3.8A, slab gels of GelMA, P1:G1, P1:G2 and P1:G3 had 92 ± 1%, 95 ± 1%, 94 ± 1%, 94 ± 1% water retention, respectively. Meanwhile, 3D printed

hydrogels had 91 ± 2%, 94 ± 1% and 94 ± 2% water retention for GelMA, P1:G2 and P1:G3, respectively. Results show that pectin contaning hydrogels have higher water absorption capacity. Meanwhile, pectin is already known for its high water holding property (Akhgari et al. 2010).

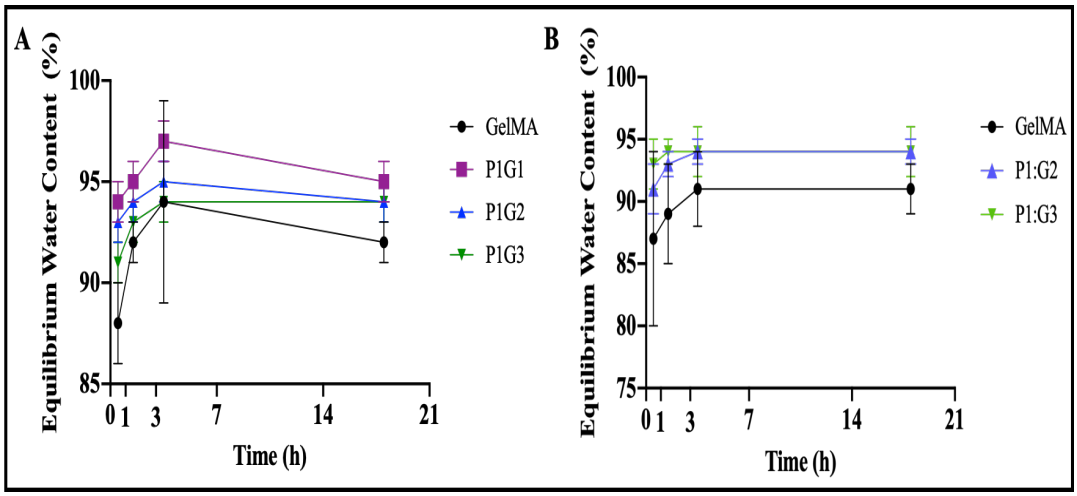

Figure 3.8 Equilibrium water content of slab gels (A) and 3D printed hydrogels (B) (n=3).

3.5.5 Oxygen Permeability of Slab Gels

An ideal skin substitute whether bioactive or not, should allow gaseous passage. Because, there are phases in wound healing as collagen synthesis that requires oxygen (B. Singh and Singh 2021). In this study, oxygen permeability was investigated via Winkler's method by calculating the amount of dissolved oxygen in water in a bottle which has a neck closed with freeze-dried slab gels. As given in Figure 3.9, the dissolved oxygen values were calculated as 7.89 ± 0.18, 7.62 ± 0.28, 7.44 ± 0.12 mg/mL and 7.47 ± 0.2 for, P1:G1, P1:G2, P1:G3 and GelMA, respectively. Meanwhile, for positive control (open flask) it was found 8.49 ± 0.07 mg/mL and negative control it was 6.49 ± 0.06 mg/mL. From these results, it can be concluded that the hydrogels allow the passage of sufficient amount of oxygen which

would contribute on wound healing. Parallel to the results of this study, Lu et al. used the Winkler method on the oxygen penetration of their chitosan based wound dressing. As a result, the oxygen amounts were calculated 8.77 ± 0.31 mg/mL for the hydrogel meanwhile, positive and negative controls were 9.26 ± 0.51 and 7.92 ± 0.35 mg/mL, respectively (Lu et al. 2010). The differences between the results of this study and theirs attributed to relative humidity and temperature of the environment.

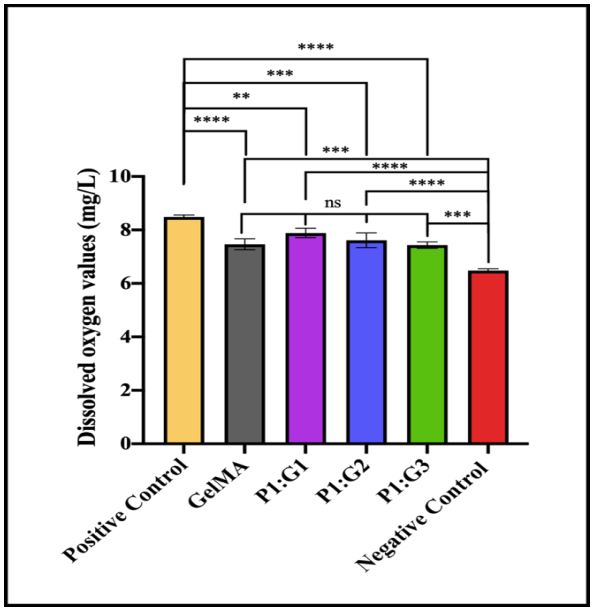

Figure 3.9 Oxygen permeability of slab hydrogels. Statistical analysis was carried out using one-way ANOVA. **$p < 0.01$, ***$p<0.001$, ****$p<0.0001$, and ns: not-significant (n=3).

3.5.6 Water Contact Angle Measurements of Slab Gels

Hydrophilicity is an essential property for wound dressing to allow the absorption of wound exudate (Xi et al. 2018). Thus, surface wettability of slab gels was analyzed with contact angle measurements. As given in Figure 3.10, water contact angles were found as 63° ± 8, 74° ± 3, 96° ± 8 and 91° ± 9 for P1:G1, P1:G2, P1:G3 and GelMA, respectively. It was reported that hydrocolloid dressings consist of polysaccharides

such as pectin are promising wound care materials prior to their high fluid absorption and creating moist environment (Andriotis et al. 2020). The results showed that increase in PeMA ratio in the hydrogel, resulted in a decrease in the contact angle and making the scaffold more hydrophilic. This is also in correlation with the water retention ability of hydrogels prepared in this study. PeMA included groups showed higher water absorption due to obtaining hydrophilic structure with the presence of pectin. Similar to the results in this study, Wang et al. reported that their GelMA hydrogel (prepared from 7% (w/v) GelMA solution) had WCA of 82° and when GelMA was incorporated with pure 1% (w/v) alginate WCA decreased to 60°. The group also reported the WCA value of pure alginate hydrogel which found less than 10° (G. Wang et al. 2019). Since, pectin and alginate are both polysaccharides and polyuronates that has similar chemical structure and gelation ability, this study confirms the water contact angle measurements of this study. It should also be noted that, even though there was a nonsignificant difference between P1:G3 and pure GelMA, for an optimal skin grafting procedure, including PeMA would be beneficial on accelerating healing due to its higher water uptake as presented in Fig.3.8.

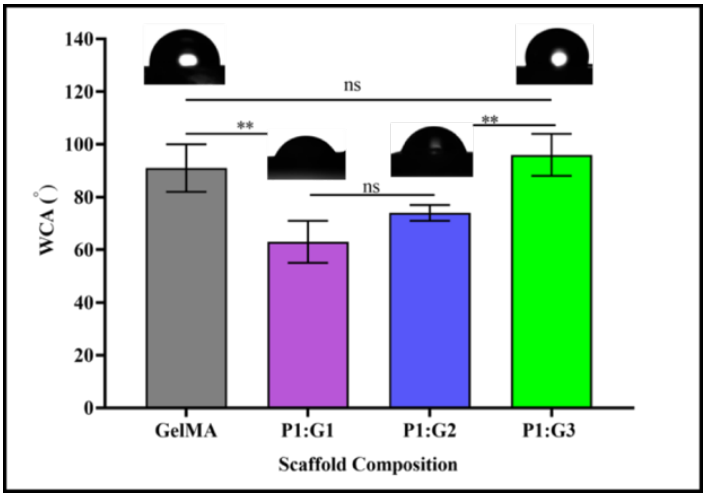

Figure 3.10 Water contact angle measurements of slab gels made from GelMA, P1:G1, P1:G2 and P1:G3. Statistical analysis was carried out using one-way ANOVA. **$p < 0.01$ and ns: not-significant (n=5).

3.5.7 *In Vitro* Curcumin Release Studies

The release studies of curcumin containing hydrogels were performed by immersing in ethanol:PBS (1:9, v/v) media (which was reported by Comotto et al. 2019) with two different pH (7.4 and 5.0) and incubating at 37°C. As shown in Fig.3.11, release studies were performed both in slab (A) and 3D printed hydrogels (B). It was found in general that, release from slab gels are faster than 3D printed hydrogels. This result confirms the *in situ* degradation study which 3D printed hydrogels were found a bit more stable.

Both hydrogel groups showed initial bursts at pH 7.4 for 3h then showed sustained release for 8 days. At 7.4, 3D printed hydrogel had released 5.24 ± 0.18% of the curcumin while, slab gel had released 8.12 ± 0.88% in 3 h. On the other hand, initial burst was lower at pH 5.0 as 0.49 ± 0.05% and 1.4 ± 0.03% for 3D prints and slab gels, respectively. This could occur due to two reasons. First, as Wang et al. reported in their study, curcumin has low solubility in acidic conditions thus release was slower at pH 5.0 (Wang et al. 2019). Secondly, both pectin and gelatin have carboxyl groups in their structure. Carboxyl groups are reported to ionize at pH above 7 thus, the hydrogels were expected to swell more in pH 7.4 and would provide faster release (Sookkasem et al. 2015). The results suggested that curcumin release was dependent on the pH of the media. Considering that the natural pH of the skin is acidic and around 5.5 - 6.0 and it increases in the cases of chronic wounds, the curcumin loaded hydrogels can provide a controlled release for the healing (Abrigo, McArthur, and Kingshott 2014). Parallel to the release results in this study, Yoon et al. reported similar release profile where around 50% cumulative release was observed in 7 days in PBS (pH 7.4) from their hydrogel consist of gylcol chitosan (Yoon et al. 2017).

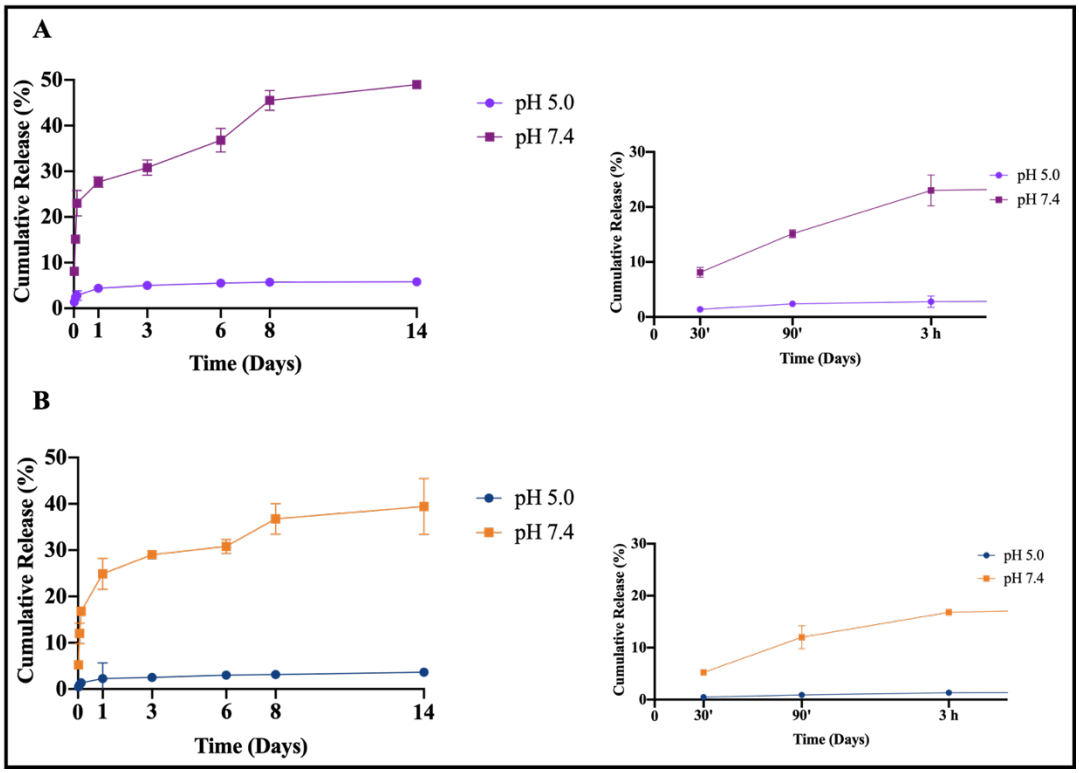

Figure 3.11 Curcumin release from slab gels in PBS pH 7.4 (fuschia), pH 5.0 (purple) (A), from 3D printed hydrogels in PBS pH 7.4 (orange) and pH 5.0 (dark green), (B). Close view of the release profile in the first 3 h is presented as an inset.

3.5.8 Antibacterial Studies

Chronic wounds are separated from acute wounds by having high risk of infections which prolongs the healing time and require medical assistance (Dart, Bhave, and Kingshott 2019). Therefore, it is important to prevent both the passage of microorganisms into the wound site and growth of pathogens around the wound. The two properties of the skin grafts were assessed on penetration and anti-growth assays.

3.5.8.1 Bacterial Penetration

Bacterial penetration assay was performed on the slab gels only, due to the visible large pores present on 3D printed hydrogels. As presented in Figure 3.12, although

slab gels did not include the anti-bacterial drug, curcumin, all groups have prevented contamination within the broth as much as negative control (glasses with caps on).

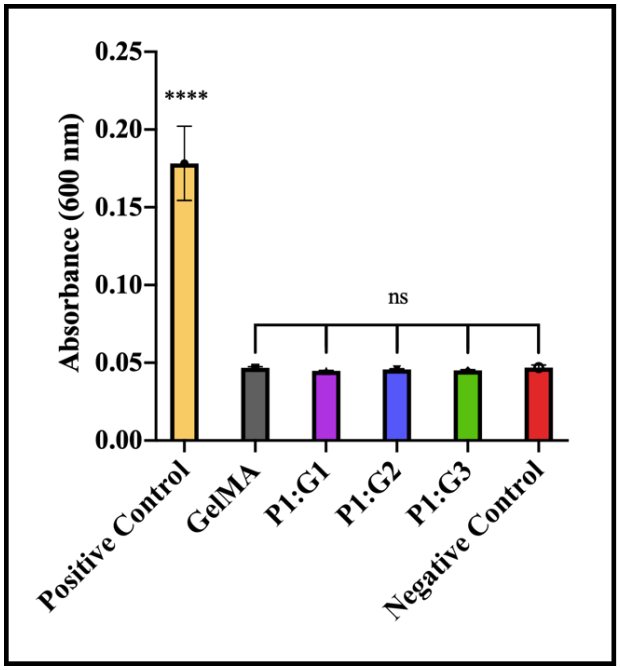

Figure 3.12 Bacterial penetration results of slab gels. The contamination in broth were analyzed after 5 days at 600 nm. Statistical analysis was carried out using one-way ANOVA. ****$p<0.0001$ and ns: not-significant. The tests were performed in triplicates.

3.5.8.2 Anti-Bacterial Activities of Curcumin Loaded Hydrogels

Curcumin was chosen to provide anti-bacterial property and added into the hydrogels. Therefore, the zones of inhibition analyses were performed on curcumin containing slabs and 3D printed hydrogels. The impact of curcumin was tested on Gram negative (*E.coli*) and Gram positive bacteria (*S.aureus*). After 24 h incubation, the photographs of the hydrogels were taken (Fig.3.13), and the zones were measured via ImageJ software. For *S.aureus,* diffusion zones were found as 0.63 ± 0.05 and 1.50 ± 0.27 mm for 3D printed and slab gels having 150 µg/mL curcumin,

respectively, and the difference was significant. For 3D printed and slab gels containing 100 µg/mL curcumin, these values were 0.30 ± 0.1 and 0.45 ± 0.2, respectively, and the difference was non-significant (Table 3.1). Slab gels showed higher zone areas than the 3D printed hydrogels having the same amount of curcumin in both concentrations. When compared with *in situ* degradation studies, 3D printed hydrogels had higher stability and shape fidelity than the slab gels. Therefore, curcumin release from slab gels was expected to be higher that resulted in zone larger than obtained for 3D print gels.

The minimum inhibitory concentration (MIC) values of *E.coli* and *S.aureus* were reported as 250 µg/mL and 150 µg/mL (Sandikci Altunatmaz et al. 2016) which equals to 678 µM and 407 µM, respectively. Similarly, Comotto et al. observed a zone on *S.aureus* of their hydrogel which contained 150 µg/mL curcumin. In their study, they have also tested 300 µg/mL of curcumin loaded hydrogel but it showed cytotoxic effects on human keratinoctyes (Comotto et al. 2019). In this study, it was observed that when the concentration of curcumin was higher than 150 µg/mL, curcumin prevented the penetration of UV light towards the inner parts of the polymers and therefore inhibited the gelation of slab gels (Appendix F). Tummalapalli et al. conducted disk diffusion study on their electrospun gelatin fibers. They immersed their fibers into 40% (w/v) curcumin solution which equals to 400 mg/mL in this study, that showed the success rate of 93% on inhibiting both strains. However, this concentration caused apoptosis in NIH 3T3 fibroblasts everyday for 3 days long incubation period. The untreated cells showed around 1400 relative fluorescence units (RFU) where cells treated with 40% (w/v) curcumin had around 800 RFU viability. Thus, the group added aloe vera into the fibers to minimize tha toxic effect of curcumin (Tummalapalli et al. 2016a).

Table 3.1. Inhibition zones of *S.aureus* incubated with 3D printed and slab gels having two different curcumin concentrations (n=3).

3D Printed Hydrogels		**Slab Gels**	
100 µg/mL	150 µg/mL	100 µg/mL	150 µg/mL
$0.3 \pm 0.1^{\#}$	$0.63 \pm 0.05^{***}$	$0.45 \pm 0.2^{\#}$	$1.5 \pm 0.27^{***}$

*** indicates statistical difference between the two groups ($p<0.001$).

# indicates no significant difference between the two groups.

Meanwhile, no visible zones were obtained on *E.coli*. This can be explained with Gram positive bacteria are more sensitive to curcumin than Gram negative (Shlar et al. 2017). Furthermore, considering that *S.aureus* is a common bacteria found in infected wounds and is a part of natural skin flora (Comotto et al. 2019), the impact of the hydrogels in this study, can present an effective wound dressing material or skin substitute material. Furthermore, for *in vivo* applications of the hydrogel skin substitute the concentration of curcumin will be increased.

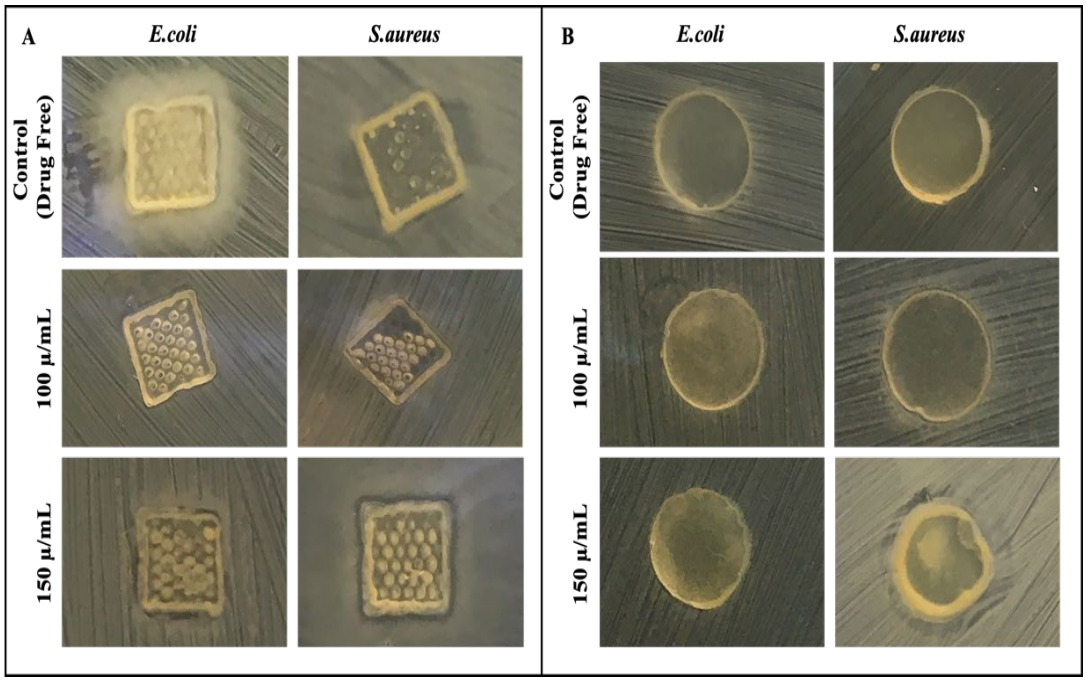

Figure 3.13 Disk diffusion images of 3D printed hydrogels (A) and slab gels (B) containing two curcumin dosages tested on *S.aureus* and *E.coli*.

3.5.9 *In vitro* Cell Culture Studies

3.5.9.1 Cell Proliferation on Slab Gels and 3D Printed Hydrogels

In literature, it was already reported that both pectin and gelatin were cytocompatible materials. However, methacrylated pectin and gelatin's impact on cell viability was assessed with Live/Dead analyses, alamar blue assay and DAPI/Phalloidin staining. For this purpose, the cytotoxicity tests first applied to the slab gels by 7 days of cultivation.

Fig.3.14A represents cell viability images of GelMA and P1:G1, P1:G2 and P1:G3 slab hydrogels and Fig.3.14B gives the percentage of live cells on slab gels analyzed with ImageJ software from Live/Dead images. The Alamar blue analysis (Fig.3.14C) showed that the hydrogels were cytocompatible by promoting cell proliferation. Nonetheless, it can be also clearly seen in Fig.3.14A that cell proliferation was

slower in P1:G1 than the other blend groups. This can be explained with the difference in surface wettability of hydrogels. From the swelling and water contact angle tests, it was obtained that among all groups P1:G1 showed the highest water absorption and also it was the softest hydrogel group which these properties effect the gels' cytocompatibility. A similar comparison was performed by Xu et al. on photocrosslinkable gellan gum hydrogels and modified methacrylated gellan gum hydrogels with higher gellan gum chains that made the gel slightly more hydrophobic. Briefly, the decrease in wettability which was observed with increase in water contact angle (37.3 ± 1.3 to 69.2 ± 2.3) had supported protein adsorption and cell adhesion (Xu et al. 2021). Thus, although the hydrogels are made from same polymers, a significant change in surface wettability, mechanical stability and water retention ability effected the overall biocompatibility of P1:G1 slab gel. Furthermore, it should be also stated that at day 7, proliferation of GelMA gel tends to decrease while P1:G3 gel shows superior cell viability.

Apart from cell quantification, cell morphology on empty slab gels was investigated with DAPI/Phalloidin staining (Fig 3.15). Even at day 1, L929 cells started to elongate and by day 7 cell elongation and proliferation increased with time indicating that the biomaterials were ideal for cell adhesion and cell growth. It should be also noted that cell elongation and migration were higher in P1:G2 and P1:G3 groups than GelMA group (indicated with red arrows in Fig.3.15). This was in parallel with study reported by Zhuang et al., where GelMA was combined with gellan gum and 3D printed scaffolds showed higher cell spreading in gellan gum and GelMA containing groups than pure GelMA hydrogel (Zhuang et al. 2019).

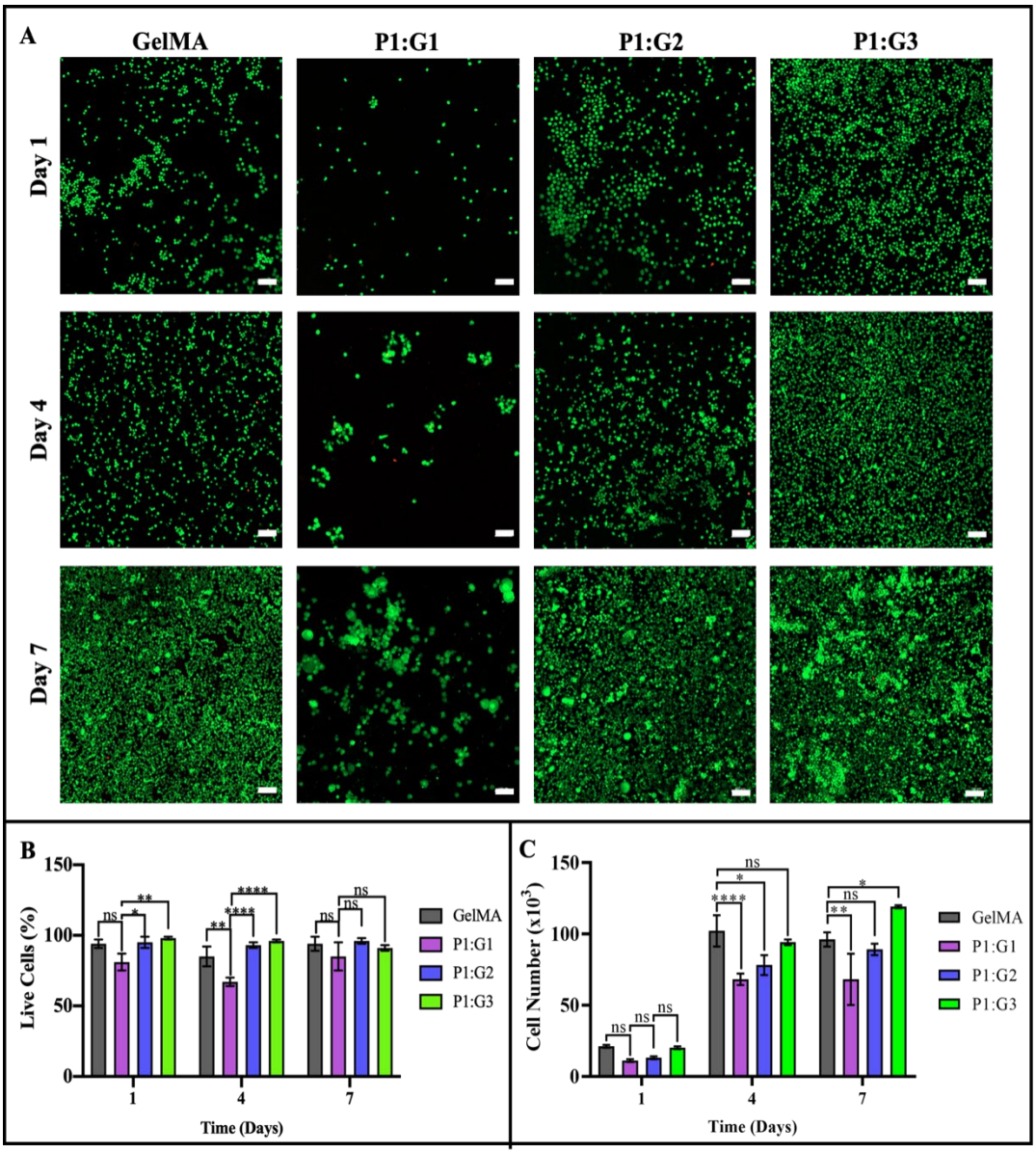

Figure 3.14 Confocal images of Live/Dead staining of cells seeded on slab gels at days 1, 4 and 7 (Green: Live, Red: Dead, Scale bar: 100 µm, initial seeding $3x10^4$ cells/hydrogel) (A), percent of live cells on gels obtained from Live/Dead images using ImageJ software (B). Alamar Blue viability results at days 1, 4 and 7. Statistical analysis was carried out using one-way ANOVA. *p<0.1, **p < 0.01, ****p<0.0001 and ns: not-significant. (C).

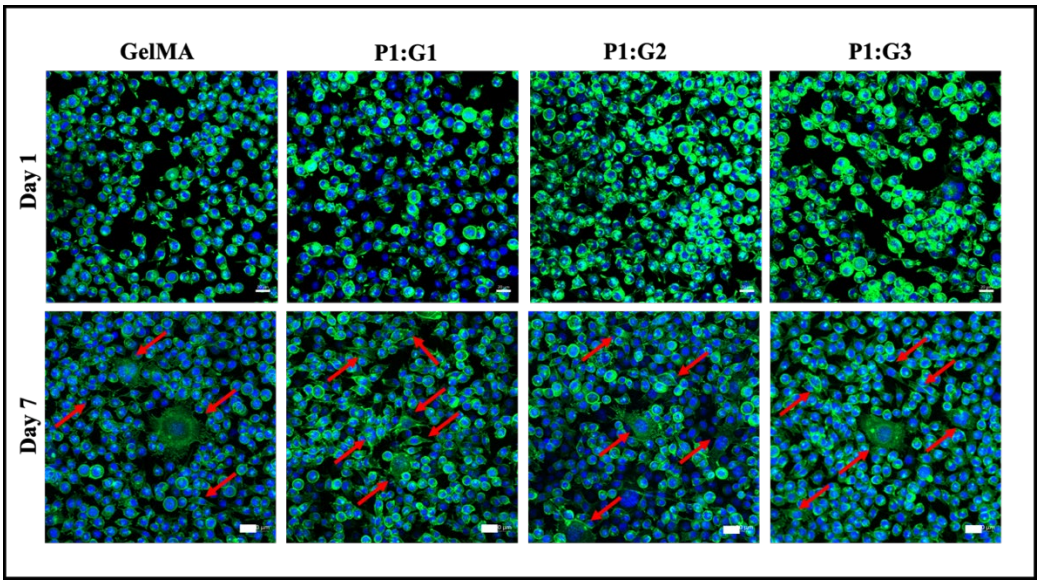

Figure 3.15 Confocal images of fibroblasts stained for nucleus (DAPI, blue in color) and cytoskeletal elements (phalloidin, green in color). Red arrows indicate cell elongation (scale bar: 20 µm).

Cell viability study conducted on slab gels showed that P1:G3 was superior than the other groups including the control, GelMA (Fig.3.14C). Therefore, for the rest of the study, P1:G3 was chosen for drug delivery, anti-bacterial properties and cellular activity studies. Fig.3.16A represents cell viability images of 3D printed P1:G3 and control GelMA hydrogels and in Fig.3.16B percent of live cells on gels obtained from Live/Dead images at different time points using ImageJ software is given. As seen in Fig 3.16A cells adhered and populated around the pores when seeded on 3D printed hydrogels. This might occur due to the roughness around the edges of the pores.

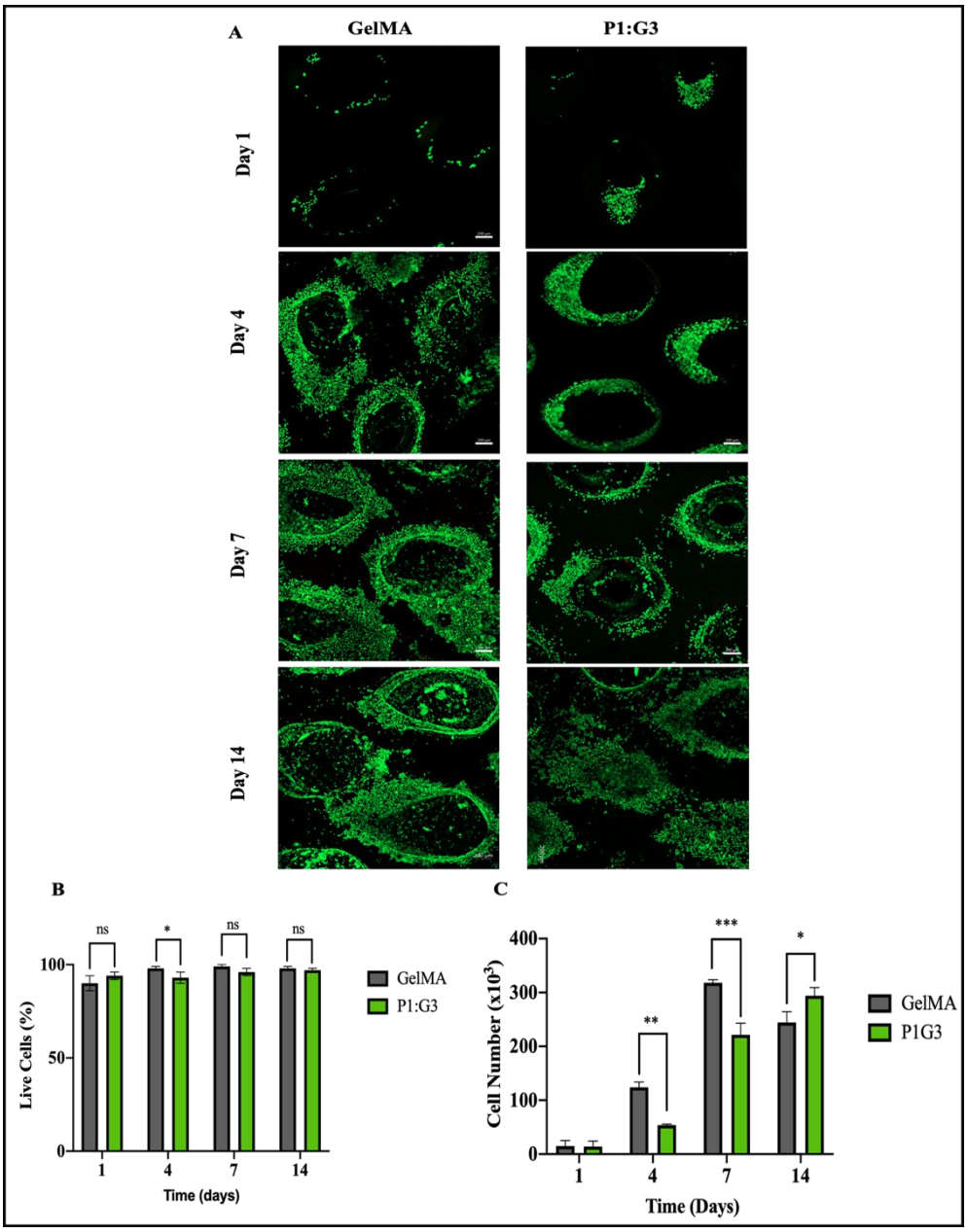

Figure 3.16 Confocal images of Live/Dead staining of cells seeded on 3D printed gels at days 1, 4, 7 and 14 (Green: Live, Red: Dead, Scale bar: 100 µm, initial seeding $3x10^4$/hydrogel) (A), percent of live cells on gels obtained from Live/Dead images using ImageJ software (B). Alamar Blue viability results at days 1, 4, 7 and 14. Statistical analysis was carried out using one-way ANOVA. *p<0.1, **p < 0.01, ***p<0.001 and ns: not-significant. (C).

3.5.9.2 Cell Proliferation on Curcumin and Vitamin-C Loaded Slab Gels and 3D Printed Hydrogels

In order to determine optimal drug concentration, the biocompatibility of curcumin and Vitamin-C loaded 3D printed and slab hydrogels were assessed, seperately.

3.5.9.2.1 L929 Proliferation on Curcumin Loaded Slab Gels and 3D Printed P1:G3 Hydrogels

Dose dependent cytotoxicity was conducted for curcumin (Appendix G). It was observed that above 3.7 µg/mL curcumin concentration, the cell viability decreased. However, MIC values of *E.coli* and *S.aureus* for curcumin are 250 µg/mL and 150 µg/mL, respectively. For the hydrogels to have antibacterial property, doses around MIC values should be loaded. Since curcumin has low solubility in aqueous media its release from the hydrogels would be slow. Therefore, new concentrations of 100 and 150 µg/mL of curcumin were chosen and encapsulated into 3D printed hydrogels and slab gels. The effect of curcumin on L929 fibroblast cell viability was compared with the viability observed in control group which did not contain curcumin. The Live/Dead images given for slab gels in Fig.3.17A and B and for 3D printed hydrogels in Fig.3.18A and B showed that both concentrations loaded in the hydrogels did not show any any cytotoxic effect based on percentage of live cells determined with ImageJ analysis. At day 7, cell proliferation observed via Alamar Blue assay in hydrogel groups (slab and 3D printed) loaded with 100 µg/mL curcumin and the control was similar, however, cell proliferation observed in hydrogel group loaded with 150 µg/mL was significantly lower than observed in the control group (Fig.3.17C and Fig.3.18C). As given in the previous sections, the primary aim in curcumin concentration was to choose an optimal concentration that would both show antibacterial property and not to inhibit cell proliferation. Yu et al. reported that curcumin concentration below 150 µg/mL supported MC3T3-E1 osteoblast proliferation on their photocrosslinked hydrogel consisting of

methacrylated hyaluronic acid, chitosan and silk fibroin (Yu et al. 2021). Therefore, for bioprinting and in vitro drug release studies 100 µg/mL curcumin concentration was chosen for loading of the hydrogels.

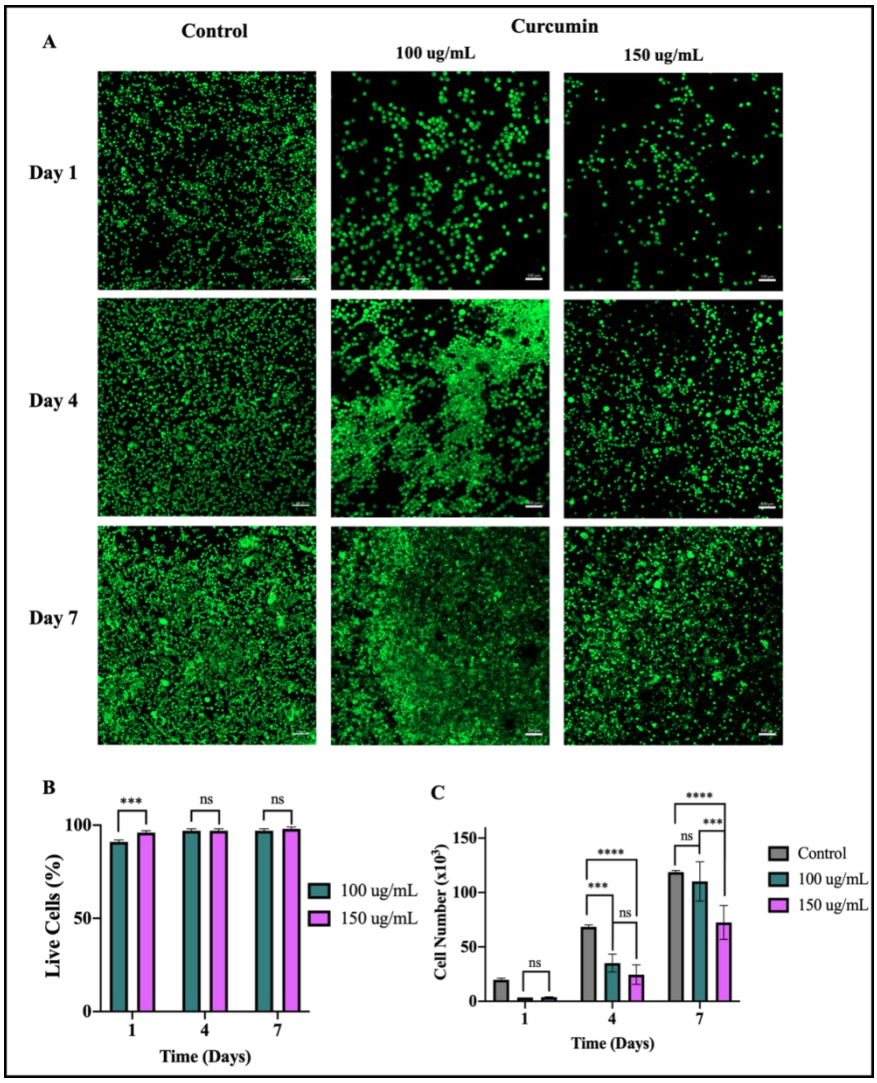

Figure 3.17 Confocal images of Live/Dead staining of unloaded (control), 100 µg/mL and 150 µg/mL curcumin loaded slab gels at days 1, 4 and 7 (Green: Live, Red: Dead, Scale bar: 100 µm, initial seeding $3x10^4$/hydrogel) (A), percent of live cells on gels obtained from Live/Dead images using ImageJ software (B). Alamar Blue viability results at days 1, 4 and 7 (C). Statistical analysis was carried out using one-way ANOVA. ***p<0.001, ****p<0,0001 and ns: not-significant.

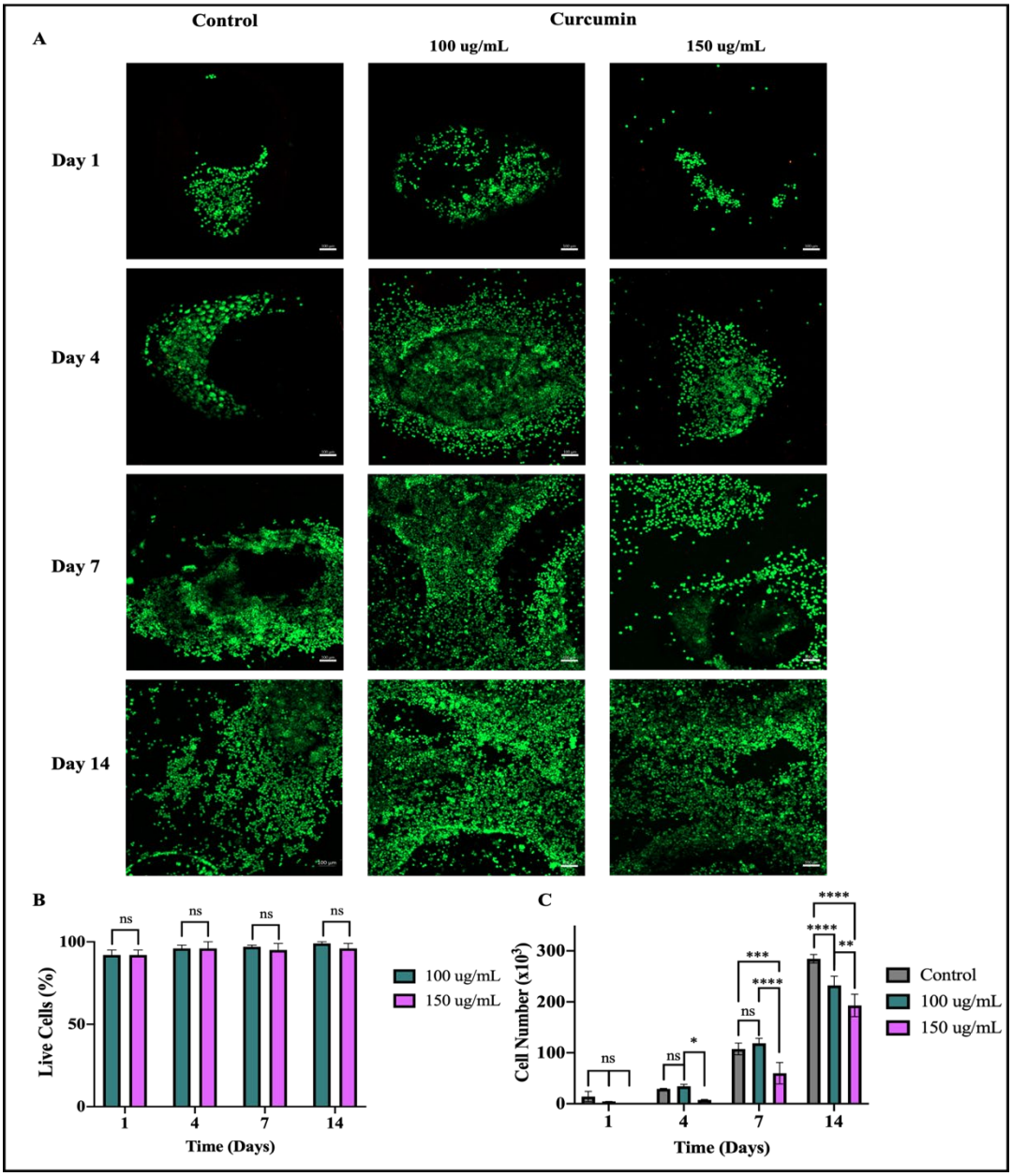

Figure 3.18 Confocal images of Live/Dead staining of unloaded (control), 100 µg/mL and 150 µg/mL curcumin loaded 3D printed hydrogels at days 1, 4, 7 and 14 (Green: Live, Red: Dead, Scale bar: 100 µm, initial seeding $3x10^4$ cells/hydrogel) (A), percent of live cells on gels obtained from Live/Dead images using ImageJ software (B). Alamar Blue viability results at days 1, 4, 7 and 14 (C). Statistical analysis was carried out using one-way ANOVA. *p<0.1, **p < 0.01, ***p<0.001 and ns: not-significant.

3.5.9.2.2 Proliferation of L929 Fibroblasts on Vitamin-C Loaded Slab Gels and 3D Printed P1:G3 Hydrogels

Effect of Vitamin-C on cells was examined apart of curcumin. Similar tests were carried out for Vitamin-C by using 0.25 mM and 0.75 mM. These amounts of Vitamin-C were encapsulated in slab and 3D printed hydrogels and the effect on cell proliferation was evaluated. From Live/Dead staining in Fig.3.19A and Fig.3.20A, the live cell percentages on hydrogels were above 80% and 90% for each day for slab gels and 3D printed hydrogels, respectively. However, for 0.25 mM Vitamin-C the difference between this group and control can clearly be seen especially at days 1 and 4. The difference was also observed in Alamar blue results (Fig.3.19C). Briefly, the concentrations of 0.25 mM and 0.75 mM were chosen from dose dependent cytotoxicity studies directly on L929 cells (Appendix G) where 0.25 mM was found more effective on cell proliferation while 0.75 mM was found cytotoxic. However, the impact was the opposite for loading these concentrations into hydrogels. We observed that absorbance of Vitamin-C decreased. This could have arosen from probable interaction of Vitamin-C with unreacted Irgacure 2959. Such interaction might have caused lower release from the gels and thereby the effect of Vitamin-C was lower. However, increasing Vitamin-C concentration to 0.75 mM has overcome this problem and we observed the positive effect at this higher concentarion. Therefore, for bioprinting application 0.75 mM was chosen. There is no study in the literature reporting that concentrations of Vitamin-C similar to 0.25 mM showing no impact or negative impact on cells. Vivcharenko et al. used 0.56 mM of Vitamin-C for their films because above this concentration they observed that cell viability decreased. However, at this concentration they did not observe a significant difference in cell proliferation between Vitamin-C included scaffolds and the control. The authors did not report an impact of Vitamin-C either on collagen synthesis or cell proliferation (Vivcharenko et al. 2020). On the other hand, Fan et al. reported the boosting effect of Vitamin-C loaded into their electrospun fibers.

They immersed the fibers into Vitamin-C of different concentrations (14 and 42 mM) for loading into the fibers (Fan et al. 2012).

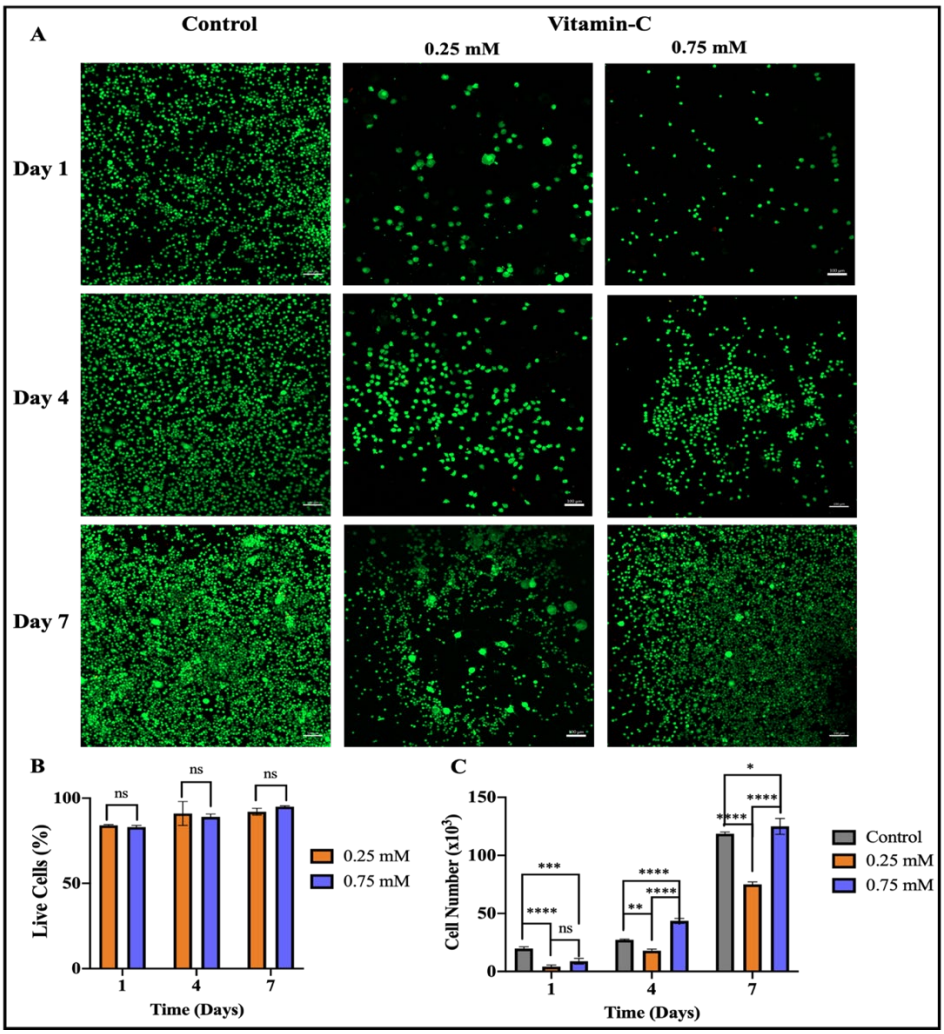

Figure 3.19 Confocal images of Live/Dead staining of unloaded (control), 0.25 mM and 0.75 mM Vitamin-C loaded slab gels at days 1, 4 and 7 (Green: Live, Red: Dead, Scale bar: 100 µm, initial seeding density: $3x10^4$/hydrogel) (A), percent of live cells on gels obtained from Live/Dead images using ImageJ software (B). Alamar Blue viability results at days 1, 4 and 7 (C). Statistical analysis was carried out using one-way ANOVA. *p<0.1, **p < 0.01, ***p<0.001, ****p<0.0001 and ns: not-significant.

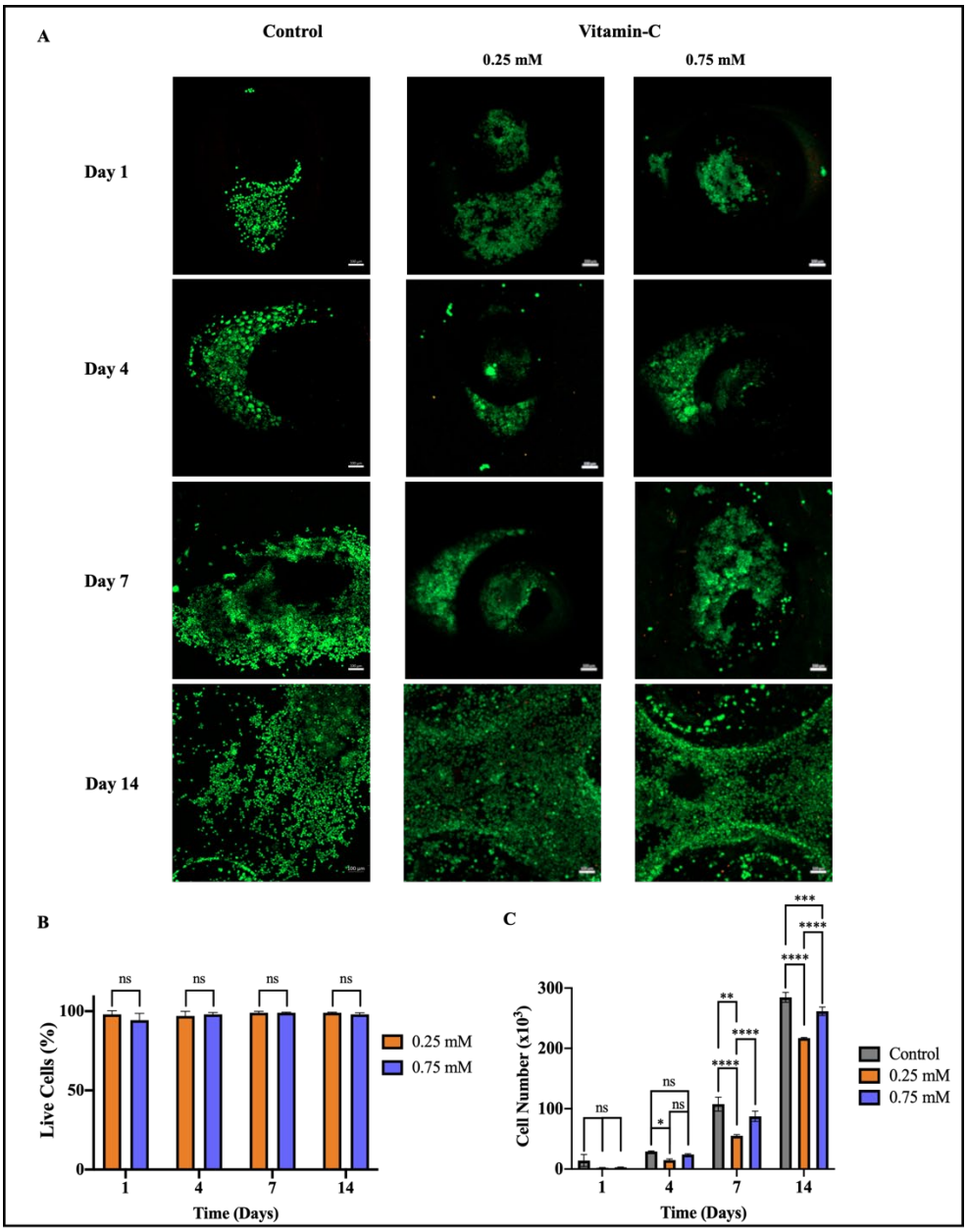

Figure 3.20 Confocal images of Live/Dead staining of unloaded (control), 0.25 mM and 0.75 mM Vitamin-C loaded 3D printed hydrogels at days 1, 4, 7 and 14 (Green: Live, Red: Dead, Scale bar: 100 µm, initial seeding density: $3x10^4$/hydrogel) (A), percent of live cells on gels obtained from Live/Dead images using ImageJ software (B). Alamar Blue viability results at days 1, 4, 7 and 14 (C). Statistical analysis was carried out using one-way ANOVA. *p<0.1, **p < 0.01, ***p<0.001, ****p<0.0001 and ns: not-significant.

3.5.9.2.3 L929 Proliferation on Curcumin and Vitamin-C Loaded 3D Bioprinted P1:G3 Hydrogels

In bioprinting experiments, 100 µg/mL curcumin and 0.75 mM Vitamin-C were chosen based on the tests explained in previous sections. Bioink solution containing $5x10^6$ cells/mL, 100 µg/mL curcumin and 0.75 mM Vitamin-C were prepared for fabrication of 3D bioprinted hydrogels. A control bioink that did not contain Vitamin-C and curcumin was used as control. From the confocal images given in Fig. 3.21, through the cultivation period, majority of the cells were viable. In fact, at day 14, the control had slightly less cells than curcumin and Vitamin-C containing bioink where the pores of the scaffolds were filled with L929 fibroblasts cells

The percent of live cells (Fig.3.21B) was found lower than on the cell seeded 3D printed hydrogels until day 4 and significant difference was observed with the control and Vitamin-C and curcumin loaded bioprints. This result could occur from two reasons: first, during 3D bioprinting, the polymer solution is objected to a pressure through the nozzle which has a negative on all cell types (Blaeser et al. 2016). Secondly, after bioprinting is completed, the hydrogel is subjected to UV light for 10 s. On the other hand, for 3D printed hydrogels, only the polymer is subjected to pressure and UV light, and after the formation of scaffolds the cells were seeded on them. Therefore, the viability percent of cells on those hydrogels was found to be higher. However, starting from day 7 to day 14, drug loaded samples did not show significant difference with control. Similar results were reported by Si et al. which developed a 3D bioprinted photocrosslinked hydrogel consisting of methacrylated hyaluronic acid and sodium hyaluronate using nafcillin as drug for wound dressing application. $3x10^6$ ml/ hDF cells were encapsulated and the viability was assessed for 7 days. It was found that at day 1, significantly lower cell viability was observed in the hydrogels than the control (gel without the drug). The authors explained this as a result of the pressure during 3D bioprinting and unreacted Irgacure 2959. Starting from day 4, drug loaded bioprints showed similar cell viability results as the control (Si et al. 2019).

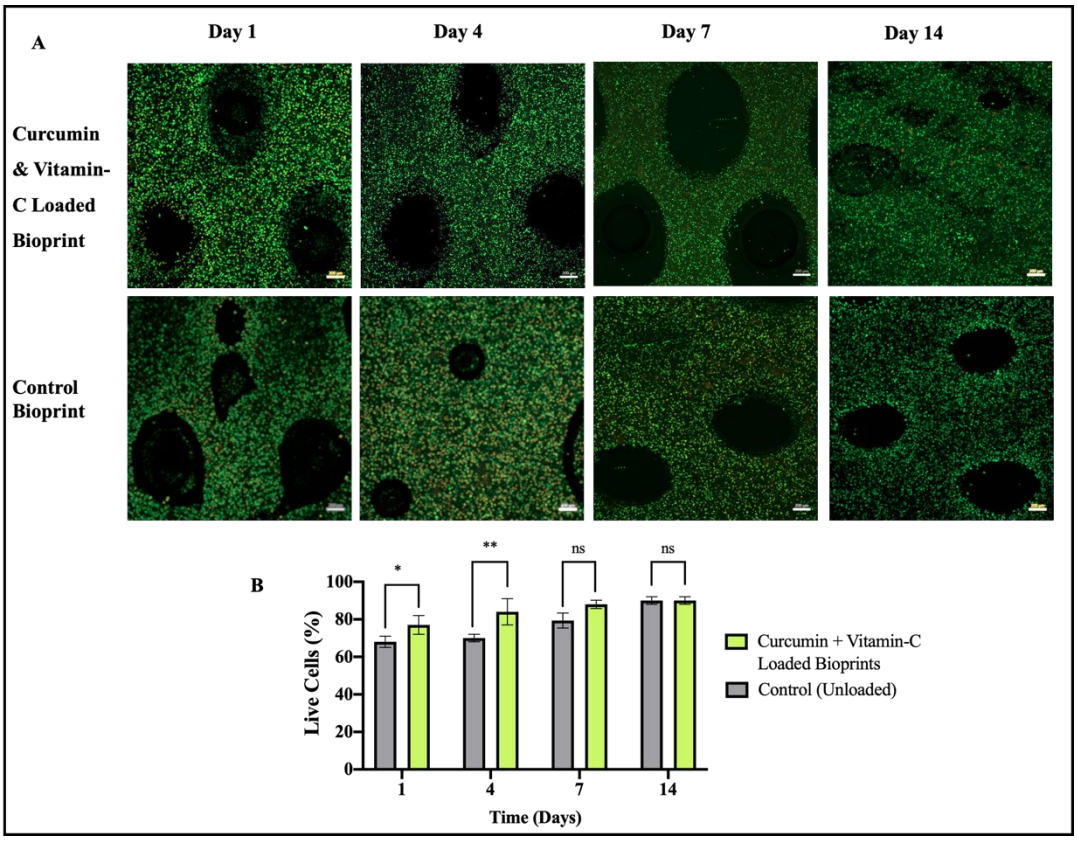

Figure 3.21 Confocal images of Live/Dead staining of unloaded (control), 0.75 mM Vitamin-C and 150 µg/mL curcumin loaded 3D bioprinted hydrogels at days 1, 4, 7 and 14 (Green: Live, Red: Dead, Scale bar: 200 µm, cell density in bioink; $5x10^6$ cells/mL) (A), percent of live cells on gels obtained from Live/Dead images using ImageJ software (B). Statistical analysis was carried out using one-way ANOVA. *$p<0.1$, **$p < 0.01$and ns: not-significant.

3.5.9.2.4 Analysis of Collagen Type I Deposition by Fibroblasts With Immunocytochemistry (ICC)

Vitamin-C was known to accelerate collagen synthesis (Peng et al. 2016) thus, immunostaining was performed at pre-determined time points on fixed samples in order to investigate collagen deposition by the cells. The ratio of collagen type I positive areas to number of nuclei stained with DAPI was calculated (Fig.3.22B, Fig

3.23B and Fig 3.24B). It can be seen that collagen type I deposition can be detected starting from day 7 for both slab and Vitamin-C containing hydrogels. Similar immunocytostaining study was performed by Pereira et al. on 3D printed pectin hydrogels where collagen deposition was observed for hNDF fibroblasts on day 14. Therefore, it can be said that addition of Vitamin-C accelerated the collagen synthesis for cells. Moreover, the collagen type I deposition was found significantly higher for fibroblasts seeded on slab and 3D printed hydrogels loaded with 0.25 mM and 0.75 mM Vitamin-C than control. For slab gels, at the end of day 7, there was no significant difference between two doses of Vitamin-C in terms of collagen type deposition however, for 3D printed hydrogels 0.75 mM Vitamin-C was found more efficient than 0.25 mM. In addition to collagen synthesis, Alamar Blue results showed that L929 viability was higher than 0.25 mM of Vitamin-C (Fig.3.19C, Fig3.20C), therefore, 0.75 mM Vitamin-C was chosen for bioprinting.

When compared to cell seeded hydrogel, bioprinted scaffolds showed limited staining. Although, the staining was procedure was repeated and the incubation period for DAPI and Phalloidin was prolonged, it was not helpful to obtain similar images as in cell seeded hydrogels. For this problem, there is no available literature however, it is foreseen that the opaque color of P1:G3 gaining an orange/red color due to curcumin inhibiting taking imagesof high quality with confocal microcopy.

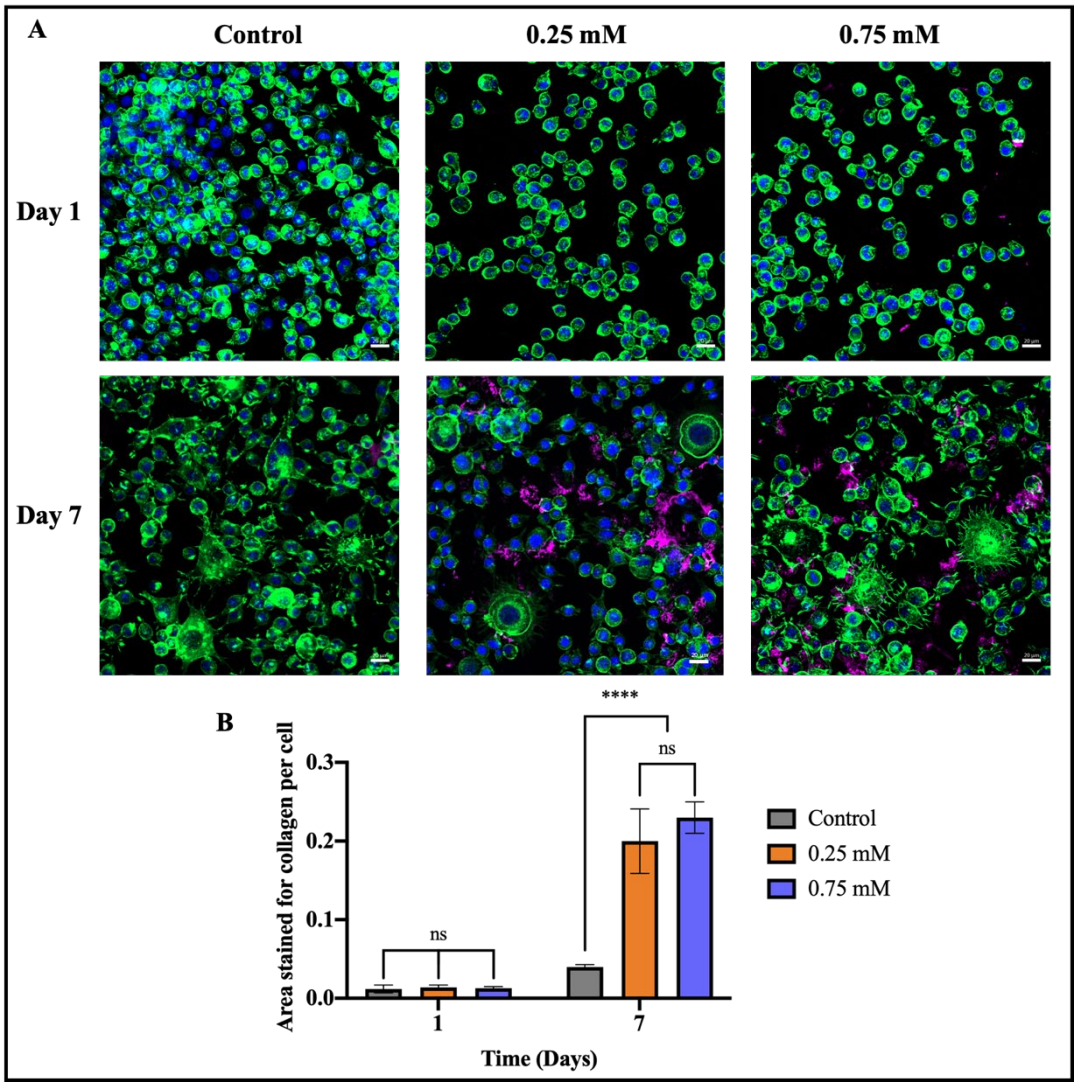

Figure 3.22 Confocal images of unloaded (control), 0.25 and 0.75 mM Vitamin-C loaded slab gels which were stained for collagen type I. (DAPI, blue in color, cytoskeletal elements stained with phalloidin, green in color and collagen type I stained in pink, Scale bar: 20 µm, initial seeding $3x10^4$/hydrogel), (A). Ratio of area stained for collagen type I to the total number of cells which was determined by DAPI staining of nuclei (B). Statistical analysis was carried out using one-way ANOVA., ****$p<0.0001$ and ns: not-significant.

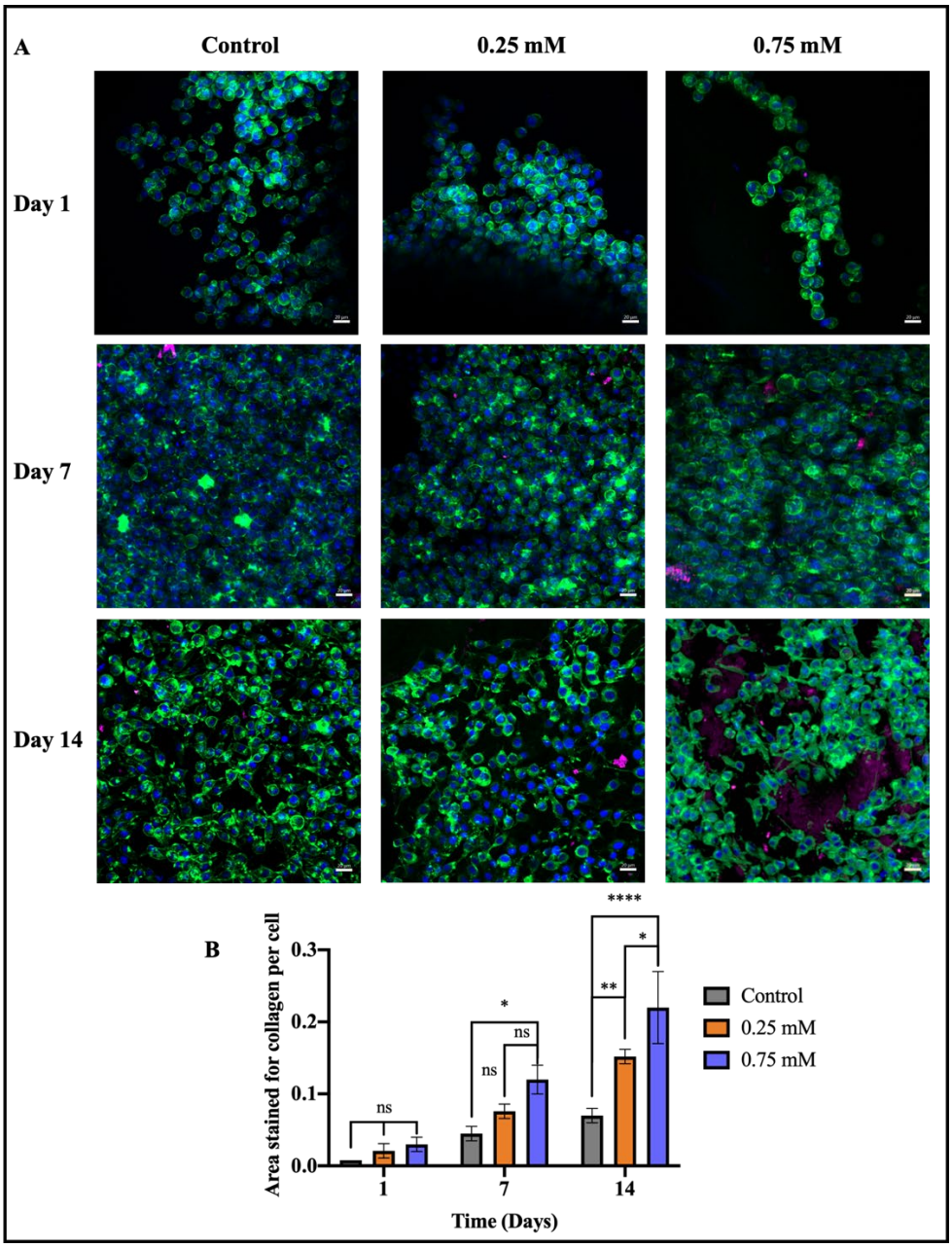

Figure 3.23 Confocal images of unloaded (control), 0.25 and 0.75 mM Vitamin-C loaded 3D printed hydrogels which were stained for collagen type I. (DAPI, blue in color, cytoskeletal elements stained with phalloidin, green in color and collagen type I stained in pink, Scale bar: 20 µm, initial seeding $3x10^4$/hydrogel), (A). Ratio of area stained for collagen type I to the total number of cells determined by DAPI staining of nuclei (B). Statistical analysis was carried out using one-way ANOVA. *p<0.1, **p < 0.01, ***p<0.001 and ns: not-significant.

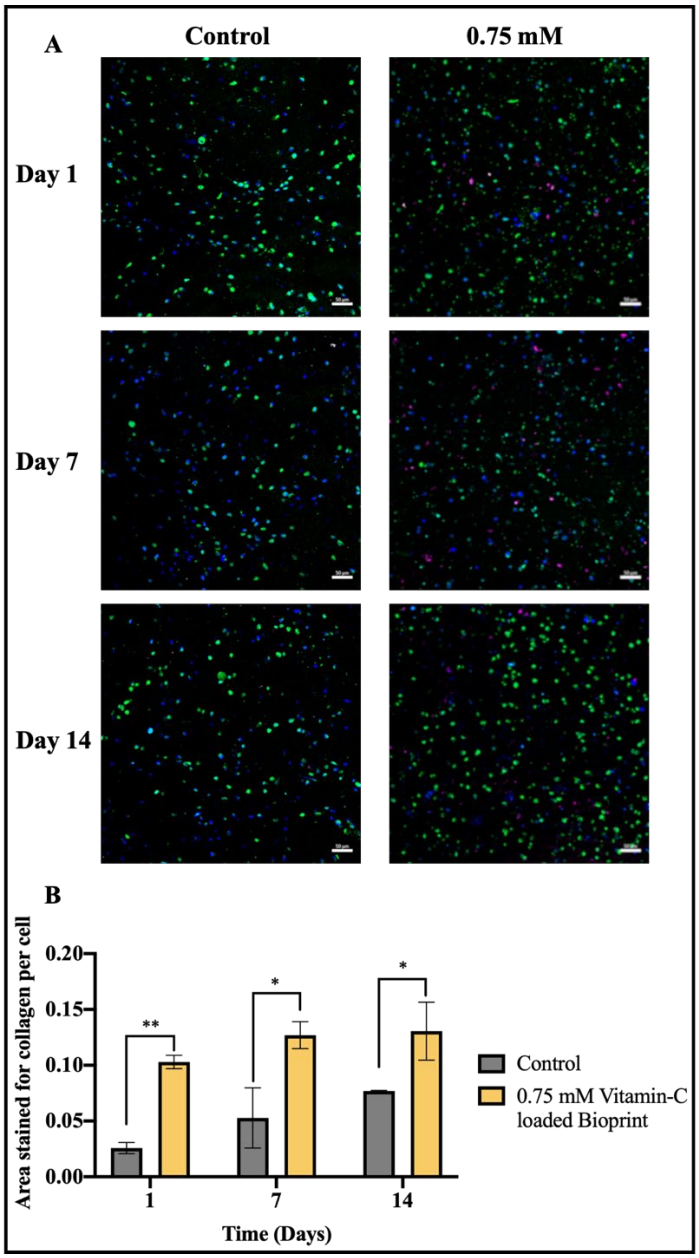

Figure 3.24 Confocal images of unloaded (control) and 0.75 mM and 100 µg/mL curcumin loaded 3D bioprinted hydrogels stained with anti-collagen type I (DAPI, blue in color, cytoskeletal elements stained with phalloidin, green in color and anti-collagen type I stained areas are seen in pink, Scale bar: 20 µm, cell density in bioink; $5x10^6$ cells/mL). Ratio of area stained for collagen type I to the total number of cells which was determined by DAPI staining (B). Statistical analysis was carried out using one-way ANOVA. *$p<0.1$, **$p < 0.01$ and ns: not-significant.

3.5.9.2.5 Evaluation of Collagen Deposition with Sirius Red Staining

Sirius red staining was also performed on Vitamin-C containing slab gels, 3D printed gels and curcumin containing 3D bioprinted hydrogels. The majority of the hydrogels consisted of GelMA, all hydrogel was stained in red because gelatin is a collagen derivative. However, when the backgorund was minimized the cells were observed in dark red while collagen was observed as bright red dots. In literature, Onat et al. used sirius red staining for detecting collagen deposition by SaOS-2 and hFOB cells seeded on poly(4-hydroxy-L-proline ester) based scaffolds. Significant difference in collagen deposition was observed between the samples treated with differentiation medium containing Vitamin-C than the untreated control group was observed from 6-10%. In this study, amount of collagen staining to cell number was found from 0.01-0.30 depending on days and concentration (Fig.3.25B, 3.26B and 3.27B). At day 1, there was no significant difference between the control and Vitamin-C containing groups. In slab gels, difference was observed between control and 0.75 mM at day 7. However, biggest difference between two concentrations of Vitamin-C was observed at day 14 of 3D printed hydrogels. Sridhar et al. reported a study based on scaffolds immersed in Vitamin-C (28 mM) (Sridhar et al. 2015). In their study, collagen expression was detected via picrosirius red staining around 9 days. This may be the reason of Vitamin-C including slab gels not having a significant difference fromeach other. If the study was prolonged for slab gels, we may have observed the gap between two concentrations as in 3D printed conjugates.

It should also be noted that, in bioprinting confocal microcopy could not present high quality images therefore, a comparison between control and bioprints could not be held. However, since sirius red also stained the hydrogel, however collagen deposited areas are bright red areas (Fig. 3.27A). Although at day 7 (Fig.3.27B), there was no significant difference among the groups, however, as in cell seeded 3D printed hydrogels, difference was observed at day 14. Collagen expression per cell number was calculated as 0.26 for bioprints while it was 0.11 for the control. From these results, it can be said that 0.75 mM Vitamin-C containing 3D bioprint was

found effective on collagen synthesis of the encapsulated fibroblasts and would be efficient on possible burn wounds.

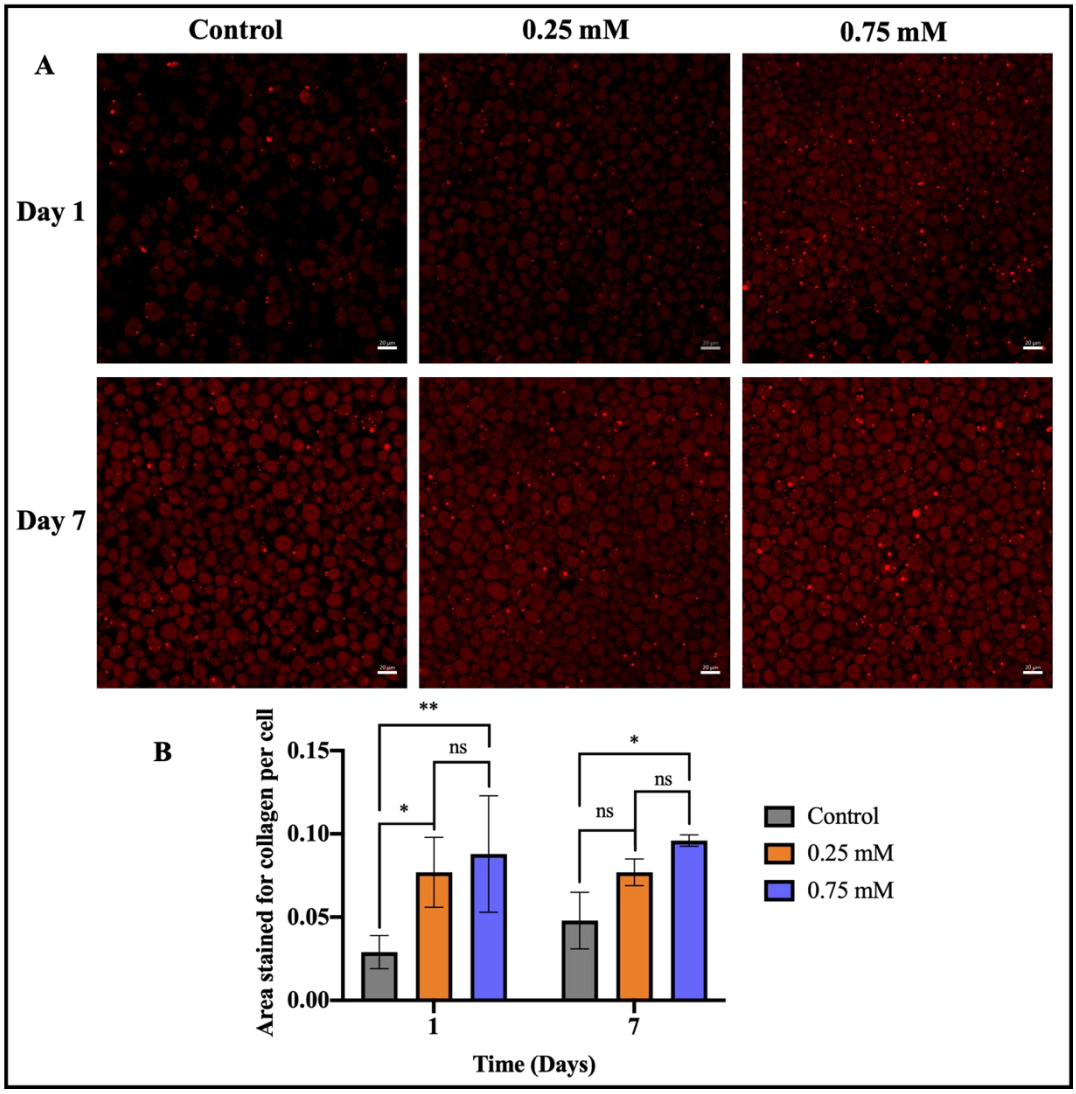

Figure 3.25 Confocal images of unloaded (control), 0.25 mM and 0.75 mM Vitamin-C loaded slab gels, stained with sirius red dye (bright red dots indicate collagen, Scale bar: 20 µm, initial seeding $3x10^4$/hydrogel). Ratio of area stained with sirius red to number of cells which was determined with DAPI staining (B). Statistical analysis was carried out using one-way ANOVA. *$p<0.1$, **$p < 0.01$ and ns: not-significant.

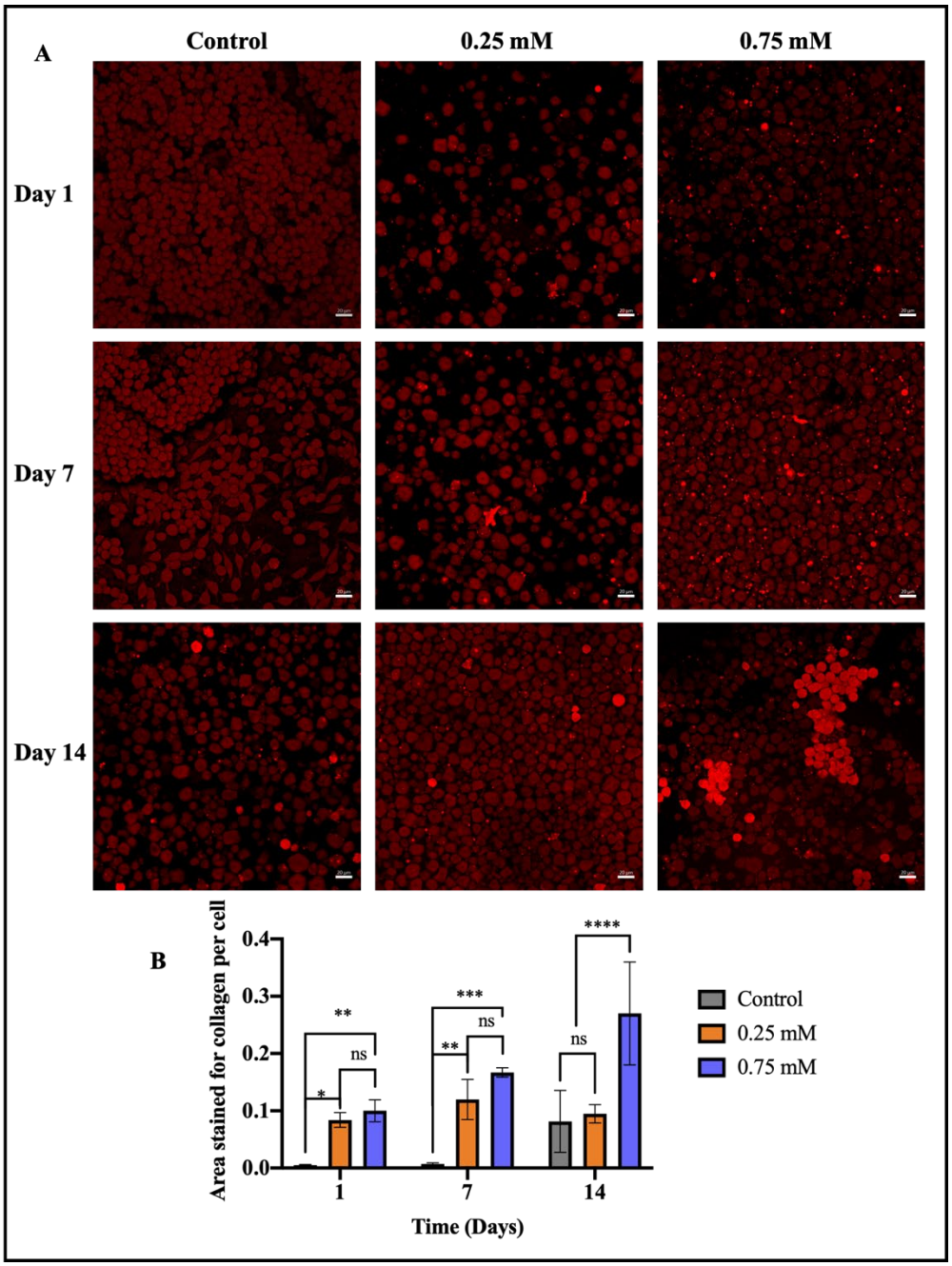

Figure 3.26 Confocal images of unloaded (control), 0.25 mM and 0.75 mM Vitamin-C loaded 3D printed hydrogels, stained with sirius red dye (bright red dots indicate collagen, Scale bar: 20 µm, initial seeding: $3x10^4$/hydrogel). Ratio of area stained with sirius red to number of cells which was determined with DAPI staining (B). Statistical analysis was carried out using one-way ANOVA. *p<0.1, **p < 0.01, ***p<0.001, ****p<0.0001 and ns: not-significant.

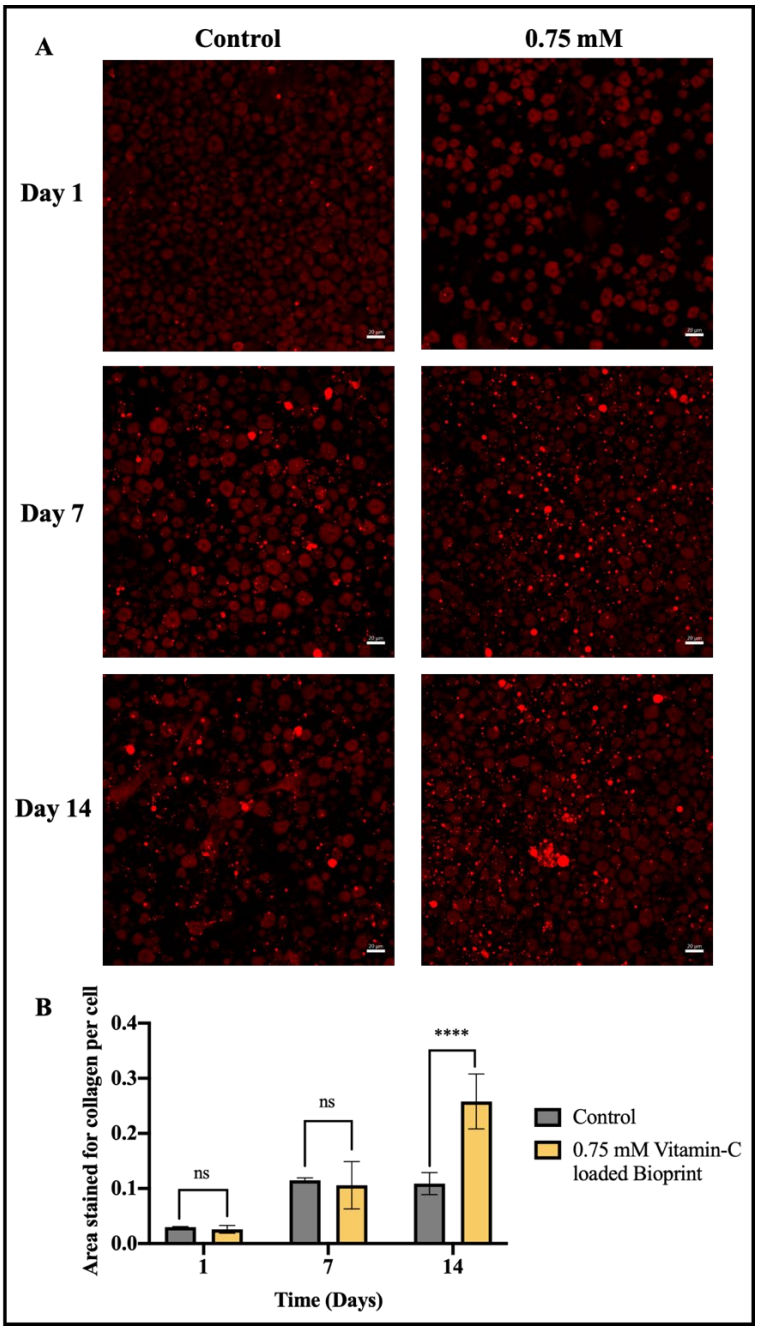

Figure 3.27. Confocal images of unloaded (control) and 0.75 mM Vitamin-C and 100 µg/mL curcumin loaded 3D bioprinted hydrogel, stained with sirius red dye (bright red dots indicate collagen, Scale bar: 20 µm, initial seeding $3x10^4$/hydrogel). Ratio of area stained with sirius red to number of cells which was determined with DAPI staining (B). Statistical analysis was carried out using one-way ANOVA, ****$p<0.0001$ and ns: not-significant.

CHAPTER 4

CONCLUSION

In this thesis study, curcumin and/or Vitamin-C loaded skin graft of methacrylated pectin and methacrylated gelatin hydrogels were produced for the first time in 3D printed and slab forms. Blend hydrogels in slab form was found to allow sufficient oxygen permeability required for wound healing as well as inhibiting microorganism penetration. Addition of PeMA have improved wettability of hydrogels. Additionally, all blend hydrogels were found biocompatible using L929 cells. In comparison to slab hydrogels, 3D printed hydrogels retained more of their initial weights throughout the incubation period and preserved their honeycomb patterned shapes. As a result of this, both zone of inhibition values and *in vitro* release of curcumin was found higher in slab gels than 3D printed hydrogels for the given curcumin concentration. Additionally, higher curcumin release at pH 7.4 compared to pH 5.0 showed that the hydrogels can be effective on chronic wounds which increases the natural pH of the skin. Lastly, combining curcumin, Vitamin-C and fibroblasts in a 3D bioprint had positive impact on cell viability as well as collagen synthesis.

In conclusion, curcumin and Vitamin-C containing 3D printed photo-crosslinked hydrogels present a potential as a skin graft for chronic burn wound treatments. *In vivo* animal studies are needed for future studies.

REFERENCES

Abrigo, M., McArthur, S.L. & Kingshott, P. (2014). Electrospun Nanofibers as Dressings for Chronic Wound Care: Advances, Challenges, and Future Prospects. *Macromolecular Bioscience*, 14, 772–792. https://doi.org/10.1002/mabi.201300561

Ahmed, A.S., Mandal U.K., Taher, M., Susanti & D., Jaffri, J. (2018). PVA-PEG Physically Cross-Linked Hydrogel Film as a Wound Dressing: Experimental Design and Optimization. *Pharmaceutical Development and Technology*, 23 (8), 751-760. https://doi.org/10.1080/10837450.2017.1295067

Akhgari, A., Farahmand, F., Garekani, A.H., Sadeghi, F. & Vandamme, T. (2010). The Effect of Pectin on Swelling and Permeability Characteristics of Free Films Containing Eudragit RL and/or RS as a Coating Formulation Aimed for Colonic Drug Delivery. *Daru*, 18 (2): 91–96.

Alipour, R., Khorshidi, A., Shojaei, A.F., Mashayekhi, F. & Moghaddam, M.J.M. (2019). Skin Wound Healing Acceleration by Ag Nanoparticles Embedded in PVA/ PVP/Pectin/Mafenide Acetate Composite Nanofibers. *Polymer Testing*, 79 (106022). https://doi.org/10.1016/j.polymertesting.2019.106022

Alven, S., Nqoro, X., & Aderibigbe, B.A. (2020). Polymer-Based Materials Loaded with Curcumin for Wound Healing Applications. *Polymers*, 12 (10): 2286. https://doi.org/10.3390/polym12102286

Ambekar, R.S. & Kandasubramanian, B. (2019). Advancements in Nanofibers for Wound Dressing: A Review. *European Polymer Journal*, 117: 302–36. https://doi.org/10.1016/j.eurpolymj.2019.05.020

Andriotis, E.G., Eleftheriadis, G.K., Karavasili, C. & Fatouros, D.G. (2020). Development of Bio-Active Patches Based on Pectin for the Treatment of

Ulcers and Wounds Using 3D-Bioprinting Technology. *Pharmaceutics*, 12 (1) 56. https://doi.org/10.3390/pharmaceutics12010056

Augustine, R. (2018). Skin Bioprinting: A Novel Approach for Creating Artificial Skin from Synthetic and Natural Building Blocks. *Progress in Biomaterials*, 7 (2): 77–92. https://doi.org/10.1007/s40204-018-0087-0

Bae, H., Ahari, A.F., Shin, H., Nichol, J.W., Hutson, C.B., Masaeli, M., Kim, S.H., Aubin, H., Yamanlar, S. & Khademhosseini, A. (2011). Cell-Laden Microengineered Pullulan Methacrylate Hydrogels Promote Cell Proliferation and 3D Cluster Formation. *Soft Matter*, 7 (5): 1903–11. https://doi.org/10.1039/C0SM00697A

Baron, R.I., Culica, M.E., Biliuta, G., Bercea, M., Gherman, S., Zavastin, D., Ochiuz, L., Avadanei, M. & Coseri, S. (2019). Physical Hydrogels of Oxidized Polysaccharides and Poly(Vinyl Alcohol) for Wound Dressing Applications. *Materials*, 12(9): 1569. https://doi.org/10.3390/ma12091569

Basara, G., Yue, X. & Zorlutuna, P. (2019). Dual Crosslinked Gelatin Methacryloyl Hydrogels for Photolithography and 3D Printing. *Gels*, 5 (34). https://doi.org/10.3390/gels5030034

Bencherif, S., Srinivasan, A., Horkay, F., Hollinger, J.O., Matyjaszewski, K. & Washburn, N.R. (2008). Influence of the Degree of Methacrylation on Hyaluronic Acid Hydrogels Properties. *Biomaterials*, 29: 1739-1749. http://dx.doi.org/10.1016/j.biomaterials.2007.11.047

Bertassoni, L.E., Cardoso J.C., Manoharan, V., Cristino, A.L., Bhise, N.S., Araujo, W.A., Zorlutuna, P., Vrana, N.E., Gheammaghami, A.M., Dokmeci, R. & Khademhosseini, A. (2014). Direct-Write Bioprinting of Cell-Laden Methacrylated Gelatin Hydrogels. *Biofabrication*, 6 (2). https://doi.org/10.1088/1758-5082/6/2/024105

Blaeser, A., Campos, D.F.D., Puster, U., Richtering, W., Stevens, M.M. & Fischer, H. (2016). Controlling Shear Stress in 3D Bioprinting is a Key Factor to

Balance Printing Resolution and Stem Cell Integrity. *Advanced Healthcare Materials*, 5 (3): 326-33. https://doi.org/10.1002/adhm.201500677

Brougham, C.M., Levingstone, T.J., Shen, N., Cooney, G.M., Jockenhoevel, S., Flanagan, T.C. & O'Brien, F.J. (2017). Freeze-Drying as a Novel Biofabrication Method for Achieving a Controlled Microarchitecture within Large, Complex Natural Biomaterial Scaffolds. *Advanced Healthcare Materials*, 6 (21):1700598. https://doi.org/10.1002/adhm.201700598

Brown, M.S., Ashley, B. & Koh. A. (2018). Wearable Technology for Chronic Wound Monitoring: Current Dressings, Advancements, and Future Prospects. *Frontiers in Bioengineering and Biotechnology*, 6: 6-47. https://doi.org/10.3389/fbioe.2018.00047

Browning, J.A. & Cindass, R. (2020). Burn Debridement, Grafting, and Reconstruction. StatPearls Publishing, 2020. https://www.ncbi.nlm.nih.gov/books/NBK551717/

Capo, J.T., Kokko, K.P., Rizzo, M., Adams, J.E., Shamian, B., Abernathie, B. & Melamed, E. (2014). The Use of Skin Substitutes in the Treatment of the Hand and Upper Extremity. *Hand*, 9(2):156–65. https://doi.org/10.1007%2Fs11552-013-9587-5

Castañeda-Reyes, E.D., Perea-Flores, M.d.J., Davila-Ortiz, G., Lee, Y. & Gonzalez de Mejia, E. (2020). Development, Characterization and Use of Liposomes as Amphipathic Transporters of Bioactive Compounds for Melanoma Treatment and Reduction of Skin Inflammation: A Review. *International Journal of Nanomedicine*, 15: 7627–50. https://doi.org/10.2147/IJN.S263516

Chan, S.Y., Choo, W.S., Young, D.J. & Loh, X.J. (2016). Thixotropic Supramolecular Pectin-Poly(Ethylene Glycol) Methacrylate (PEGMA) Hydrogels. *Polymers*, 8 (11):404. https://doi.org/10.3390/polym8110404

Choi, J.R., Yong, K.W., Choi, J.Y. & Cowie, A.C. (2019). Recent Advances in Photo-Crosslinkable Hydrogels for Biomedical Applications. *Biotechniques*, 66 (1):40-53. https://doi.org/10.2144/btn-2018-0083

Chou, A.I. & Nicoll, S.B. (2009) Characterization of Photocrosslinked Alginate Hydrogels for Nucleus Pulposus Cell Encapsulation. *Journal of Biomedical Materials Research Part A*, 91 (1): 187–94.

Čoma, M., Fröhlichová, L., Urban, L., Zajíček, R., Urban, T., Szabo, P., Novák, S., Fetissov, V., Dvorankova, B., Smetana Jr., K. & Gal, P. (2021). Molecular Changes Underlying Hypertrophic Scarring Following Burns Involve Specific Deregulations at All Wound Healing Stages (Inflammation, Proliferation and Maturation). *International Journal of Molecular Science*, 22 (2): 897. https://doi.org/10.3390/ijms22020897

Comotto, M., S. Saghazadeh, S. Bagherifard, B. Aliakbarian, M. Kazemzadeh-Narbat, F. Shafiri, S.A.M. Shaegh, et al. 2019. Breathable Hydrogel Dressings Containing Natural Antioxidants for Management of Skin Disorders.*Journal of Biomaterials Applications* 33 (9): 1265–76.

Coutinho, D.F., Sant, S.V., Shin, H., Oliveira, L.T., Gomes, M.E., Neves N.M., Khademhosseini, A. & Reis, R.L. (2010). Modified Gellan Gum Hydrogels with Tunable Physical and Mechanical Properties. *Biomaterials*, 31: 7494–7502. https://doi.org/10.1016/j.biomaterials.2010.06.035

Curti, F., Stancu, I.C., Voicu, G., Iovu, H., Dobrita, C.I., Ciocan, L.T., Marinescu, R. & Iordache, F. (2020). Development of 3D Bioactive Scaffolds through 3D Printing Using Wollastonite–Gelatin Inks. *Polymers*, 12(10) 2420. https://doi.org/10.3390/polym12102420

Dart, A., Bhave, M. & Kingshott, P. (2019). Antimicrobial Peptide-Based Electrospun Fibers for Wound Healing Applications. *Macromolecular Bioscience*, 19 (1800488). https://doi.org/10.1002/mabi.201800488

Derakhshanfar, S., Mbeleck, R., Xu, K., Zhang, X., Zhong, W. & Xing, M. (2018). 3D Bioprinting for Biomedical Devices and Tissue Engineering: A Review of Recent Trends and Advances. *Bioactive Materials*, 3(2):144–56. https://doi.org/10.1016/j.bioactmat.2017.11.008

Dılgın, Y., & Nışlı, G. (2003). Fluorimetric Determination of Ascorbic Acid in Vitamin C Tablets Using Methylene Blue. *Chemical and Pharmaceutical Bulletin*, 53 (10): 1251–54. https://doi.org/10.1248/cpb.53.1251

Ehterami, A., Salehi, M., Farzamfar, S., Vaez, A., Samadian, H., Sahrapeyma, H., Mirzai, M., Ghorbani, S. & Goodarzi, A. (2018). In Vitro and in Vivo Study of PCL/COLL Wound Dressing Loaded with Insulin-Chitosan Nanoparticles on Cutaneous Wound Healing in Rats Model. *International Journal of Biological Macromolecules*, 117: 601–9. https://doi.org/10.1016/j.ijbiomac.2018.05.184

Eke, G., Mangir, N., Hasırcı, N., MacNeil, S. & Hasırcı, V. (2017). Development of a UV Crosslinked Biodegradable Hydrogel Containing Adipose Derived Stem Cells to Promote Vascularization for Skin Wounds and Tissue Engineering. *Biomaterials*, 129: 188–198. https://doi.org/10.1016/j.biomaterials.2017.03.021

El-Sherbiny, I.M. & Yacoub, M.H. (2013). Hydrogel Scaffolds for Tissue Engineering: Progress and Challenges. *Global Cardiology Science and Practice*, 3: 316-342. https://doi.org/10.5339/gcsp.2013.38

Esentürk, İ., Erdal, M.S. & Güngör, S. (2016). Electrospinning Method to Produce Drug-Loaded Nanofibers for Topical/ Transdermal Drug Delivery Applications. *İstanbul Eczacılık Fakültesi Dergisi,* 46 (1): 46–69.

Fereydouni, N., Movaffagh, J., Amiri, N., Darroudi, S., Gholoobi, A., Goodarzi, A., Hashemzadeh, A. & Darroudi, M. (2021). Synthesis of Nano-Fibers Containing Nano-Curcumin in Zein Corn Protein and Its Physicochemical

and Biological Characteristics. *Scientific Reports*, 11 (1902). https://doi.org/10.1038/s41598-020-73678-w

Franco, R.A., Nguyen, T.H. & Lee, B.T. (2011). Preparation and Characterization of Electrospun PCL/PLGA Membranes and Chitosan/Gelatin Hydrogels for Skin Bioengineering Applications. *Journal of Materials Science: Materials in Medicine*, 22 (2207–2218). https://doi.org/10.1007/s10856-011-4402-8

Gao, Y. & Jin, X. (2019). Dual Crosslinked Methacrylated Alginate Hydrogel Micron Fibers and Tissue Constructs for Cell Biology. *Marine Drugs*, 17 (10): 557. https://doi.org/10.3390/md17100557

Gawkowska, D., Cybulska, J. & Zdunek, A. (2018). Structure-Related Gelling of Pectins and Linking with Other Natural Compounds: A Review. *Polymers,* 10 (7):762. https://doi.org/10.3390/polym10070762

GhavamiNejad, A., Ashammakhi, N., Wu, Y.X. & Khademhosseini, A. (2020). Crosslinking Strategies for 3D Bioprinting of Polymeric Hydrogels. *Small*, 16 (35) 2002931. https://doi.org/10.1002/smll.202002931

Ghilan, A., Chiriac, A.P., Nita, L.E., Rusu, A.G., Neamtu, I. & Chiriac, V.M. (2020). Trends in 3D Printing Processes for Biomedical Field: Opportunities and Challenges. *Journal of Polymers and the Environment*, 28: 1345–67. https://doi.org/10.1007/s10924-020-01722-x

Ghomi, E.R., Khalili, S., Khorasani, S.N., Neisiany, R.E. & Ramakrishna, S. (2019). Wound Dressings: Current Advances and Future Directions. *Journal of Applied Polymer Science*, 136 (7):47738. https://doi.org/10.1002/app.47738

Gizaw, M., Thompson, J., Faglie, A., Lee, S.Y., Neuenschwander, P. & Chou, S.F. (2018). Electrospun Fibers as a Dressing Material for Drug and Biological Agent Delivery in Wound Healing Applications. *Bioengineering,* 5 (1): 9. https://doi.org/10.3390/bioengineering5010009

Holback, H., Yeo, Y. & Park, K. (2011). Hydrogel Swelling Behavior and Its Biomedical Applications. In Biomedical Hydrogels, edited by Steve Rimmer, 3–24. Woodhead Publishing.

Hu, X., Wang, Y., Zhang, L. & Xu, M. (2020). Formation of Self-Assembled Polyelectrolyte Complex Hydrogel Derived from Salecan and Chitosan for Sustained Release of Vitamin C. *Carbohydrate Polymers*, 234 (115920). https://doi.org/10.1016/j.carbpol.2020.115920

Huyan, Y., Lian, Q., Zhao, T., Li, D. & He, J. (2020). Pilot Study of the Biological Properties and Vascularization of 3D Printed Bilayer Skin Grafts. International *Journal of Bioprinting*, 6 (1): 246. http://dx.doi.org/10.18063/ijb.v6i1.246

II Stone, R., Natesan, S., Kowalczewski, C.J., Mangum, L.H., Clay, N.E., Clohessy, R.M., Carlsson, A.H., Tassin, D.H., Chan, R.K., Rizzo, J.A. & Christy, R.J. (2018). Advancements in Regenerative Strategies Through the Continuum of Burn Care. *Frontiers in Pharmacology*, 9 (672). https://doi.org/10.3389/fphar. 2018.00672.

Ilhan, E., Cesur, S., Güler, E., Topal, F., Albayrak, D., Güncü, M.M., Cam, M.E., Taskin, T., Sasmazel, H.T., Aksu B., Oktar, F.N. & Gunduz, O. (2020). Development of Satureja Cuneifolia-Loaded Sodium Alginate/Polyethylene Glycol Scaffolds Produced by 3D-Printing Technology as a Diabetic Wound Dressing Material. *International Journal of Biological Macromolecules*, 161: 1040–54. https://doi.org/10.1016/j.ijbiomac.2020.06.086

De Isla, N., Huseltein, C., Jessel, N., Pinzano, A., Decot, V., Magdalou, J., Bensoussan, D. & Stoltz, J.F. (2010). Introduction to Tissue Engineering and Application for Cartilage Engineering. *Bio-Medical Materials and Engineering*, 20 (3): 127–33. https://doi.org/10.1186/s40634-015-0026-0

Jia, W., Gungor-Ozkerim, P.S., Zhang, Y.S., Yue, K., Zhu, K., Liu, W., Pi, O., Byambaa, B., Dokmeci, M.R., Shin, S.R. & Khademhosseini A. (2016).

Direct 3D Bioprinting of Perfusable Vascular Constructs Using a Blend Bioink. *Biomaterials*, 106: 58–68. https://doi.org/10.1016/j.biomaterials.2016.07.038

Jin, L., Wang, T., Zhu, M.L., Leach, M.K., Naim, Y.I., Corey, J.M. & and Feng, Z.Q. (2012). Electrospun Fibers and Tissue Engineering. *Journal of Biomedical Nanotechnology*, 8 (1): 1–9. http://dx.doi.org/10.1166/jbn.2012.1360

Kannaiyan, J., Khare, S., Narayanan, S. & Mahuvawalla, F. (2019). Fabrication of Electrospun Polycaprolactone/Gelatin Composite Nanofibrous Scaffolds with Cellular Responses. *American Journal of Nano Research and Applications*, 7 (2): 11–20. doi: 10.11648/j.nano.20190702.11

Karakurt, I., Aydoğdu, A., Çıkrıkçı, S., Orozco, J. & Lin, L. (2020). Stereolithography (SLA) 3D Printing of Ascorbic Acid Loaded Hydrogels: A Controlled Release Study. *International Journal of Pharmaceutics*, 584 (119428). https://doi.org/10.1016/j.ijpharm.2020.119428

Kaur, A., Midha, S., Giri, S. & Mohanty, S. (2019). Functional Skin Grafts: Where Biomaterials Meet Stem Cells. *Stem Cells International*, 1286054. https://doi.org/10.1155/2019/1286054

Keirouz, A., Chung, M., Kwon, J., Fortunato, G. & Radacsi, N. (2020). 2D and 3D Electrospinning Technologies for the Fabrication of Nanofibrous Scaffolds for Skin Tissue Engineering: A Review. *WIREs Nano*, 12 (4): e01626. https://doi.org/10.1002/wnan.1626

Khamrai, M., Banerjee, S.L., Paul, S., Samanta, S. & Kundu, P.P. (2019). Curcumin Entrapped Gelatin/Ionically Modified Bacterial Cellulose Based Self-Healable Hydrogel Film: An Eco-Friendly Sustainable Synthesis Method of Wound Healing Patch. *International Journal of Biological Macromolecules*, 122: 940–53. https://doi.org/10.1016/j.ijbiomac.2018.10.196

Kılıç-Bektaş, C. & Hasırcı, V. (2020). Cell Loaded 3D Bioprinted GelMA Hydrogels for Corneal Stroma Engineering. Biomaterials Science, 8: 438–49. https://doi.org/10.1039/C9BM01236B

Lantigua, D., Nguyen, M.A., Wu, X., Suvarnapathaki, S., Kwon, S., Gavin, W. & Camci-Unal, G. (2020). Synthesis and Characterization of Photocrosslinkable Albumin-Based Hydrogels for Biomedical Applications. *Soft Matter*, 16 :9242-9252. https://doi.org/10.1039/D0SM00977F

Lara-Espinoza, C., Carjaval-Millán, E., Balandrán-Quintana, R., López-Franco, Y. & Rascón-Chu, A. (2018). Pectin and Pectin-Based Composite Materials: Beyond Food Texture. *Molecules*, 23(4): 942. https://doi.org/10.3390/molecules23040942

Lee, B.H., Shirahama, H., Cho, N.J. & Tan, L.H. (2015). Efficient and Controllable Synthesis of Highly Substituted Gelatin Methacrylamide for Mechanically Stiff Hydrogels. *RSC Advances*, 5 (128): 106094–97. https://doi.org/10.1039/C5RA22028A

Li, H., Wang, M., Williams, G.R., Wu, J., Sun, X., Lv, Y. & Zhu, L.M. (2016). Electrospun Gelatin Nanofibers Loaded with Vitamins A and E as Antibacterial Wound Dressing Materials. *RSC Advances*, 6:50267-50277. https://doi.org/10.1039/C6RA05092A

Lin, C.H., Su, J.J.M., Lee, S.Y. & Lin, Y.M. (2018). Stiffness Modification of Photopolymerizable Gelatin-Methacrylate Hydrogels Influences Endothelial Differentiation of Human Mesenchymal Stem Cells. *Journal of Tissue Engineering and Regenerative Medicine,* 12 (10): 2099–2111. https://doi.org/10.1002/term.2745

Long, J., Etxeberria, A.E., Nand, A.V., Bunt, C.R., Ray, S. & Seyfoddin, A. (2019). A 3D Printed Chitosan-Pectin Hydrogel Wound Dressing for Lidocaine T Hydrochloride Delivery. *Materials Science & Engineering C*, 104 (109873). https://doi.org/10.1016/j.msec.2019.109873

Lu, G., Ling, K., Zhao, P., Xu, Z., Deng, C., Zheng, H., Huang, J. &Chen, J. (2010). A Novel in Situ-Formed Hydrogel Wound Dressing by the Photocross-Linking of a Chitosan Derivative.*Wound Repair and Regeneration,* 18 (70–79). https://doi.org/DOI:10.1111/j.1524-475X.2009.00557.x.

Mansuroğlu, B., Kızılbey, K., Poyraz, F.Ş., Yurttaş, Z., Fuerkaiti, S.N., Abaoğlu, İ.Y., & Başat, H.N. (2020). Chitosan/Dextran Sulphate Sodium Hydrogels for Wound Healing Material: Preparation, Characterisation and in Vitro Evaluation. *Materials Technology*, 1800297. https://doi.org/10.1080/10667857.2020.1800297

Mantha, S., Pillai, S., Khayambashi, P., Upadhyay, A., Zhang, Y., Tao, O., Pham, H.M., & Tran, S.D. (2019). Smart Hydrogels in Tissue Engineering and Regenerative Medicine. *Materials*, 12(20): 3323. https://doi.org/10.3390/ma12203323

Maver, T., Smrke, D.M., Kurecic, M., Gradisnik, L., Maver, U. & Kleinschek, S. (2018). Combining 3D Printing and Electrospinning for Preparation of Pain-Relieving Wound-Dressing Materials. *Journal of Sol-Gel Science and Technology*, 88: 33–48. https://doi.org/10.1007/s10971-018-4630-1

McCormick, P.G. (1972). The Determination of Dissolved Oxygen by the Winkler Method. *Journal of Chemical Education*, 49 (12): 839–41.

Metcalfe, A.D. & Ferguson, M.W.J. (2007). Tissue Engineering of Replacement Skin: The Crossroads of Biomaterials, Wound Healing, Embryonic Development, *Stem Cells and Regeneration. Journal of Royal Society: Interface*, 4 (413–437). https://doi.org/10.1098/rsif.2006.0179

Mihaila, S.M., Gaharwar, A.K., Reis, R.L., Marques, A.P., Gomes, M.E. & Khademhosseini, A. (2013). Photocrosslinkable Kappa-Carrageenan Hydrogels for Tissue Engineering Applications. *Advanced Healthcare Materials*, 2: 895–907. https://doi.org/10.1002/adhm.201200317

Minzanova, S.T., Mironov, V.F., Arkhipova, D.M., Khabibullina, A.V., Mironova, L.G., Zakirova, Y.M. & Milyukov, V.A. (2018). Biological Activity and Pharmacological Application of Pectic Polysaccharides: A Review. *Polymers*, 10 (1407). https://doi.org/10.3390/polym10121407.

Mishra, R.K., Majeed, A.B.A. & Banthia, A.K. (2011). Development and Characterization of Pectin/Gelatin Hydrogel Membranes for Wound Dressing. *International Journal of Plastics Technology*, 15 (1): 82–95. https://doi.org/10.1007/s12588-011-9016-y

Moghadamtousi, S.Z., Kadir, H.A., Hassandarvish, P., Tajik, H., Abubakar, S. & Zandi, K. (2014). A Review on Antibacterial, Antiviral, and Antifungal Activity of Curcumin. *BioMed Research International*, 186864. https://doi.org/10.1155/2014/186864

Mogoşanu, G.D & Grumezescu, A.M. (2014). Natural and Synthetic Polymers for Wounds and Burns Dressing. *International Journal of Pharmaceutics*, 463: 127–36. https://doi.org/10.1016/j.ijpharm.2013.12.015

De Mori, A., Fernandez, M.P., Blunn, G., Tozzi, G. & Roldo, M. (2018). 3D Printing and Electrospinning of Composite Hydrogels for Cartilage and Bone Tissue Engineering. *Polymers*, 10(3): 285. https://doi.org/10.3390/polym10030285

Myers, S.R. Partha, V.N., Soranzo, C., Price, R.D. & Navsaria, H.A. (2007). Hyalomatrix: A Temporary Epidermal Barrier, Hyaluronan Delivery, and Neodermis Induction System for Keratinocyte Stem Cell Therapy. *Tissue Engineering*, 13 (11):2733-2741. https://doi.org/10.1089/ten.2007.0109

Naves, L.B., Dhand, C., Almeida, L., Rajamani, L. & Ramakrishna, S. (2016). In Vitro Skin Models and Tissue Engineering Protocols for Skin Graft Applications. *Essays in Biochemistry*, 60(4): 357–69. https://doi.org/10.1042/EBC20160043

Nordby, M.H., Kjøniksen, A.L., Nyström, B. & Roots, J. (2003). Hermoreversible Gelation of Aqueous Mixtures of Pectin and Chitosan. *Rheology. Biomacromolecules*, 4: 337–43. https://doi.org/ 10.1021/bm020107+

Noreen, A., Nazli, Z.H., Akram, J., Rasul, I., Mansha, A., Yaqoob, N., Iqbal, R., Tabasum, S., Zuber, M. & Zia, M.K. (2017). Pectins Functionalized Biomaterials; a New Viable Approach for Biomedical Applications: A Review. *International Journal of Biological Macromolecules*, 101: 254–72. https://doi.org/10.1016/j.ijbiomac.2017.03.029

Dehkordi, A.N., Mirahmadi Babaheydari, F., Chehelgerdi, M. & Dehkordi, S.R. (2019). Skin Tissue Engineering: Wound Healing Based on Stem-Cell-Based Therapeutic Strategies. *Stem Cell Research & Therapy*, 10 (1): 111. https://doi.org/10.1186/s13287-019-1212-2

O'Brien, F.J. (2011). Biomaterials & Scaffolds for Tissue Engineering. *Materials Today*, 14 (3): 88-95. https://doi.org/10.1016/S1369-7021(11)70058-X

Okur, M.E., Karantas, I.D., Şenyiğit, Z., Üstündağ Okur, N. & Siafaka, P.I. (2020). Recent Trends on Wound Management: New Therapeutic Choices Based on Polymeric Carriers. *Asian Journal of Pharmaceutical Sciences*, 15 (6): 661–84. https://doi.org/10.1016/j.ajps.2019.11.008

Onat, B., Tunçer, S., Ulusan, S., Banerjee, S. & Erel-Göktepe, İ. (2019). Biodegradable Polymer Promotes Osteogenic Differentiation in Immortalized and Primary Osteoblast-like Cells. *Biomedical Materials*, 14(4): 045003. https://doi.org/10.1088/1748-605X/ab0e92

Ono, S., Imai, R., Ida, Y., Shibata, D., Komiya, T. & Matsumura, H. (2015). Increased Wound PH as an Indicator of Local Wound Infection in Second Degree Burns. *Burns*, 41: 820–24. https://doi.org/10.1016/j.burns.2014.10.023

Peng, H., Chen, S., Luo, M., Ning, F., Zhu, X. & Xiong, H. (2016). Preparation and Self-Assembly Mechanism of Bovine Serum Albumin−Citrus Peel Pectin

Conjugated Hydrogel: A Potential Delivery System for Vitamin C. *Journal of Agricultural and Food Chemistry*, 64: 7737-7384. https://doi.org/10.1021/acs.jafc.6b02966

Pepelanova, I., Kruppa K., Scheper T. & Lavrentieva, A. (2018). Gelatin-Methacryloyl (GelMA) Hydrogels with Defined Degree of Functionalization as a Versatile Toolkit for 3D Cell Culture and Extrusion Bioprinting. *Bioengineering*, 5 (3):55. https://doi.org/10.3390/bioengineering5030055

Pereira, R.F., Sousa, A., Barrias, C.C., Bartolo, P.J. & Granja, P.L. (2018). A Single-Component Hydrogel Bioink for Bioprinting of Bioengineered 3D Constructs for Dermal Tissue Engineering. *Materials Horizons,* 5: 1100–1111. https://doi.org/10.1039/C8MH00525G

Pereira, R.F., Sousa, A., Barrias, C.C., Bayat, A., Granja, P.L. & Bartolo, P.J. (2017). Advances in Bioprinted Cell-Laden Hydrogels for Skin Tissue Engineering. *Biomanufacturing Reviews 2*,(1). https://doi.org/10.1007/s40898-017-0003-8

Pettinelli, N., Llamazares-Rodriguez, S., Abella, V., Barral, L., Bouza, R., Farrag, Y. & Lago, F. (2019). Entrapment of Chitosan, Pectin or κ-Carrageenan within Methacrylate Based Hydrogels: Effect on Swelling and Mechanical Properties. *Materials Science & Engineering C*, 96: 583–90. https://doi.org/10.1016/j.msec.2018.11.071

Przekora, A. (2020). A Concise Review on Tissue Engineered Artificial Skin Grafts for Chronic Wound Treatment: Can We Reconstruct Functional Skin Tissue In Vitro?. *Cells*, 9 (7): 1622. https://doi.org/10.3390/cells9071622

Rashaan, Z.M., Krijnen, P., Allema, J.H., Vloemans, A.F., Schipper, I.B. & Breederveld, R.S. (2017). Usability and Effectiveness of Suprathel® in Partial Thickness Burns in Children. *European Journal of Trauma and Emergency Surgery*, 43: 549–56. https://doi.org/10.1007/s00068-016-0708-z

Rezaei, E., Beiraghi-Toosi, A., Ahmadabadi, A., Tavousi, S.H., Tabrizi, A.A., Fotuhi, K., Nooghabi, M.J., Manafi, A. Moghadam, S.A. (2017). Can Skin Allograft Occasionally Act as a Permanent Coverage in Deep Burns? A Pilot Study. *World Journal of Plastic Surgery*, 6 (1): 94–99.

Rice, M.A., Sanchez-Adams, J. & Anseth, K.S. (2006). Exogenously Triggered, Enxymatic Degradation of Photopolymerized Hydrogels with Polycaprolactone Subunits: Experimental Observation and Modeling of Mass Loss Behavior. Biomacromolecules, 7 (6): 1968-1975. https://dx.doi.org/10.1021%2Fbm060086%2B

Rider, P., Kačarević, Z.P., Alkildani, S., Retnasingh, S. & Barbeck, M. (2018). Bioprinting of Tissue Engineering Scaffolds. *Journal of Tissue Engineering*, 9: 1–16. https://doi.org/10.1177%2F2041731418802090

Rieger, K.A., Birch, N.P. & Schiffman, J.D. (2013). Designing Electrospun Nanofiber Mats to Promote Wound Healing – a Review. *Journal of Materials Chemistry B,* (1):4531-41. https://doi.org/10.1039/C3TB20795A

Rnjak-Kovacina, J. & Weiss, A.S. (2011). Increasing the Pore Size of Electrospun Scaffolds. *Tissue Engineering: Part B*, 17 (5). https://doi.org/10.1089/ten.teb.2011.0235

Saraiva, S.M., Miguel, S.P., Ribeiro, M.P., Coutinho, P. & Correia. I.J. (2015). Synthesis and Characterization of a Photocrosslinkable Chitosan–Gelatin Hydrogel Aimed for Tissue Regeneration. *RSC Advances*,17 (5): 63478-88. https://doi.org/10.1039/C5RA10638A

Serra, M.B., Barroso, W.A., da Silva, N.N., do Nascimento Silva, S., Romão Borges, A.C., Abreu, I.C. & da Rocha Borges, M.O. (2017). From Inflammation to Current and Alternative Therapies Involved in Wound Healing. *International Journal of Inflammation*, 3406215. https://doi.org/10.1155/2017/3406215

Sharma, M., Sahu, K., Singh, S.P. & Jain, B. (2018). Wound Healing Activity of Curcumin Conjugated to Hyaluronic Acid: In Vitro and in Vivo Evaluation.

Artificial Cells, *Nanomedicine and Biotechnology*, 46 (5): 1009–17. https://doi.org/10.1080/21691401.2017.1358731

Sheikh, Zeeshan, Nader Hamdan, Yuichi Ikeda, Marc Grynpas, Bernhard Ganss, and Michael Glogauer. 2017. Natural Graft Tissues and Synthetic Biomaterials for Periodontal and Alveolar Bone Reconstructive Applications: A Review. *Biomaterials Research*, 21 (9). https://doi.org/10.1186/s40824-017-0095-5

Shin, H., Olsen, B.D. & Khademhosseini, A. (2012). The Mechanical Properties and Cytotoxicity of Cell-Laden Double-Network Hydrogels Based on Photocrosslinkable Gelatin and Gellan Gum Biomacromolecules. *Biomaterials*, 33 (11): 3143–52. https://doi.org/10.1016/j.biomaterials.2011.12.050

Si, H., Xing, T., Ding, Y., Zhang, H., Yin, R. & Zhang, W. (2019). 3D Bioprinting of the Sustained Drug Release Wound Dressing with Double-Crosslinked Hyaluronic-Acid-Based Hydrogels. *Polymers*, 11 (10): 1584. https://doi.org/10.3390/polym11101584

Singh, B., & J. Singh. (2021). Application of Tragacanth Gum and Alginate in Hydrogel Wound Dressing's Formation Using Gamma Radiation.*Carbohydrate Polymer Technologies and Applications,*2 (100058). https://doi.org/https://doi.org/10.1016/j.carpta.2021.100058.

Singh, D., Singh, D. & Han, S.S. (2016). 3D Printing of Scaffold for Cells Delivery: Advances in Skin Tissue Engineering. *Polymers*, 8 (1): 19. https://doi.org/10.3390/polym8010019

Snyder, D.L., Sullivan, N. & Schoelles, K.M. (2012). Skin Substitutes for Treating Chronic Wounds: Technology Assessment Report. https://www.ncbi.nlm.nih.gov/books/NBK554220/

Sookkasem, A., Chatpun, S., Yuenyongsawad, S. & Wiwattanapatapee. (2015). Alginate beads for colon specific delivery of self-emulsifying curcumin.

Journal of Drug Delivery Science and Technology, 29: 159-166. http://dx.doi.org/10.1016/j.jddst.2015.07.005

Sridhar, S., Venugopal, J.R. & Ramakrishna, S. (2015). Improved Regeneration Potential of Fibroblasts Using Ascorbic Acid-Blended Nanofibrous Scaffolds. *Journal of Biomedical Materials Research Part A*, 103A (11): 3431–40. https://doi.org/10.1002/jbm.a.35486

Suhaeri, M., Noh, M.H., Moon, J.H., Kim, I.G., Oh, S.J., Ha, S.S., Lee, H.J. & and Park, K. (2018). Novel Skin Patch Combining Human Fibroblast-Derived Matrix and Ciprofloxacin for Infected Wound Healing. *Theranostics*, 8 (18): 5025–38. doi:10.7150/thno.26837

Suhail, S., Sardashti, N. Jaiswal, D., Rudraiah, S., Misra, M. & Kumbar, S.G. (2019). Engineered Skin Tissue Equivalents for Product Evaluation and Therapeutic Applications. *Biotechnology Journal*, 14 (7): 1900022. https://doi.org/10.1002/biot.201900022

Sun, B.K., Siprashvili, Z. & Khavari, P.A. (2014). Advances in Skin Grafting and Treatment of Cutaneous Wounds. *Science,* 346 (6212). doi: 10.1126/science.1253836

Tamay, D.G., Ünal, T.D., Alagöz, A.S., Yücel, D., Hasırcı, N. & Hasırcı, V. (2019). 3D and 4D Printing of Polymers for Tissue Engineering Applications. *Frontiers in Bioengineering and Biotechnology*, 7 (164). https://doi.org/10.3389/fbioe.2019.00164

Tavakoli, S. & Klar, A.S. (2020). Advanced Hydrogels as Wound Dressings. *Biomolecules*, 10 (8): 1169. https://doi.org/10.3390/biom10081169

Tomal W. & Ortyl, J. (2020). Water-Soluble Photoinitiators in Biomedical Applications. *Polymers*, 12 (5): 1073.https://doi.org/10.3390/polym12051073

Tsai, R.Y, Chen, P.W., Kuo, T.Y., Lin, C.M., Wang, D.M., Hsien, T.Y. & and Hsieh, H.J. 2014. Chitosan/Pectin/Gum Arabic Polyelectrolyte Complex: Process-Dependent Appearance, Microstructure Analysis and Its Application. *Carbohydrate Polymers,* 101: 752–59. https://doi.org/10.1016/j.carbpol.2013.10.008

Tummalapalli, M., Berthet, M., Verrier, B., Deopura, B.L., Alam, M.S., & Gupta, B. (2016a). Composite Wound Dressings of Pectin and Gelatin with Aloe Vera and Curcumin as Bioactive Agents. *International Journal of Biological Macromolecules,* 82: 104–13. https://doi.org/10.1016/j.ijbiomac.2015.10.087

Tummalapalli, M., Berthet, M., Verrier, B., Deopura, B.L., Alam, M.S., & Gupta, B. (2016b). Drug Loaded Composite Oxidized Pectin and Gelatin Networks for Accelerated Wound Healing. *International Journal of Pharmaceutics*, 505: 234–45. https://doi.org/10.1016/j.ijpharm.2016.04.007

Tytgat, L., Van Damme, L., del Pilar Ortega Arevalo, M., Declercq, H., Thienport, H., Otteveare, H., Blondeel, P., Dubruel, P. & Van Vlierberghe, S. (2019). Extrusion-Based 3D Printing of Photo-Crosslinkable Gelatin and κ-Carrageenan Hydrogel Blends for Adipose Tissue Regeneration. *International Journal of Biological Macromolecules*, 140: 929–38. https://doi.org/10.1016/j.ijbiomac.2019.08.124

Varkey, M., Ding, J. & Tredget, E.E. (2015). Advances in Skin Substitutes—Potential of Tissue Engineered Skin for Facilitating Anti-Fibrotic Healing. *Journal of Functional Biomaterials*, 6 (3): 547. https://doi.org/10.3390/jfb6030547

Vig, K., Chaudhari, A., Tripathi, S., Dixit, S., Sahu, R., Pillai, S., Dennis, V.A. & Singh, S.R. (2017). Advances in Skin Regeneration Using Tissue Engineering. *International Journal of Molecular Sciences*, 18 (4): 789. https://doi.org/10.3390/ijms18040789

Vivcharenko, V., Wojcik, M. & Przekora. A. (2020). Cellular Response to Vitamin C-Enriched Chitosan/Agarose Film with Potential Application as Artificial Skin Substitute for Chronic Wound Treatment. *Cells,* 9 (1185). https://doi.org/10.3390/cells9051185

Wan, W., Cai, F., Huang, J., Chen, S. & Liao, Q. (2019). A Skin-Inspired 3D Bilayer Scaffold Enhances Granulation Tissue Formation and Anti-Infection for Diabetic Wound Healing. *Journal of Materials Chemistry B*, 7: 2954-61. https://doi.org/10.1039/c8tb03341b.

Wang, G., Jia, L., Han, F., Wang, J., Yu, L., Yu, Y., Turnbull, G., Guo, M., Shu, W. & Li, B. (2019). Microfluidics-Based Fabrication of Cell-Laden Hydrogel Microfibers for Potential Applications in Tissue Engineering. *Molecules*, 24 (8): 1633. https://doi.org/10.3390/molecules24081633.

Wang, H., Zhou, L., Liao, J. & Tan, Y. (2014). Cell-Laden Photocrosslinked GelMA-DexMA Copolymer Hydrogels with Tunable Mechanical Properties for Tissue Engineering.*Journal of Materials Science: Materials in Medicine,* 25 (9): 2173–83. https://doi.org/10.1007/s10856-014-5261-x.

Wang, H., Gong, X., Guo, X., Liu, C., Fan, Y-Y., Zhang, J., Niu, B. & Li, W. (2019). Characterization, release, and antioxidant activity of curcumin-loaded sodium alginate/ZnO hydrogel beads. *International Journal of Biological Macromolecules,* 121: 1118-1125. https://doi.org/10.1016/j.ijbiomac.2018.10.121

Wang, Q., Zhang, H., Huang, J., Xia, N., Li, T. & Xia, Q. (2018). Self-Double-Emulsifying Drug Delivery System Incorporated in Natural Hydrogels: A New Way for Topical Application of Vitamin C. *Journal of Microencapsulation*, 35 (1): 90–101. https://doi.org/10.1080/02652048.2018.1425752

Wang, S., Lee, J.M. & Yeong, W.Y. (2015). Smart Hydrogels for 3D Bioprinting.*International Journal of Bioprinting*, 1 (1): 3–14. http://dx.doi.org/10.18063/IJB.2015.01.005

Wang, Y., Ma, M., Wang, J., Zhang, W., Lu, W., Gao, Y., Zhang, B. & Guo, Y. (2018). Development of a Photo-Crosslinking, Biodegradable GelMA/PEGDA Hydrogel for Guided Bone Regeneration Materials. *Materials*, 11 (8): 1345. https://doi.org/10.3390/ma11081345

Wang, Y., Beekman, I., Hew, J., Jackson, S., Issler-Fisher, A.C., Parungao, R., Lajevardi, S.S., Li, Z. & Maitz, P.K.M. (2018). Burn Injury: Challenges and Advances in Burn Wound Healing, Infection, Pain and Scarring. *Advanced Drug Delivery Reviews,* 123: 3–17. https://doi.org/10.1016/j.addr.2017.09.01

Wei, L.G., Chang, H.I., Wang, Y., Hsu, S.H., Dai, L.G., Fu, K.Y. & Dai., N.T. (2019). A Gelatin/Collagen/Polycaprolactone Scaffold for Skin *Regeneration. PeerJ*, 7 (e6358). https://doi.org/10.7717/peerj.6358

Wickett, R.R. & Visscher, M.O. (2006). Structure and Function of the Epidermal Barrier. *American Journal of Infection Control*, 34 (10): 98–110. https://doi.org/10.1016/j.ajic.2006.05.295

Xi, Y., Ge, J., Guo, Y., Lei, B. & Ma, P.X. (2018). Biomimetic Elastomeric Polypeptide-Based Nanofibrous Matrix for Overcoming Multidrug-Resistant Bacteria and Enhancing Full-Thickness Wound Healing/Skin Regeneration. *ACS Nano*, 12: 10772–84. https://pubs.acs.org/doi/abs/10.1021/acsnano.8b01152.

Yamamoto, T., Iwase, H., King, T.W., Hara, H. & Cooper, D.K.C. (2018). Skin Xenotransplantation: Historical Review and Clinical Potential. *Burns*, 44 (7): 1738–49. https://doi.org/10.1016/j.burns.2018.02.029

Yan, J.K., Qiu, W.Y., Wang, Y.Y. Wu, J.Y. (2017). Biocompatible Polyelectrolyte Complex Nanoparticles from Lactoferrin and Pectin as Potential Vehicles for

Antioxidative Curcumin. *Journal of Agricultural Food Chemistry*, 65: 5720–30. 10.1021/acs.jafc.7b01848

Yan, W.C., Davoodi, P., Vijayavenkataraman, S., Tian, Y., Ng, W.C., Fuh, J.Y.H., Robinson, K.S. & Wang, C.H. (2018). 3D Bioprinting of Skin Tissue: From Pre-Processing to Final Product Evaluation. *Advanced Drug Delivery Reviews*, 132: 270–95. https://doi.org/10.1016/j.addr.2018.07.016

Yin, J., Yan, M., Wang, Y., Fu, J. & Suo, H. (2018). 3D Bioprinting of Low-Concentration Cell-Laden Gelatin Methacrylate (GelMA) Bioinks with a Two-Step Cross-Linking Strategy. *ACS Applied Materials and Interfaces*, 10: 6849–57. https://doi.org/10.1021/acsami.7b16059

Ying, H., Zhou, J., Wang, M., Su, D., Ma, Q., Lv, G. & Chen, J. (2019). In Situ Formed Collagen-Hyaluronic Acid Hydrogel as Biomimetic Dressing for Promoting Spontaneous Wound Healing. *Materials Science and Engineering: C*, 10: 487–98. https://doi.org/10.1016/j.msec.2019.03.093

Zeng, Q., Macri, L.K. Prasad, A., Clark, R.A.F., Zeugolis, D.I., Hanley, C., Garcia, Y. et al. (2011). 6.20 Skin Tissue Engineering. In Comprehensive Biomaterials II, 6:334–82.

Zepon, K.M., Martins, M.M., Souza Marques, M., Maia Heckler, J., Dal Pont Morisso, F., Griebeler Moreira, M., Luiza Ziulkoski, A. & Kanis, L.A. (2019). Smart Wound Dressing Based on κ–Carrageenan/Locust Bean Gum/Cranberry Extract for Monitoring Bacterial Infections. *Carbohydrate Polymers*, 206: 362–70. https://doi.org/10.1016/j.carbpol.2018.11.014

Zhao, X, Sun, X., Yıldırımer, L., Lang, Q., Lin, Z.Y., Zheng, R., Zhang, Y., Cui, W., Annabi, N. & Khademhosseini, A. (2017). Cell Infiltrative Hydrogel Fibrous Scaffolds for Accelerated Wound Healing. *Acta Biomaterialia*, 49: 66–77. https://doi.org/10.1016/j.actbio.2016.11.017

Zhuang, P., Ng, W.L., An, J., Kai Chua, C. & Tan, L.P. (2019). Layer-by-Layer Ultraviolet Assisted Extrusion- Based (UAE) Bioprinting of Hydrogel

Constructs with High Aspect Ratio for Soft Tissue Engineering Applications. *PLos One,* 14 (6): e0216776. https://doi.org/10.1371/journal.pone.0216776

APPENDICES

A. Curcumin Calibration Curve

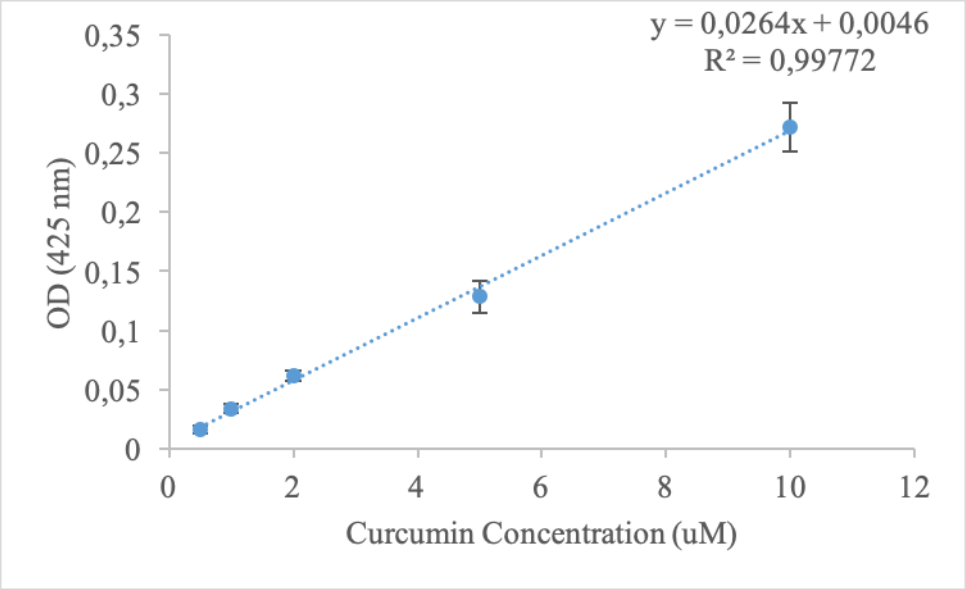

Figure A1. Calibration curve of curcumin constructed with different concentrations of curcumin in PBS (0.1 M, pH 7.2) (n=3).

B. Reduction of Values of PBS containing Irgacure 2959 and Vitamin-C

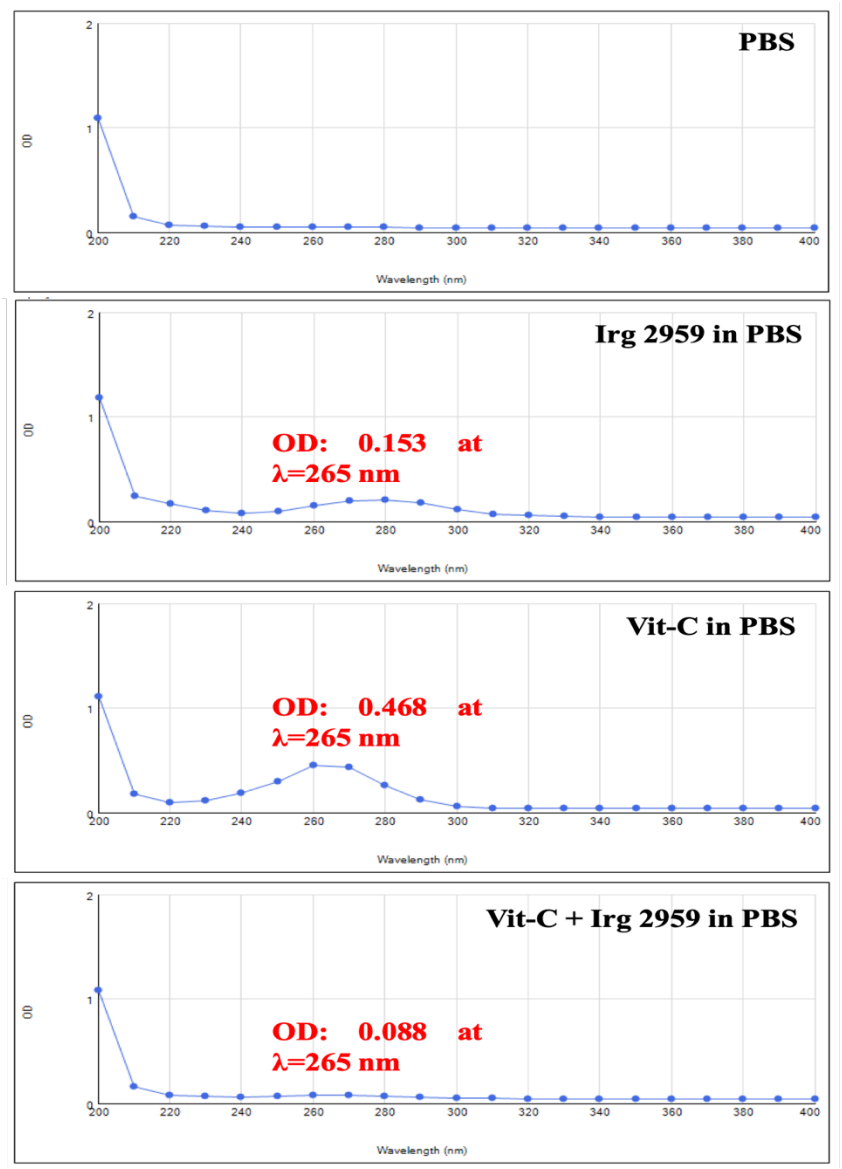

Figure B1. Effect of Irgacure 2959 on Absorbance readings of Vitamin-C solution

C. Calibration Curve of Vitamin-C

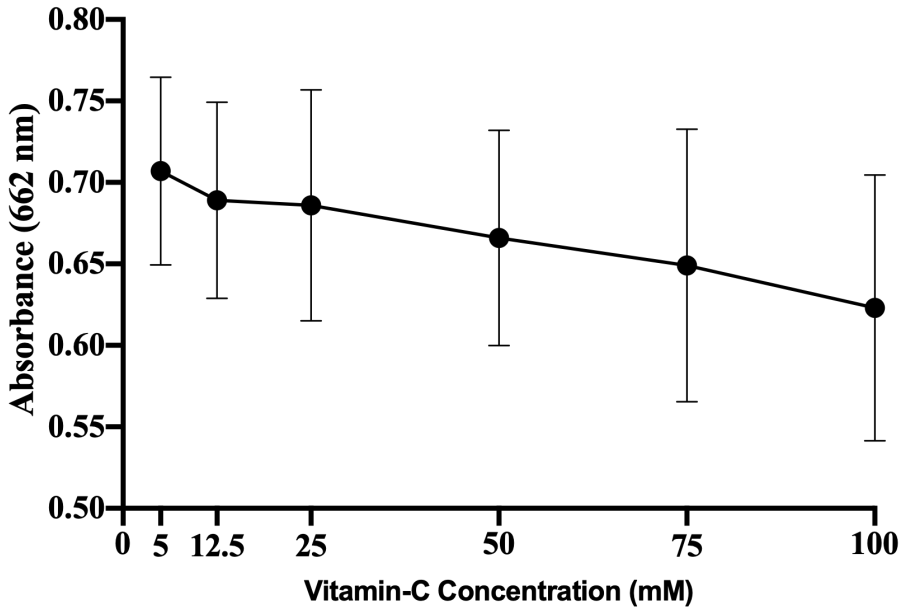

Figure C1. Calibration curve of Vitamin-C using 0.025 M methylene blue.

D. Alamar Blue Calibration Curve

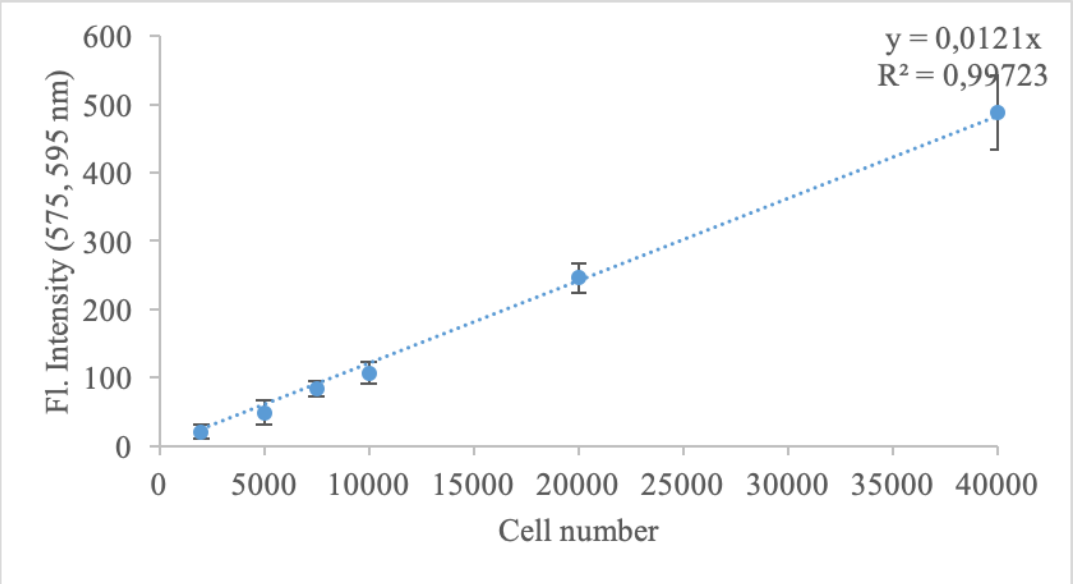

Figure D1. Calibration curve of cell number for Alamar Blue viability assay using fluorescence measurements (n=5).

E. The reaction of methacrylation of pectin and gelatin

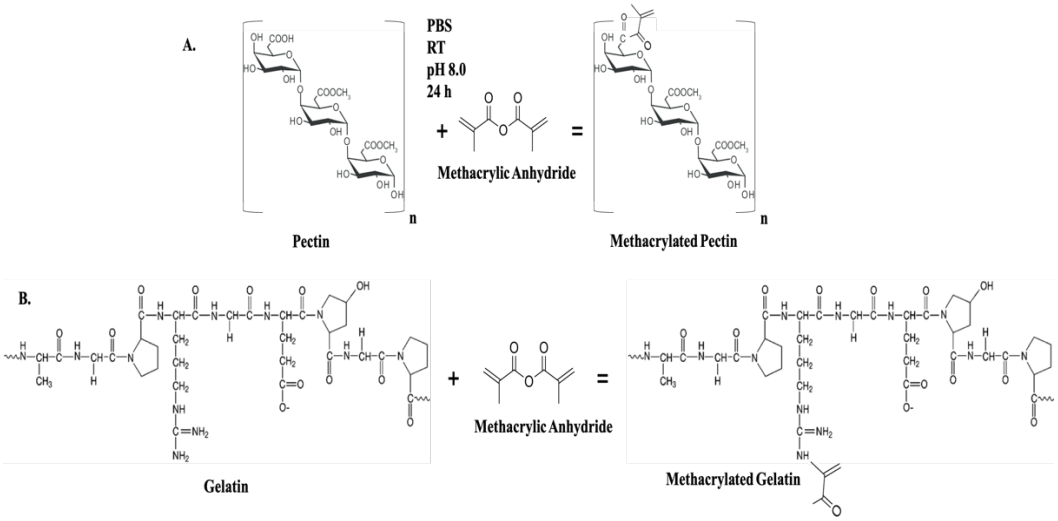

Figure E1. The reaction of methacrylation of pectin (A, in PBS, at RT) and gelatin (B, in CB Buffer, pH 9.0 at 60ºC).

F. The Effect of Curcumin Concentration on the Formation of Photocrosslinked P1:G3 Gels

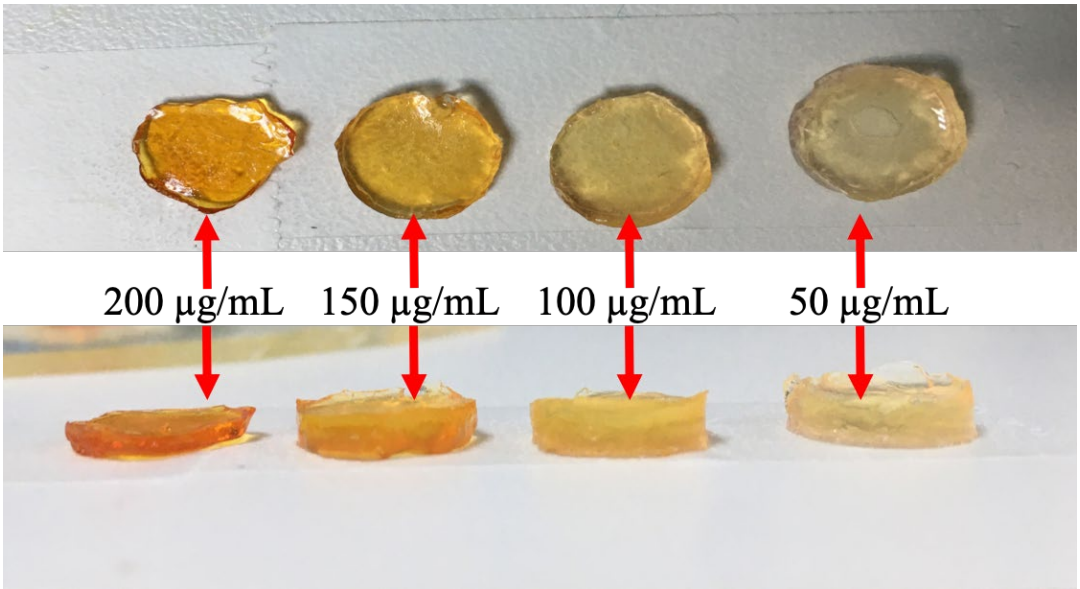

Figure F1. Photographs of photocrosslinked P1:G3 slab gels loaded with different concentrations of curcumin.

G. Dose Dependent Cytotoxicity Study of Vitamin-C and Curcumin to L929 Fibroblast Cells

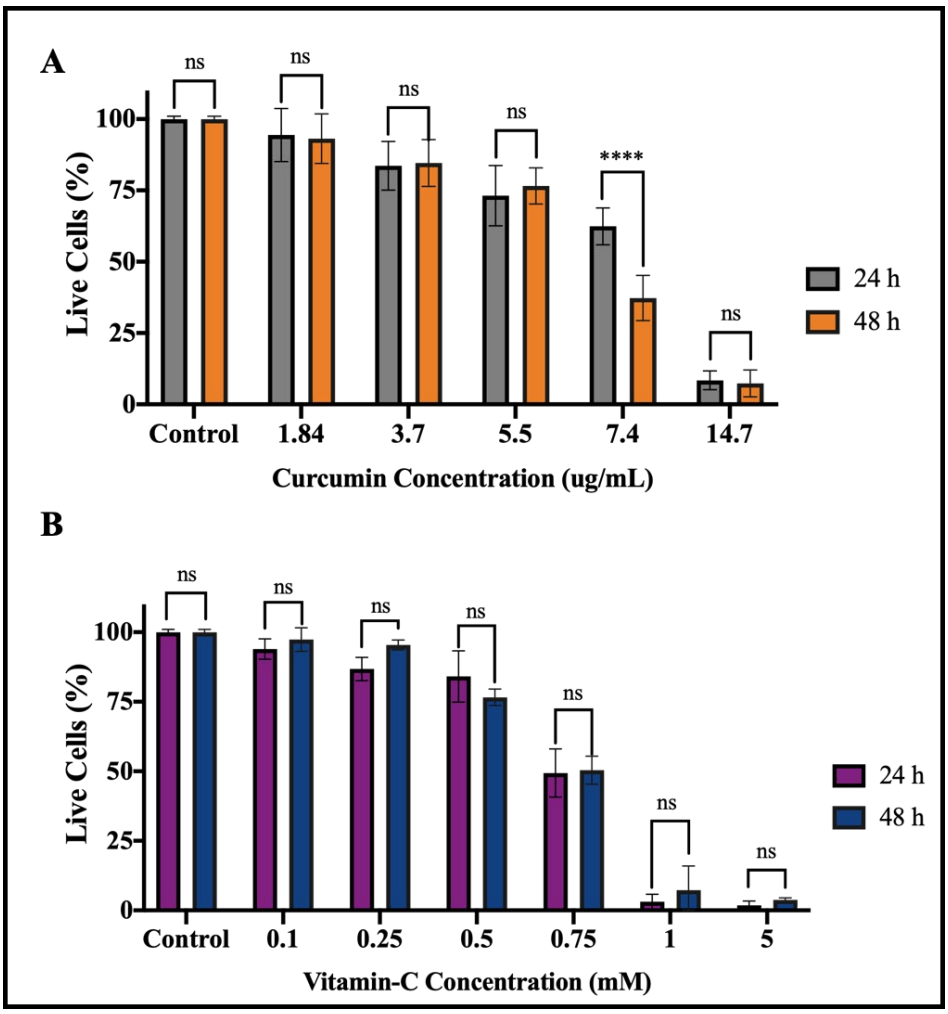

Figure G1. The impact of different concentrations of curcumin and Vitamin-C on L929 viability.